Latvijas Biozinātņu un tehnoloģiju universitāte

Veterinārmedicīnas fakultāte

Klīniskais institūts

Mg.med.vet. **Gundega Štelfa**

promocijas darbā iekļautās zinātniskās publikācijas

PIRMSKLĪNISKO PĒTĪJUMU EKSPERIMENTĀLIE MODEĻI GALVAS TRAUMU PĒTĪJUMIEM AR JAUNĀM ZĀĻU VIELĀM

EXPERIMENTAL MODELS FOR PRECLINICAL INVESTIGATIONS OF NOVEL DRUGS FOR TRAUMATIC BRAIN INJURY

zinātnes doktora grāda

Zinātnes doktore (Ph.D) Veterinārmedicīnas zinātnē

iegūšanai

Promocijas darba vadītājs
Profesors, **Dr. med.vet**. Ilmārs Dūrītis _____

Promocijas darba vadītāja
Profesore, **Dr. pharm.** Maija Dambrova _____

Promocijas darba konsultante
Dr.med. Līga Zvejniece _____

Promocijas darba autore _____

Jelgava 2024

JOURNAL OF NEUROTRAUMA 37:295–304 (January 15, 2020)
Mary Ann Liebert, Inc.
DOI: 10.1089/neu.2019.6524

Skull Fractures Induce Neuroinflammation and Worsen Outcomes after Closed Head Injury in Mice

Liga Zvejniece,[1] Gundega Stelfa,[1,2] Edijs Vavers,[1] Einars Kupats,[1,3] Janis Kuka,[1] Baiba Svalbe,[1] Baiba Zvejniece,[1,4] Christiane Albert-Weissenberger,[5] Anna-Leena Sirén,[5] Nikolaus Plesnila,[6] and Maija Dambrova[1,3]

Abstract

The weight-drop model is used widely to replicate closed-head injuries in mice; however, the histopathological and functional outcomes may vary significantly between laboratories. Because skull fractures are reported to occur in this model, we aimed to evaluate whether these breaks may influence the variability of the weight-drop (WD) model. Male Swiss Webster mice underwent WD injury with either a 2 or 5 mm cone tip, and behavior was assessed at 2 h and 24 h thereafter using the neurological severity score. The expression of interleukin (IL)-6, IL-1β, tumor necrosis factor-α, matrix metalloproteinase-9, and tissue inhibitor of metalloproteinase-1 genes was measured at 12 h and 1, 3, and 14 days after injury. Before the injury, micro-computed tomography (micro-CT) was performed to quantify skull thickness at the impact site. With a conventional tip diameter of 2 mm, 33% of mice showed fractures of the parietal bone; the 5 mm tip produced only 10% fractures. Compared with mice without fractures, mice with fractures had a severity-dependent worse functional outcome and a more pronounced upregulation of inflammatory genes in the brain. Older mice were associated with thicker parietal bones and were less prone to skull fractures. In addition, mice that underwent traumatic brain injury (TBI) with skull fracture had macroscopic brain damage because of skull depression. Skull fractures explain a considerable proportion of the variability observed in the WD model in mice—i.e., mice with skull fractures have a much stronger inflammatory response than do mice without fractures. Using older mice with thicker skull bones and an impact cone with a larger diameter reduces the rate of skull fractures and the variability in this very useful closed-head TBI model.

Keywords: neuroinflammation; skull fracture; traumatic brain injury; weight-drop model

Introduction

Traumatic brain injury (TBI) may result from falls, motor vehicle accidents, sports injuries, and explosions and is one of the leading causes of neurological deficits in persons under the age of 45. The TBI is heterogeneous with many etiologies and clinical presentations and encompasses diffuse, focal, penetrating, or blast injury.[1,2] Diffuse axonal injury results from movement of the brain within the skull and is related to closed-head injury (CHI), the most common type of TBI in humans.[3] During the last decade, substantial attention has been paid to the study of TBI. Reproducible animal models are crucial to clarify the biochemical/molecular mechanisms of injury and to assess preclinical drug efficacy and safety.

Numerous animal models have been used to study TBI, including open and CHI.[4] While mechanical force is delivered to the intact skull in CHI,[4] in open head injury, a craniotomy has to be performed, and the impact is directed toward the dura mater.[5,6] To perform CHI, several models are used, such as variations in weight-drop (WD),[5–7] piston-driven,[8–10] and blast injury[11] TBI models. The WD models that use a free falling weight are used most widely to induce CHI.[12]

Although WD models have been used for several decades, there is a substantial difference in performance and protocols between laboratories. For example, the weight of the falling cylinder varies from 5 g to 500 g, and the drop height varies from 1 cm to 167 cm.[13–16] As a consequence, the biochemical outcome— i.e., the expression of inflammatory cytokines, such as tumor necrosis

[1]Latvian Institute of Organic Synthesis, Riga, Latvia.
[2]Latvia University of Life Sciences and Technologies, Jelgava, Latvia.
[3]Riga Stradins University, Riga, Latvia.
[4]University of Latvia, Riga, Latvia.
[5]Department of Neurosurgery, University Hospital Würzburg, Würzburg, Germany.
[6]University of Munich, Institute for Stroke and Dementia Research, Munich, Germany.

factor (TNF)-α, interleukin (IL)-6, IL-12, and IL-1β, is highly variable.[17–21]

Controlled cortical impact and fluid percussion injury models, procedures that need a craniotomy, induce comparable high cytokine expression.[12,22–24] Because in a previous study we observed that approximately 30% of mice experienced skull fractures after WD injury (unpublished data), we hypothesize that injury to the skull may be one of the main triggers for the expression of inflammatory genes in the brain after WD injury and may thus contribute to the variability observed in this valuable TBI model. Therefore, the aim of the present study was to compare the inflammatory response after WD injury in the hippocampus and striatum of mice and correlate these findings with the presence and severity of skull fractures.

Methods

Animals

One hundred and nine male Swiss Webster (Laboratory Animal Centre, University of Tartu, Tartu, Estonia) 10-week-old mice were used for the WD model and 13 male Swiss Webster 10- and 20-week-old mice were used for micro-computed tomography (micro-CT). The mice weighed 28–46 g; all animals were housed under standard conditions (21–23°C, 12 h light/dark cycle) with unlimited access to standard food (Lactamin AB, Mjölby, Sweden) and water.

The mice were assigned randomly to one of three experimental groups. Body weight was recorded throughout the study as a measure of general health. The experimental design was to expose 10-week-old mice to CHI using a weight-drop device with 2 or 5 mm cone tip or sham treatment. The skull was then examined for evidence of visible fractures, as defined below. Animals with CHI were subdivided into non-fracture and fracture (mild, moderate, severe) groups for comparison. The neurobehavioral status of the mice was obtained at 2 and 24 h after injury. Blood and brain tissue were collected at 12 h or 1, 3, and 14 days post-TBI for quantitative reverse transcription-polymerase chain reaction (RT-PCR) and enzyme-linked immunosorbent assay (ELISA), as described below. Before injury, a micro-CT was performed to quantify skull thickness at the impact site.

The timeline of experimental procedures is depicted in Figure 1. All studies involving animals were reported in accordance with the Animal Research: Reporting *In Vivo* Experiments guidelines.[25,26] The experimental procedures were performed in accordance with the guidelines reported in the EU Directive 2010/63/EU and in accordance with local laws and policies; all procedures were approved by the Latvian Animal Protection Ethical Committee of Food and Veterinary Service in Riga, Latvia.

Chemicals

Isoflurane was purchased from Chemical Point (Deisenhofen, Germany). Tramadol solution was purchased from KRKA (Novo Mesto, Slovenia). Physiological saline (0.9%) was purchased from Fresenius Kabi (Warsaw, Poland). Oxygen and nitrous oxide gases were purchased from AGA (Riga, Latvia).

WD model

The WD model was performed as described previously.[5,6] Briefly, the mice were anesthetized with 4% isoflurane in a mixture of 50% nitrous oxide and 50% oxygen, and 2% isoflurane was maintained during the surgical procedure using a face mask. The depth of anesthesia was monitored by toe pinch. Before trauma induction, the mice received a subcutaneous (SC) injection of tramadol (10 mg/kg). A midline longitudinal scalp incision was made, and the skull was exposed. A cone with a tip diameter of 2 or 5 mm was placed 2 mm posterior and lateral to bregma, and a weight of 90 g was dropped from a height of 8 cm onto the cone.

Oxygen was applied for 20–40 sec immediately after TBI. Then, the scalp wound was closed with a polypropylene 6-0 suture (Surgipro™ II, Covidien, Mansfield, MA), and the mice were returned to their home cages with free access to water and food. Sham animals underwent the same procedures as the animals in the TBI group, but without the release of the weight.

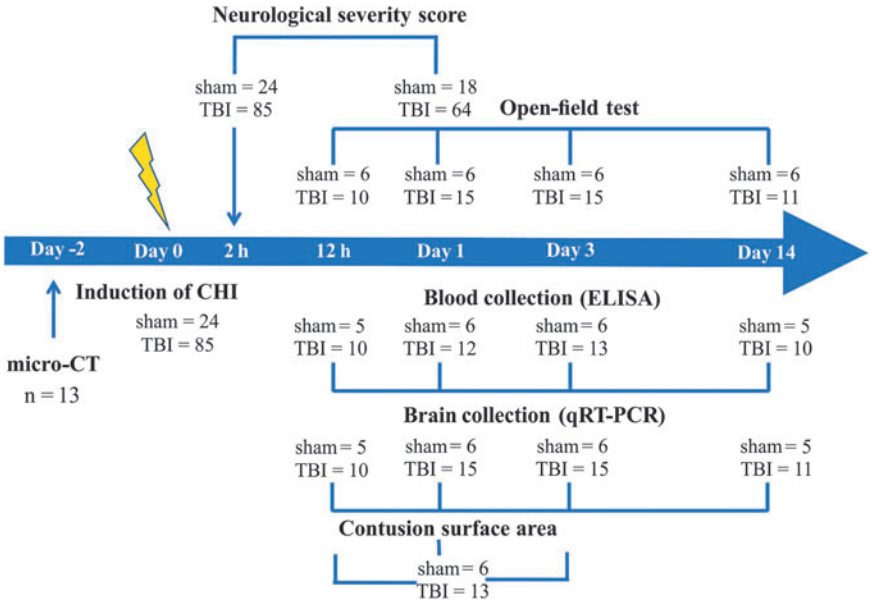

FIG. 1. Schematic illustration of the experimental design. TBI, traumatic brain injury; CHI, closed head injury; ELISA, enzyme-linked immunosorbent assay; micro-CT, micro-computed tomography; qRT-PCR, quantitative reverse transcription: polymerase chain reaction. Color image is available online.

Neurological severity score (NSS)

Behavioral testing was performed by experienced scientists blinded to the experimental group. The neurobehavioral status of the mice was obtained by the NSS.[5] The general neurological state of the mice was evaluated at baseline and 2 h and 24 h post-injury during the light part of the light–dark cycle. The NSS consists of nine individual parameters, including motor function, alertness, and physiological behavior tasks.

The following items were assessed: presence of paresis; impairment of seeking behavior; absence of perceptible startle reflex; inability to get down from a rectangle platform (34 × 27 cm); inability to walk on 3-, 2-, and 1-cm wide beams; and inability to balance on a 0.7-cm–wide beam and a 0.5 cm-diameter round beam for at least 15 sec. If a mouse showed impairment in one of these items, then a value of 1 was added to its NSS. Thus, higher values for the NSS indicate more severe neurological impairment.

The severity of skull fractures was determined based on the parameters used to evaluate skull fractures in patients with small modifications: non (skull bone without changes/no signs of fracture), mild (isolated linear fracture with no evidence of intracranial lesion), moderate (linear depressed or diastatic fracture with minimal dural tear, no macroscopic evidence of hematoma or parenchyma injury), and severe (complicated fracture with macroscopic intracranial lesions, including parenchyma injury and hematomas).[27,28]

The severity of skull fracture was evaluated immediately after injury by macroscopic visualization, which is a rapid and simple method. Post-mortem micro-CT analysis of the parietal bone plates could provide more detailed results than macroscopic visualization, however.

Open-field test

To detect the motor activity of the animals, an open-field test was performed before and at 12 h and 1, 3, and 14 days after TBI. The test apparatus was a square arena (44 × 44 cm) with a black floor. The moved distance and velocity in a 5-min session were recorded and analyzed using the EthoVision video tracking system (version XT 11.5; Noldus, Wageningen, The Netherlands).

Quantitative RT-PCR analysis

To quantify the inflammatory response, the mouse brains were collected at 12 h and 1, 3, and 14 days after trauma. Brain tissues were collected immediately after decapitation of the animals. Individual brain structures from both hemispheres were separated on ice and snap frozen in liquid nitrogen. The brain samples were stored at -80°C until ribonucleic acid (RNA) isolation.

Quantitative RT-PCR was performed using a previously described method[29] with slight modifications. Total RNA was isolated from brain tissues using an RNA mini kit (Life Technologies, Grand Island, NY) according to the manufacturer's instructions. The extracted RNA was dissolved in 50 μL nuclease-free distilled water and stored at -80°C until further analysis. First-strand complementary deoxyribonucleic acid (cDNA) was synthesized using a high-capacity cDNA reverse transcription kit (Thermo Fisher Scientific, Waltham, MA) following the manufacturer's protocol.

Quantitative RT-PCR analysis for IL-6, IL-1β, TNF-α, tissue inhibitor of metalloproteinase (TIMP)-1, matrix metalloproteinase (MMP)-9 and β-actin was performed using SYBR® Green Master Mix (Life Technologies). The primer sequences used in this study were as follows: IL-6 (NM_001314054.1), 5 - TCT ATA CCA CTT CAC AAG TCG GA - 3 (forward) and 5 – GAA TTG CCA TTG CAC AAC TCT TT – 3 (reverse); IL-1β (NM_008361.4), 5 – GGG CCT CAA AGG AAA GAA TC – 3 (forward) and 5 – TTG CTT GGG ATC CAC ACT CT – 3 (reverse); TNF-α (NM_013693.3), 5 – CCC TCA CAC TCA GAT CAT CTT CT – 3 (forward) and 5 – GCT ACG ACG TGG GCT ACA G – 3 (reverse); TIMP-1 (NM_011593.2), 5 – CAG TAA GGC CTG TAG CTG TGC – 3 (forward) and 5 - AGG TGG TCT CGT TGA TTT CTG – 3 (reverse); MMP-9 (NM_031055.1), 5 – TCG AAG GCG ACC TCA AGT G – 3 (forward) and 5 – TTC GGT GTA GCT TTG GAT CCA – 3 (reverse); and β-actin (NM_007393.5), 5 – CCT CTA TGC CAA CAC AGT GC– 3 (forward) and 5 – CAT CGT ACT CCT GCT TGC TG– 3 (reverse).

The primers were obtained from Metabion (Steinkirchen, Germany). The relative expression levels for each gene were calculated with the $\Delta\Delta$Ct method, normalized to the expression of β-actin and compared with the age-matched sham group.

TIMP-1 and TNF-α measurement in plasma

Blood samples were collected after decapitation of the animals. Heparin was used to prevent blood clot formation. Blood samples were centrifuged at 3000 rpm and 4°C for 10 min (Heraeus™ Biofuge™ Stratos™ Centrifuge, Thermo Fisher Scientific) to separate the plasma. Plasma was stored at -80°C. The ELISA was performed using Mouse TIMP1 SimpleStep ELISA® Kit (Abcam, Boston, MA) and a Mouse TNF-α ELISA Kit (EMD Millipore, Burlington, MA) following the manufacturer's instructions.

Micro-CT analysis

The micro-CT imaging was performed before TBI. The mice were anesthetized using 4% isoflurane in a mixture of 50% nitrous oxide and 50% oxygen, followed by 1–1.5% isoflurane throughout the procedure. The micro-CT scans were acquired using 30 keV, 0.95 mA lamp energy with an exposure time of 250 ms using a Trifoil InSyTe FLECT® imager (Chatsworth, CA). A total of 720 projections were acquired per rotation. Three-dimensional images on selected skull areas were reconstructed with a voxel size of 25 μm using FluoroView 1.5 and Cobra 7.12.9 software. Qualitative and quantitative data were analyzed using VivoQuant 1.23 software.

To evaluate parietal bone thickness and density, a coronal section was taken. The frontal plane represents the coronal plane at the middle of the bregma and lambda sutures. By using coronal sections, the parietal bone gray scale value (radiological density) was measured in three regions (Fig. 6B) of interest at five points in an equal interval. The coronal skull micro-CT images were divided into bone and non-bone regions by determining the threshold value using the automated Otsu method.[30] The gray scale values of the mouse skull were used to evaluate bone density.[31–33]

Measurement of contusion surface area

Mice were anesthetized using a combination of ketamine (200 mg/kg) and xylazine (15 mg/kg) and perfused transcardially with 0.01 M phosphate-buffered saline (1X PBS) for 5 min at a speed of 3 mL/min to remove blood from the tissue. Perfusion was switched to 4% paraformaldehyde (PFA) solution in 1X PBS until stiffening of the mouse body. The brains were dissected carefully and fixed overnight in 4% PFA at 4°C. The dissected brains were washed in 1X PBS, dried, and photographed using a digital camera (Sony A900, Japan). The cortical contusion area was quantified using ImageJ software (version 1.52j).

Statistical analysis

The statistical calculations were performed using the GraphPad Prism 8.1 software package (GraphPad Software, Inc., La Jolla, CA). The Shapiro-Wilk test was used to examine the distribution of the data. The Kruskal-Wallis test followed by the Dunn test was used for non-normally distributed data sets. A *post hoc* test was performed if analysis of variance (ANOVA) or the Kruskal-Wallis test indicated statistically significant differences.

Time and group interactions were analyzed by using two-way ANOVA and the Tukey test as the *post hoc* test for multiple

comparisons. Student *t* test was used to compare differences between mouse weight and occurrence of fracture and differences between parietal bone thickness and gray scale values in animals without and with skull fractures. The Pearson correlation test was used to analyze the correlation between parietal bone thickness and animal weight. The *p* values less than 0.05 were considered significant.

Results

Health status assessment after CHI

Two mice in the ''with fracture'' group died immediately after injury. All other mice were included in the data analysis. One mouse in the ''with fracture'' group had spontaneous seizures. In animals with skull fracture, there was a minor loss of body weight during the first three post-injury days; however, no significant differences were observed between the groups (data not shown). During the immediate time after injury, apnea (<3 sec) was observed in three animals. The remaining animals breathed spontaneously during and after the procedure and were fully awake within 1 min.

NSS

The animals were divided into two groups: animals with and without skull fractures after TBI. The NSS was significantly higher in traumatized than in sham-operated mice at 2 h and 24 h after surgery (Fig. 2A; main effects of time [$F_{(2, 135)} = 98.4$, $p < 0.0001$] and group [$F_{(2, 76)} = 25.8$, $p < 0.0001$], and interaction between time and group [$F_{(4, 152)} = 26.9$, $p < 0.0001$]).

Two hours after TBI, the average scores for animals without and with skull fractures were 2.5 ± 0.2 and 4.8 ± 0.5 points, respectively (Fig. 2A). Twenty-four hours after TBI, the NSS for animals without and with skull fracture was 2.9 ± 0.2 and 4.8 ± 0.4 points, respectively (Fig. 2A), and there was a significant difference between the groups (Fig. 2A). In addition, we observed that the NSS increased significantly depending on the skull fracture severity (Fig. 2B).

We compared the impact of cone tips on the occurrence of fracture using a cone with a 2 mm or 5 mm tip. The cone with a 2 mm tip caused skull fractures in 33% of animals, while only 10% of animals had fractures when traumatized with the 5 mm cone (Fig. 2D). The functional outcome was similar in mice traumatized with the 2 or 5 mm cone at 2 h and 24 h after TBI (Fig. 2C; main effects of time [$F_{(2, 34)} = 18.8$, $p < 0.0001$] and group [$F_{(2, 22)} = 5.3$, $p < 0.05$] and the interaction between time and group [$F_{(4, 44)} = 3.4$, $p < 0.05$]).

Open-field test

The mice were tested in an open-field test to assess locomotor activity at 12 h, 1, 3, and 14 days after injury. There were no significant differences in the distance traveled and velocity between groups (data not shown).

Inflammation-related gene expression in the brain after TBI

To detect the impact of skull fracture on inflammatory gene expression in brain tissue, we measured IL-6, IL-1β, TNF-α, MMP-9, and TIMP-1 gene expression in the hippocampus and striatum at

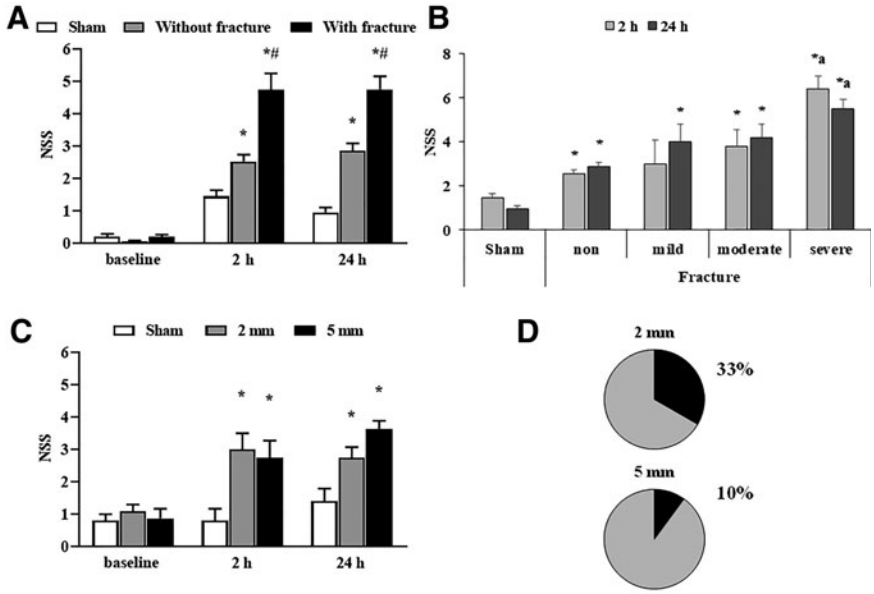

FIG. 2. Functional outcome after traumatic brain injury (TBI). (**A**) Comparison of the neurobehavioral responses in animals without or with skull fractures using the Neurological Severity Score (NSS). Data are shown as the mean ± standard error of the mean (SEM). (sham-operated, $n = 24$; without fracture, $n = 52$; with fracture, $n = 33$). $^{*}p < 0.05$ vs. sham-operated; $^{\#}p < 0.05$ without vs. with skull fracture (repeated measures two-way analysis of variance (ANOVA) followed by the Tukey test). (**B**) Relation of the severity of skull fracture and NSS at 2 h and 24 h after TBI. Data are shown as the mean with 95% confidence interval (sham-operated, $n = 24$; non-fracture, $n = 52$; mild fracture, $n = 7$; moderate fracture, $n = 12$; severe fracture, $n = 14$). $^{*}p < 0.05$ vs. sham-operated; $^{a}p < 0.05$ non vs. severe fracture (Kruskal Wallis test followed by the Dunn test). (**C**) NSS after TBI using 2 mm and 5 mm tips in animals without skull fractures. Data are shown as the mean ± SEM. $^{*}p < 0.05$ vs. sham-operated (repeated measures two-way ANOVA followed by the Tukey test) and (**D**) occurrence of fractures using cone with a 2 mm or 5 mm diameter tip (sham-operated, $n = 5$; 2 mm, $n = 12$; 5 mm, $n = 8$).

12 h, 1, 3, and 14 days after TBI. For gene expression data F values, degrees of freedom and *p* values are summarized in Supplementary Table S1. A significant 71- and 90-fold increase was observed for TIMP-1 at 12 h and 1 day after injury, respectively, in the ipsilateral hippocampus of animals with skull fractures (Fig. 3A). In addition, TIMP-1 was increased in the contralateral hippocampus 1 day after injury (Fig. 3A).

The TIMP-1 mRNA expression in the ipsilateral striatum of animals with skull fractures was increased 16- and 130-fold at 12 h and 1 day after injury, respectively (Fig. 3B). In addition, TIMP-1 mRNA was increased in the contralateral striatum at 1 and 3 days after injury (Fig. 3B).

The TNF-α mRNA expression in animals with skull fractures was significantly increased 13-fold and six-fold in the ipsilateral hippocampus at 12 h and 1 day after injury, respectively (Fig. 3A). The TNF-α mRNA expression was significantly increased 67-fold and five-fold in the ipsilateral and contralateral striatum, respectively, in animals with skull fractures at 12 h after injury (Fig. 3B). The MMP-9 gene was significantly downregulated at 12 h after trauma in the ipsilateral hippocampus of animals with skull fractures (Fig. 3A). No differences in IL-6 gene expression were detected between groups in the hippocampus and striatum (Fig. 3A, B).

Significant increase was observed for TIMP-1 mRNA at 1 day after injury in the ipsilateral hippocampus of animals without skull fractures (Fig. 3A). No significant changes for IL-6, IL-1β, TNF-α, and MMP-9 gene expression were observed at 12 h and 1, 3, and 14 days after TBI in animals without skull fractures (Fig. 3A, B).

The TIMP-1 and TNF-α genes showed a significant correlation with the severity of TBI at 12 h and 24 h after injury (Fig. 4). In the ipsilateral hippocampus, 50- and 146-fold increases in TIMP-1 gene expression were observed after moderate and severe skull fractures, respectively (Fig. 4A). Similarly, 14- and 173-fold increases in TIMP-1 gene expression in the ipsilateral striatum were observed after moderate and severe skull fractures, respectively (Fig. 4B). After severe skull fracture, TNF-α mRNA showed 14- and 130-fold increases in the ipsilateral hippocampus and striatum, respectively (Fig. 4C and 4D).

TIMP-1 and TNF-α levels in plasma

The TIMP-1 and TNF-α protein concentrations were measured in plasma at 12 h and 1, 3, and 14 days after TBI. Slightly increased TIMP-1 plasma levels were observed in animals with fractures (Fig. 5; main effects of time [$F_{(3, 53)} = 6.0$, $p < 0.01$] and group [$F_{(2, 53)} = 6.6$, $p < 0.01$] and interaction between time and group [$F_{(6, 53)} = 1.9$,

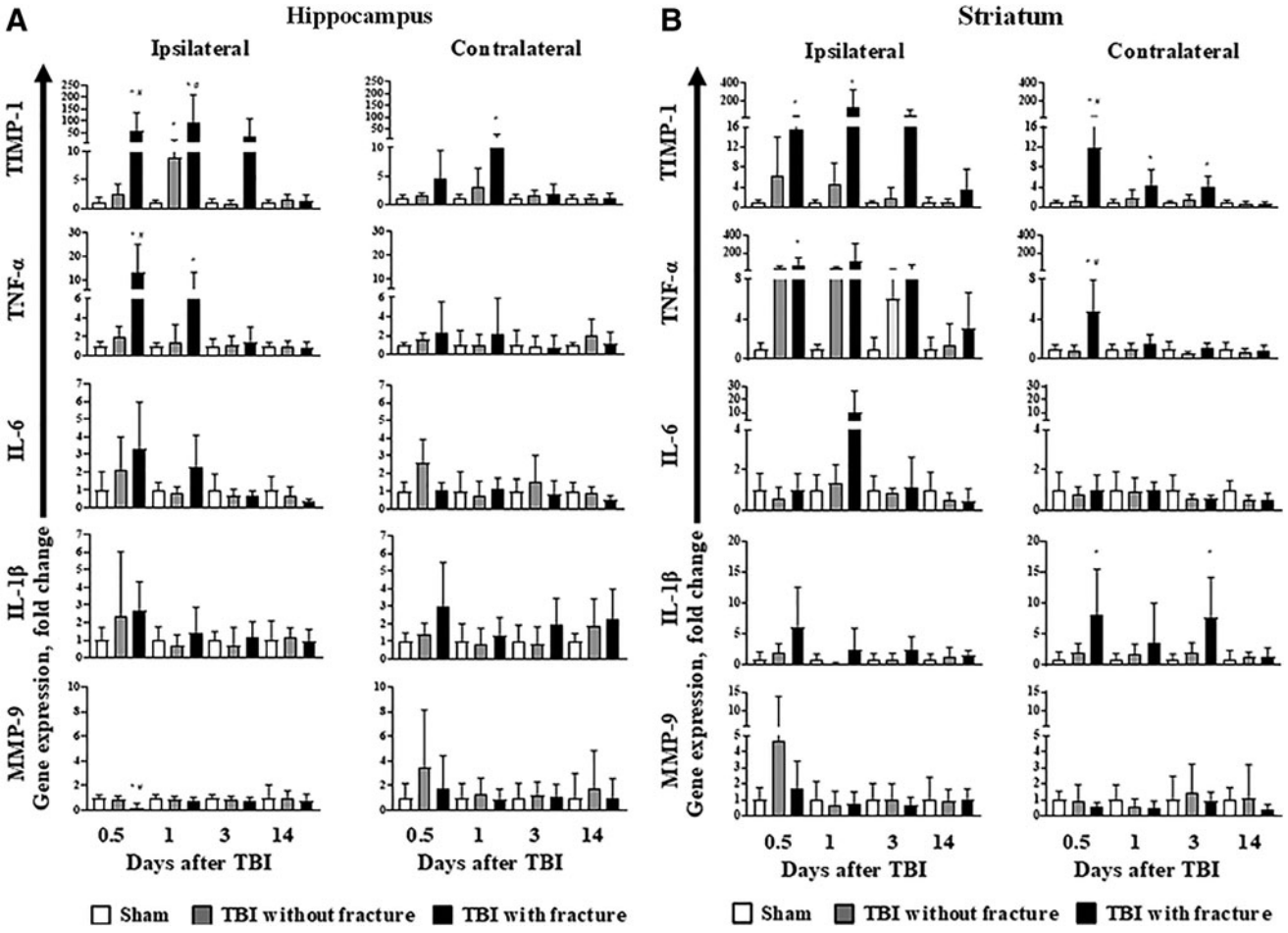

FIG. 3. Inflammation-related gene expression in the ipsilateral and contralateral (**A**) hippocampus and (**B**) striatum after traumatic brain injury (TBI). Data are expressed as the mean with 95% confidence interval ($n = 5$–9). $^{*}p < 0.05$ vs. sham-operated; $^{\#}p < 0.05$ TBI without vs. TBI with skull fracture (ordinary two-way analysis of variance followed by the Tukey test; see Supplementary Table S1 for F values, degrees of freedom, and *p* values). TIMP-1, tissue inhibitor of metalloproteinase-1; TNF-α, tumor necrosis factor-α ;IL, interleukin; MMP-9, matrixmetalloproteinase-9.

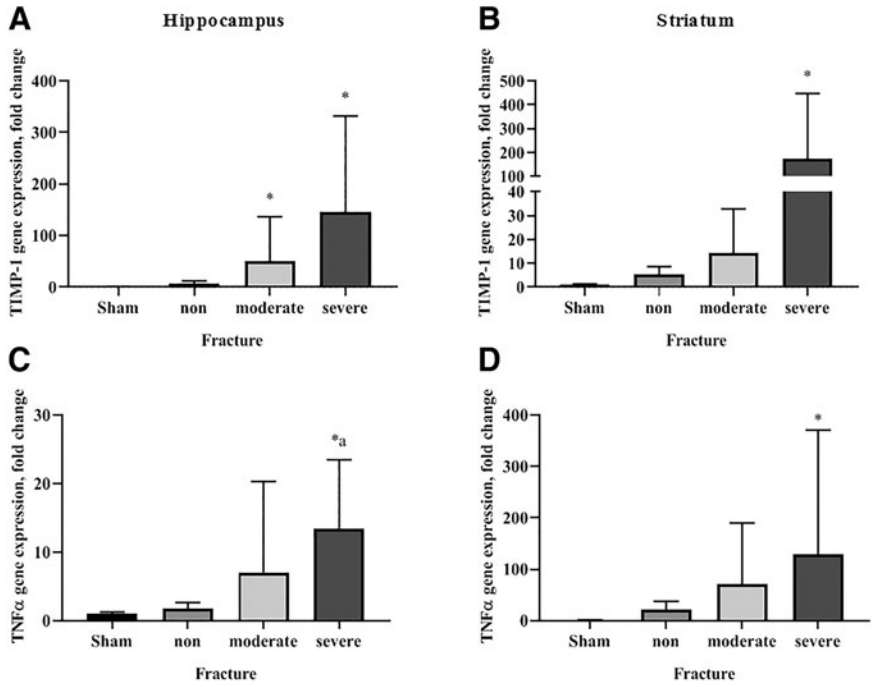

FIG. 4. Inflammation-related gene expression in the ipsilateral brain at 12 h and 24 h after traumatic brain injury with various severities of skull fracture. Tissue inhibitor of metalloproteinase-1 (TIMP-1) gene expression in the hippocampus (**A**) and striatum (**B**) and tumor necrosis factor-α (TNF-α) gene expression in the hippocampus (**C**) and striatum (**D**). Data are expressed as the mean with 95% confidence interval ($n = 5$–13). *$p < 0.05$ vs. sham-operated; [a]$p < 0.05$ vs. non-fracture; [b]$p < 0.05$ vs. mild fracture; [c]$p < 0.05$ vs. moderate fracture (Kruskal-Wallis test followed by the Dunn test).

$p > 0.05$]); however, there were no significant differences when compared with sham-operated animals. Plasma levels of TNF-α were not elevated after TBI (<1.5 pg/mL).

Evaluation of the skull bone by micro-CT

Micro-CT examination of the parietal bone revealed variations in thickness and gray scale values. The average parietal bone thickness varied from 0.17 to 0.44 mm (mean, 0.3 ± 0.1 mm), depending on the localization. The parietal bone became thinner as it reached the sagittal suture (Fig. 6B). The lateral periphery of the parietal bone had a thicker structure with a higher gray scale value, ranging from 3.7 to 10.2 (mean, 6.7 ± 1.7). The parietal bone gray scale value was higher in 20-week-old mice than in 10-week-old mice (mean, 7.2 vs. 7.5; 10 weeks vs. 20 weeks, respectively). Lower parietal bone gray scale values were associated significantly with skull fracture.

Skull thickness increased proportionally with age and weight of the animals. Parietal bone thickness correlated with animal weight (Pearson $r = 0.75$, $p < 0.01$), and animal weight was inversely associated with skull fractures. Decreased parietal bone thickness and gray scale values were significantly associated with an increased risk of fracture (Fig. 7).

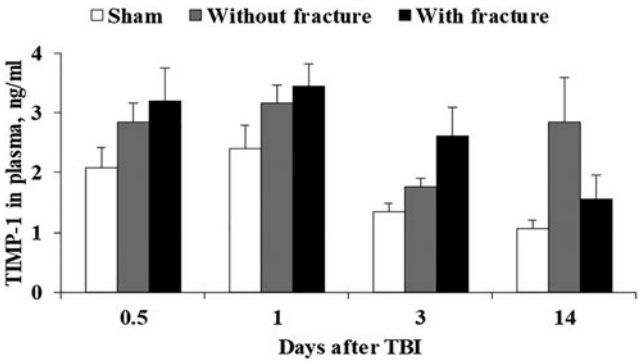

FIG. 5. Tissue inhibitor of metalloproteinase-1 (TIMP-1) concentration in the plasma of animals without or with skull fractures at 12 h, 1, 3, and 14 days after traumatic brain injury (TBI). Data are expressed as the mean ± standard deviation (n = 5–7). *$p < 0.05$ vs. sham-operated (ordinary two-way analysis of variance followed by the Tukey test).

Evaluation of the contusion surface area

Macroscopic observation demonstrated that the brains of sham-operated mice and mice that underwent TBI without skull fracture showed no signs of cortical injury (Fig. 8). The TBI with skull fracture resulted in mild to severe brain damage because of skull depression (Fig. 8). In addition, skull fractures were associated with epidural and subdural hematomas and intraparenchymal hemorrhage.

Discussion

A TBI is a complex and heterogeneous injury that includes hematomas, contusions, subarachnoid hemorrhage, hypoxia, ischemia, and axonal and vascular injuries. This heterogeneity is a particular challenge when performing experimental TBI research.[12] The WD model is the most commonly used experimental method to study the pathophysiology of CHI.[4] Nevertheless, this model is not well standardized and generates results with

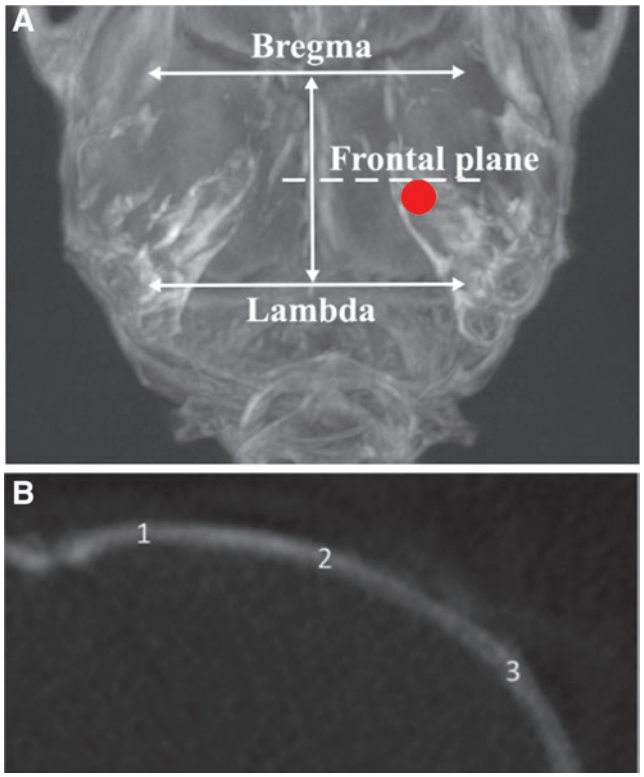

FIG. 6. Micro-CT image of a mouse skull with schematic illustration of the measurement parameters of mouse parietal bone thickness and density. (**A**) Frontal plane at a distance between coronal suture and lambdoid suture, which indicates the impact location (red circle) in the weight-drop traumatic brain injury model. (**B**) The landmarks shown on a coronal section of parietal bone represent thickness and density measurement points (medial periphery–1, midline–2, and lateral periphery–3). Color image is available online.

substantial variability regarding histopathological, biochemical, and functional outcomes.[7–11,15,28,36–38] Our results demonstrated that animals experiencing skull fractures after undergoing the WD model show a substantial inflammatory response in the brain, while animals without skull fractures do not, thus demonstrating how skull fractures contribute to the heterogeneity of the WD model.

When reviewing published literature (articles published on the CHI model in PubMed from 2001 to 2018), skull fractures were evaluated in only 18 of 97 studies (18.6%), and animals with fractures were excluded. A significant number of studies (81.4%) did not mention the incidence of skull fractures, showing that injury to the skull has been neglected in most CHI experiments.

Moreover, significant heterogeneity was observed in the parameters of falling weight, drop height, and impact tip diameter that led to different impact energies delivered to brain tissue. The falling weight ranged from 5 to 500 g, and the drop height ranged from 1 to 167 cm. Impact tip diameters ranged from 1 to 5 mm or were not reported. The calculated amount of energy as a function of the mass and height varied from 0.04 to 1.10 J. Thus, these studies do not share a common methodological indicator that would allow a comparison of the results of experiments between laboratories.

Our current study investigating the influence of skull fractures after WD represents a first step to reduce heterogeneity in this very useful CHI model. Skull fracture is an independent risk factor for intracranial hemorrhage in patients with TBI.[34,35] Intracranial hemorrhage is associated with increased intracranial pressure, oxidative damage, vasogenic edema, cytotoxic edema, heme toxicity, and iron toxicity and may thus contribute to secondary brain injury.[36]

Approximately one-half of depressed skull fractures in patients with TBI result in dural tearing, which is associated with cranial infections.[37,38] In patients, skull fracture with hemorrhage results in increased inflammation and neuronal excitability because of the

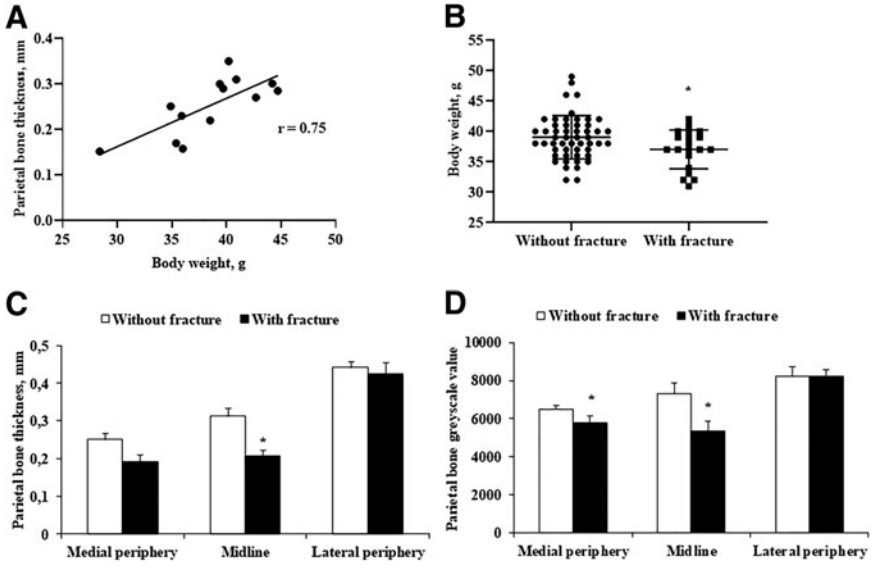

FIG. 7. Correlation between parietal bone thickness, mouse body weight and skull fracture. (**A**) Midline parietal bone thickness as a function of animal body weight ($n = 13$). Parietal bone thickness was measured using a Trifoil InSyTe FLECT® imager (Pearson $r = 0.748$, $^*p < 0.01$). (**B**) Difference between mouse weight and occurrence of fracture. Data were analyzed using GraphPad Prism 8.1 software (without fracture, $n = 52$; with fracture, $n = 20$). $^*p < 0.05$ vs. group without fracture (Student t test). (**C**) Difference between parietal bone thickness and **(D)** gray scale values in animals without and with skull fracture. Parietal bone thickness and gray scale values were measured at three points using a Trifoil InSyTe FLECT® imager. Data are shown as the mean ± standard error of the mean of five animals. $^*p < 0.05$ without vs. with fracture (Student t test).

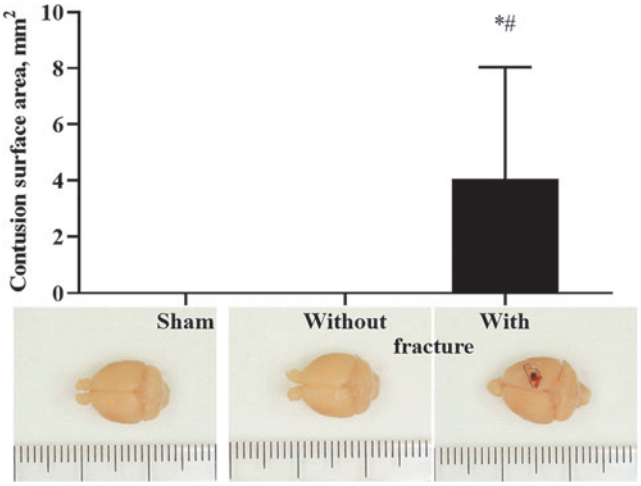

FIG. 8. Average contusion surface area observed up to 3 days after traumatic brain injury. Data are shown as the mean ± 95% confidence interval. (sham-operated, $n = 6$, without fracture, $n = 6$, with fracture, $n = 7$). Representative images of brains are shown under the graph. $^{*}p < 0.05$ vs. sham-operated; $^{\#}p < 0.05$ vs. without fracture (Kruskal-Wallis test followed by the Dunn test). Color image are available online.

toxic effects of hemoglobin breakdown and the generation of reactive oxygen species.[39]

Thus, our results demonstrating an increased neuroinflammatory response in the brain after TBI with skull fracture are well in line with the clinical features of TBI. Moreover, compared with animals without fracture, TBI in animals with moderate and severe fractures showed significant differences in responses to the NSS at 24 h but not at 2 h after TBI. Only one study reported animals with and without skull fractures and divided these animals into separate groups.[40] There was no difference in NSS between animals with or without skull fracture and sham-operated animals at 1 h post-injury.[40] The NSS was not assessed at later time points after an injury; thus, it is difficult to compare the impact of fracture on NSS in this study. Moreover, skull fracture was associated with more severe TBI outcomes, including immediate post-traumatic respiratory depression, secondary rebound injury, and death in mice.[6]

Other important factors, such as age and skull thickness, could also influence the incidence of parietal bone fracture. Skull cortical thickness is an important factor related to the deformation of the skull and fracture propensity,[41] and skull cortical bone density also influences skull fracture in humans.[42] Moreover, skull density is associated with the biomechanical threshold for concussion and may influence TBI, even without causing a skull fracture.[43] We showed that mouse parietal bone thickness and gray scale values are effective at predicting skull fractures. Thus, mouse age and weight should be taken into account in the design of the experiment.

It is important to acknowledge that in other CHI models, helmets (i.e., metallic disc on the exposed skull surface) are used to reduce the incidence of skull fractures.[7,9,44] The use of helmets helps to disperse the impact energy delivered to the brain tissue, thereby protecting the skull from the fractures. In the present study, the use of a 5 mm cone tip reduced the incidence of skull fractures, suggesting that a larger diameter should be used in the WD model.

To date, contrasting results on the neuroinflammatory response in brain tissues have been reported after CHI in mice. Our results clearly showed a significant increase in TNF-α and TIMP-1 gene expression in animals with skull fractures at 12 h and 24 h after injury, while gene expression was unchanged in animals without fracture. We did not observe a difference in the TIMP-1 plasma concentration between animals with or without fractures, however.

Many studies have demonstrated a significantly increased neuroinflammatory response in brain tissue, reaching levels greater than physiological levels within hours of injury[19,45–48]; however, only one study did not observe skull fractures.[48] For example, significantly increased brain levels of TNF-α gene and protein expression were observed on the first day after trauma,[19,47,49] while no changes in TNF-α expression were observed in other studies.[17,18,50] Interestingly, a significant increase in TNF-α expression at 4 h and 48 h after WD injury was observed using only animals with skull fractures in a WD model.[49]

Moreover, there is a significant increase in IL-1, IL-6, IL-10, and TNF-α cytokines in response to craniotomy *per se* compared with those in naïve animals,[51,52] indicating that skull fractures could cause inflammation and create outcome heterogeneity within the groups in the WD model. Recent studies found that combined closed-skull TBI and tibial fractures worsened outcome and increased inflammation compared with mice given only a TBI.[53,54] Similar to our findings, the levels of inflammatory cytokines, such as IL-1β, IL-6, and TNF-α, were not increased in isolated-TBI.[53] Interestingly, in a recent study, muscle injury combined with TBI did not significantly impact inflammatory cytokine expression or functional outcome after WD-TBI,[55] suggesting that a concurrent fracture rather than soft tissue injury may exacerbate neuroinflammation and worsen the outcomes after TBI.

Previous research demonstrated that the overexpression of TNF-α was correlated with the severity of trauma in fluid-percussion–induced TBI.[45] We observed a correlation between the levels of TNF-α and TIMP-1 gene expression and the severity of fracture. Moreover, TIMP-1 gene expression was elevated significantly in the ipsilateral hippocampus and striatum during the first 3 days after trauma with skull fracture, showing an increase of more than 100-fold.

Previous research identified an association between serum TIMP-1 levels and TBI severity and death.[56] A previous study demonstrated that the TIMP-1 gene is overexpressed in the brain at 12 h after middle cerebral artery occlusion, reaching a peak level at 2 days after stroke.[57,58] High serum TIMP-1 levels are also associated with a worse prognosis after stroke.[56,59] The TIMP-1 is constitutively expressed at a low level in many tissues, but after tissue injury and inflammation, TIMP-1 gene expression generally increases compared with that in healthy tissue.[60,61]

Pro-inflammatory cytokines increase the expression of TIMP-1 in the brain.[62] In the present study, high TIMP-1 inflammatory gene expression was observed in the first 3 days after TBI with skull fracture compared with the gene expression levels at 14 days after TBI, showing an acute response to injury. Because severe skull fracture was observed together with skull depression and bleeding, the high TIMP-1 gene expression in the brain was probably a rapid and acute response to the massive infiltration of proinflammatory cytokines that occurred in the brain after dural injury and bleeding.

Conclusion

Compared with TBI without fractures, TBI with skull fractures resulted in a more severe neurobehavioral response and a considerable increase in inflammatory gene expression in brain tissue. Our data suggest that when using the WD model, the data from animals with skull fractures must be analyzed separately from those without

skull fractures to reduce the heterogeneity of the model. Heterogeneity may also be reduced *a priori* by using animals with a thicker skull bone—i.e., older mice—and by using an impact cone with a larger diameter—i.e., 5 mm instead of 2 mm—or helmets—i.e., metallic disc—on the skull surface.

Acknowledgments

This study was supported by the framework of the EU-ERA-NET NEURON project CnsAflame.

Author Disclosure Statement

No competing financial interests exist.

Supplementary Material

Supplementary Table S1

References

1. De Guzman, E. and Ament, A. (2017). Neurobehavioral management of traumatic brain injury in the critical care setting: an update. Crit. Care Clin. 33, 423–440.
2. Berkner, J., Mannix, R., and Qiu, J. (2016). Clinical traumatic brain injury in the preclinical setting. Methods Mol. Biol. 1462, 11–28.
3. Kerr, H.A. (2013). Closed head injury. Clin. Sports Med. 32, 273–287.
4. Namjoshi, D.R., Good, C., Cheng, W.H., Panenka, W., Richards, D., Cripton, P.A., and Wellington, C.L. (2013). Towards clinical management of traumatic brain injury: a review of models and mechanisms from a biomechanical perspective. Dis. Model. Mech. 6, 1325–1338.
5. Albert-Weißenberger, C., Várrallyay, C., Raslan, F., Kleinschnitz, C., and Sirén, A.-L. (2012). An experimental protocol for mimicking pathomechanisms of traumatic brain injury in mice. Exp. Transl. Stroke Med. 4, 1.
6. Flierl, M.A., Stahel, P.F., Beauchamp, K.M., Morgan, S.J., Smith, W.R., and Shohami, E. (2009). Mouse closed head injury model induced by a weight-drop device. Nat. Protoc. 4, 1328–1337.
7. Marmarou, A., Foda, M.A.A.-E., Brink, W. van den, Campbell, J., Kita, H., and Demetriadou, K. (1994). A new model of diffuse brain injury in rats. Part 1: pathophysiolpgy and biomechanics. J. Neurosurg. 80, 291–300.
8. Namjoshi, D.R., Cheng, W., McInnes, K.A., Martens, K.M., Carr, M., Wilkinson, A., Fan, J., Robert, J., Hayat, A., Cripton, P.A., and Wellington, C.L. (2014). Merging pathology with biomechanics using CHIMERA (Closed-Head Impact Model of Engineered Rotational Acceleration): a novel, surgery-free model of traumatic brain injury. Mol. Neurodegener. 9, 55.
9. Meconi, A., Wortman, R.C., Wright, D.K., Neale, K.J., Clarkson, M., Shultz, S.R., and Christie, B.R. (2018). Repeated mild traumatic brain injury can cause acute neurologic impairment without overt structural damage in juvenile rats. PLoS One 13, e0197187.
10. Ren, Z., Iliff, J.J., Yang, L., Yang, J., Chen, X., Chen, M.J., Giese, R.N., Wang, B., Shi, X., and Nedergaard, M. (2013). 'Hit & Run' model of closed-skull traumatic brain injury (TBI) reveals complex patterns of post-traumatic AQP4 dysregulation. J. Cereb. Blood Flow Metab. 33, 834–845.
11. Cernak, I., Merkle, A.C., Koliatsos, V.E., Bilik, J.M., Luong, Q.T., Mahota, T.M., Xu, L., Slack, N., Windle, D., and Ahmed, F.A. (2011). The pathobiology of blast injuries and blast-induced neurotrauma as identified using a new experimental model of injury in mice. Neurobiol. Dis. 41, 538–551.
12. Xiong, Y., Mahmood, A., and Chopp, M. (2013). Animal models of traumatic brain injury. Nat. Rev. Neurosci. 14, 128–142.
13. Kane, M.J., Angoa-Pérez, M., Briggs, D.I., Viano, D.C., Kreipke, C.W., and Kuhn, D.M. (2012). A mouse model of human repetitive mild traumatic brain injury. J. Neurosci. Methods 203, 41–49.
14. Wu, Q., Xuan, W., Ando, T., Xu, T., Huang, L., Huang, Y.-Y., Dai, T., Dhital, S., Sharma, S.K., Whalen, M.J., and Hamblin, M.R. (2012). Low-level laser therapy for closed-head traumatic brain injury in mice: effect of different wavelengths. Lasers Surg. Med. 44, 218–226.
15. Schwarzbold, M.L., Rial, D., De Bem, T., Machado, D.G., Cunha, M.P., dos Santos, A.A., dos Santos, D.B., Figueiredo, C.P., Farina, M., Goldfeder, E.M., Rodrigues, A.L.S., Prediger, R.D.S., and Walz, R. (2010). Effects of traumatic brain injury of different severities on emotional, cognitive, and oxidative stress-related parameters in mice. J. Neurotrauma 27, 1883–1893.
16. Midura, E.F., Jernigan, P.L., Kuethe, J.W., Friend, L.A., Veile, R., Makley, A.T., Caldwell, C.C., and Goodman, M.D. (2015). Microparticles impact coagulation after traumatic brain injury. J. Surg. Res. 197, 25–31.
17. Chhor, V., Moretti, R., Le Charpentier, T., Sigaut, S., Lebon, S., Schwendimann, L., Oré, M.V., Zuiani, C., Milan, V., Josserand, J., Vontell, R., Pansiot, J., Degos, V., Ikonomidou, C., Titomanlio, L., Hagberg, H., Gressens, P., and Fleiss, B. (2017). Role of microglia in a mouse model of paediatric traumatic brain injury. Brain. Behav. Immun. 63, 197–209.
18. Albert-Weissenberger, C., Stetter, C., Meuth, S.G., Göbel, K., Bader, M., Sirén, A.L., and Kleinschnitz, C. (2012). Blocking of bradykinin receptor B1 protects from focal closed head injury in mice by reducing axonal damage and astroglia activation. J. Cereb. Blood Flow Metab. 32, 1747–1756.
19. Baratz, R., Tweedie, D., Wang, J.-Y., Rubovitch, V., Luo, W., Hoffer, B.J., Greig, N.H., and Pick, C.G. (2015). Transiently lowering tumor necrosis factor-α synthesis ameliorates neuronal cell loss and cognitive impairments induced by minimal traumatic brain injury in mice. J. Neuroinflammation 12, 45.
20. Gyoneva, S., and Ransohoff, R.M. (2015). Inflammatory reaction after traumatic brain injury: therapeutic potential of targeting cell–cell communication by chemokines. Trends Pharmacol. Sci. 36, 471–480.
21. Zhang, Q., Zhou, C., Hamblin, M.R., and Wu, M.X. (2014). Low-level laser therapy effectively prevents secondary brain injury induced by immediate early responsive gene X-1 deficiency. J. Cereb. Blood Flow Metab. 34, 1391–1401.
22. Clausen, F., Marklund, N., and Hillered, L. (2019). Acute inflammatory biomarker responses to diffuse traumatic brain injury in the rat monitored by a novel microdialysis technique. J. Neurotrauma 36, 201–211.
23. Rowe, R.K., Ellis, G.I., Harrison, J.L., Bachstetter, A.D., Corder, G.F., Van Eldik, L.J., Taylor, B.K., Marti, F., and Lifshitz, J. (2016). Diffuse traumatic brain injury induces prolonged immune dysregulation and potentiates hyperalgesia following a peripheral immune challenge. Mol. Pain 12, 174480691664705.
24. Garg, C., Seo, J.H., Ramachandran, J., Loh, J.M., Calderon, F., and Contreras, J.E. (2018). Trovafloxacin attenuates neuroinflammation and improves outcome after traumatic brain injury in mice. J. Neuroinflammation 15, 42.
25. Kilkenny, C., Browne, W., Cuthill, I.C., Emerson, M., Altman, D.G., and NC3Rs Reporting Guidelines Working Group. (2010). Animal research: reporting in vivo experiments: the ARRIVE guidelines. Br. J. Pharmacol. 160, 1577–1579.
26. McGrath, J., Drummond, G., McLachlan, E., Kilkenny, C., and Wainwright, C. (2010). Guidelines for reporting experiments involving animals: the ARRIVE guidelines. Br. J. Pharmacol. 160, 1573–1576.
27. Powell, E.C., Atabaki, S.M., Wootton-Gorges, S., Wisner, D., Mahajan, P., Glass, T., Miskin, M., Stanley, R.M., Jacobs, E., Dayan, P.S., Holmes, J.F., and Kuppermann, N. (2015). Isolated linear skull fractures in children with blunt head trauma. Pediatrics 135, e851–e857.
28. McGrath, A. and Taylor, R.S. (2019). *Pediatric Skull Fractures.* StatPearls Publishing.
29. Dambrova, M., Zvejniece, L., Skapare, E., Vilskersts, R., Svalbe, B., Baumane, L., Muceniece, R., and Liepinsh, E. (2010). The anti-inflammatory and antinociceptive effects of NF-κB inhibitory guanidine derivative ME10092. Int. Immunopharmacol. 10, 455–460.
30. Otsu, N. (1979). A Tlreshold Selection Method from Gray-Level Histograms. IEEE Transactions on Systems, Man, and Cybernetics, 9, 62–66.
31. Hasan, I., Dominiak, M., Blaszczyszyn, A., Bourauel, C., Gedrange, T., and Heinemann, F. (2015). Radiographic evaluation of bone density around immediately loaded implants. Ann. Anat 199, 52–57.
32. Monje, A., Monje, F., González-García, R., Galindo-Moreno, P., Rodriguez-Salvanes, F., and Wang, H.L. (2014). Comparison between microcomputed tomography and cone-beam computed tomography radiologic bone to assess atrophic posterior maxilla density and microarchitecture. Clin. Oral Implants Res. 25, 723–728.
33. Parsa, A., Ibrahim, N., Hassan, B., van der Stelt, P., and Wismeijer, D. (2015). Bone quality evaluation at dental implant site using multislice CT, micro-CT, and cone beam CT. Clin. Oral Implants Res. 26, e1–e7.

34. Chan, K.H., Mann, K.S., Yue, C.P., Fan, Y.W., and Cheung, M. (1990). The significance of skull fracture in acute traumatic intracranial hematomas in adolescents: a prospective study. J. Neurosurg. 72, 189–194.
35. Servadei, F., Ciucci, G., Morichetti, A., Pagano, F., Burzi, M., Staffa, G., Piazza, G., and Taggi, F. (1988). Skull fracture as a factor of increased risk in minor head injuries: indication for a broader use of cerebral computed tomography scanning. Surg. Neurol. 30, 364–369.
36. Lok, J., Leung, W., Murphy, S., Butler, W., Noviski, N., and Lo, E.H. (2011). Intracranial hemorrhage: mechanisms of secondary brain injury, in: *Acta Neurochirurgica. Supplement*. pps. 63–69.
37. Salia, S.M., Mersha, H.B., Aklilu, A.T., Baleh, A.S., and Lund-Johansen, M. (2018). Predicting dural tear in compound depressed skull fractures: a prospective multicenter correlational study. World Neurosurg. 114, e833–e839.
38. Braakman, R. (1972). Depressed skull fracture: data, treatment, and follow-up in 225 consecutive cases. J. Neurol. Neurosurg. Psychiatry 35, 395–402.
39. Agrawal, A., Timothy, J., Pandit, L., and Manju, M. (2006). Post-traumatic epilepsy: an overview. Clin. Neurol. Neurosurg. 108, 433–439.
40. McColl, T.J., Brady, R.D., Shultz, S.R., Lovick, L., Webster, K.M., Sun, M., McDonald, S.J., O'Brien, T.J., and Semple, B.D. (2018). Mild traumatic brain injury in adolescent mice alters skull bone properties to influence a subsequent brain impact at adulthood: a pilot study. Front. Neurol. 9, 372.
41. Lillie, E.M., Urban, J.E., Lynch, S.K., Weaver, A.A., and Stitzel, J.D. (2016). Evaluation of skull cortical thickness changes with age and sex from computed tomography scans. J. Bone Miner. Res. 31, 299–307.
42. Hamel, A., Llari, M., Piercecchi-Marti, M.-D., Adalian, P., Leonetti, G., and Thollon, L. (2013). Effects of fall conditions and biological variability on the mechanism of skull fractures caused by falls. Int. J. Legal Med. 127, 111–118.
43. Broglio, S.P., Lapointe, A., O'Connor, K.L., and McCrea, M. (2017). Head impact density: a model to explain the elusive concussion threshold. J. Neurotrauma 34, 2675–2683.
44. Laskowitz, D.T., McKenna, S.E., Song, P., Wang, H., Durham, L., Yeung, N., Christensen, D., and Vitek, M.P. (2007). COG1410, a novel apolipoprotein E–based peptide, improves functional recovery in a murine model of traumatic brain injury. J. Neurotrauma 24, 1093–1107.
45. Knoblach, S.M., Fan, L., and Faden, A.I. (1999). Early neuronal expression of tumor necrosis factor-α after experimental brain injury contributes to neurological impairment. J. Neuroimmunol. 95, 115–125.
46. Woodcock, T., and Morganti-Kossmann, M.C. (2013). The role of markers of inflammation in traumatic brain injury. Front. Neurol. 4, 18.
47. Shohami, E., Novikov, M., Bass, R., Yamin, A., and Gallily, R. (1994). Closed head injury triggers early production of TNFα and IL-6 by brain tissue. J. Cereb. Blood Flow Metab. 14, 615–619.
48. Homsi, S., Federico, F., Croci, N., Palmier, B., Plotkine, M., Marchand-Leroux, C., and Jafarian-Tehrani, M. (2009). Minocycline effects on cerebral edema: relations with inflammatory and oxidative stress markers following traumatic brain injury in mice. Brain Res. 1291, 122–132.
49. Ziebell, J.M., Bye, N., Semple, B.D., Kossmann, T., and Morganti-Kossmann, M.C. (2011). Attenuated neurological deficit, cell death and lesion volume in Fas-mutant mice is associated with altered neuroinflammation following traumatic brain injury. Brain Res. 1414, 94–105.
50. Semple, B.D., Bye, N., Ziebell, J.M., and Morganti-Kossmann, M.C. (2010). Deficiency of the chemokine receptor CXCR2 attenuates neutrophil infiltration and cortical damage following closed head injury. Neurobiol. Dis. 40, 394–403.
51. Lagraoui, M., Latoche, J.R., Cartwright, N.G., Sukumar, G., Dalgard, C.L., and Schaefer, B.C. (2012). Controlled cortical impact and craniotomy induce strikingly similar profiles of inflammatory gene expression, but with distinct kinetics. Front. Neurol. 3, 155.
52. Cole, J.T., Yarnell, A., Kean, W.S., Gold, E., Lewis, B., Ren, M., McMullen, D.C., Jacobowitz, D.M., Pollard, H.B., O'Neill, J.T., Grunberg, N.E., Dalgard, C.L., Frank, J.A., and Watson, W.D. (2011). Craniotomy: true sham for traumatic brain injury, or a sham of a sham? J. Neurotrauma 28, 359–369.
53. Shultz, S.R., Sun, M., Wright, D.K., Brady, R.D., Liu, S., Beynon, S., Schmidt, S.F., Kaye, A.H., Hamilton, J.A., O'Brien, T.J., Grills, B.L., and Mcdonald, S.J. (2015). Tibial fracture exacerbates traumatic brain injury outcomes and neuroinflammation in a novel mouse model of multitrauma. J. Cereb. Blood Flow Metab. 35, 1339–1347.
54. Sun, M., Brady, R.D., Wright, D.K., Kim, H.A., Zhang, S.R., Sobey, C.G., Johnstone MR, O'Brien TJ, Semple BD, McDonald SJ,and Shultz, S.R. (2017). Treatment with an interleukin-1 receptor antagonist mitigates neuroinflammation and brain damage after polytrauma. Brain. Behav. Immun. 66, 359–371.
55. Sun, M., Brady, R.D., van der Poel, C., Apted, D., Semple, B.D., Church, J.E., O'Brien, T.J., McDonald, S.J., and Shultz, S.R. (2018). A concomitant muscle injury does not worsen traumatic brain injury outcomes in mice. Front. Neurol. 9, 1089.
56. Lorente, L., Martín, M.M., Ramos, L., Cáceres, J.J., Solé-Violán, J., Argueso, M., Jiménez, A., Borreguero-León, J.M., Orbe, J., Rodríguez, J.A., and Páramo, J.A. (2015). Serum tissue inhibitor of matrix metalloproteinase-1 levels are associated with mortality in patients with malignant middle cerebral artery infarction. BMC Neurol. 15, 111.
57. Wang, L., Kang, S., Zou, D., Zhan, L., Li, Z., Zhu, W., and Su, H. (2016). Bone fracture pre-ischemic stroke exacerbates ischemic cerebral injury in mice. PLoS One 11, e0153835.
58. Wang, X., Barone, F.C., White, R.F., and Feuerstein, G.Z. (1998). Subtractive cloning identifies tissue inhibitor of matrix metalloproteinase-1 (TIMP-1) increased gene expression following focal stroke. Stroke 29, 516–520.
59. Rodríguez, J.A., Sobrino, T., Orbe, J., Purroy, A., Martínez-Vila, E., Castillo, J., and Páramo, J.A. (2013). proMetalloproteinase-10 is associated with brain damage and clinical outcome in acute ischemic stroke. J. Thromb. Haemost. 11, 1464–1473.
60. Masciantonio, M.G., Lee, C.K.S., Arpino, V., Mehta, S., and Gill, S.E. (2017). The balance between metalloproteinases and TIMPs, in: *Progress in Molecular Biology and Translational Science*. pps. 101–131.
61. White, T.E., Ford, G.D., Surles-Zeigler, M.C., Gates, A.S., LaPlaca, M.C., and Ford, B.D. (2013). Gene expression patterns following unilateral traumatic brain injury reveals a local pro-inflammatory and remote anti-inflammatory response. BMC Genomics 14, 282.
62. Gardner, J. and Ghorpade, A. (2003). Tissue inhibitor of metalloproteinase (TIMP)-1: the TIMPed balance of matrix metalloproteinases in the central nervous system. J. Neurosci. Res. 74, 801–806.

Address correspondence to:
Liga Zvejniece, MD, PhD
Latvian Institute of Organic Synthesis
Aizkraukles 21
LV-1006, Riga
Latvia

E-mail: liga@farm.osi.lv

Hindawi
Oxidative Medicine and Cellular Longevity
Volume 2020, Article ID 9364598, 12 pages
https://doi.org/10.1155/2020/9364598

Research Article

Mitochondrial-Protective Effects of R-Phenibut after Experimental Traumatic Brain Injury

Einars Kupats,[1,2] **Gundega Stelfa**,[1,3] **Baiba Zvejniece**,[1] **Solveiga Grinberga**,[1] **Edijs Vavers**,[1] **Marina Makrecka-Kuka**,[1] **Baiba Svalbe**,[1] **Liga Zvejniece**,[1] **and Maija Dambrova**[1,4]

[1]*Latvian Institute of Organic Synthesis, Riga, Latvia*
[2]*Department of Neurology and Neurosurgery, Riga Stradins University, Riga, Latvia*
[3]*Latvia University of Life Sciences and Technologies, Jelgava, Latvia*
[4]*Department of Pharmaceutical Chemistry, Riga Stradins University, Riga, Latvia*

Correspondence should be addressed to Einars Kupats; einars.kupats@farm.osi.lv

Received 15 July 2020; Revised 24 September 2020; Accepted 3 November 2020; Published 21 November 2020

Academic Editor: Luciano Saso

Altered neuronal Ca^{2+} homeostasis and mitochondrial dysfunction play a central role in the pathogenesis of traumatic brain injury (TBI). R-Phenibut ((3R)-phenyl-4-aminobutyric acid) is an antagonist of the $\alpha_2\delta$ subunit of voltage-dependent calcium channels (VDCC) and an agonist of gamma-aminobutyric acid B (GABA-B) receptors. The aim of this study was to evaluate the potential therapeutic effects of R-phenibut following the lateral fluid percussion injury (latFPI) model of TBI in mice and the impact of R- and S-phenibut on mitochondrial functionality *in vitro*. By determining the bioavailability of R-phenibut in the mouse brain tissue and plasma, we found that R-phenibut (50 mg/kg) reached the brain tissue 15 min after intraperitoneal (i.p.) and peroral (p.o.) injections. The maximal concentration of R-phenibut in the brain tissues was 0.6 μg/g and 0.2 μg/g tissue after i.p. and p.o. administration, respectively. Male Swiss-Webster mice received i.p. injections of R-phenibut at doses of 10 or 50 mg/kg 2 h after TBI and then once daily for 7 days. R-Phenibut treatment at the dose of 50 mg/kg significantly ameliorated functional deficits after TBI on postinjury days 1, 4, and 7. Seven days after TBI, the number of Nissl-stained dark neurons (N-DNs) and interleukin-1beta (IL-1β) expression in the cerebral neocortex in the area of cortical impact were reduced. Moreover, the addition of R- and S-phenibut at a concentration of 0.5 μg/ml inhibited calcium-induced mitochondrial swelling in the brain homogenate and prevented anoxia-reoxygenation-induced increases in mitochondrial H_2O_2 production and the H_2O_2/O ratio. Taken together, these results suggest that R-phenibut could serve as a neuroprotective agent and promising drug candidate for treating TBI.

1. Introduction

Traumatic brain injury (TBI) is a leading cause of mortality and disability among trauma-related injuries [1]. TBI can result in temporary, long-term, and even life-long physical, cognitive, and behavioural problems [2, 3]. Therefore, there is an increased need for effective pharmacological approaches for treating patients with TBI. Phenibut, a nootropic prescription drug with anxiolytic activity, is used in clinical practice in Eastern European countries for the treatment of anxiety, tics, stuttering, insomnia, dizziness, and alcohol abstinence [4, 5]. R-Phenibut ((3R)-phenyl-4-aminobutyric acid), which is one of the optical isomers of phenibut, binds to gamma-aminobutyric acid B (GABA-B) receptors and the $\alpha_2\delta$ subunit of voltage-dependent calcium channels (VDCC), while S-phenibut binds only to the $\alpha_2\delta$ subunit of VDCC [6–8]. Our previous studies have shown that R-phenibut treatment significantly decreased the brain infarct size and increased brain-derived neurotrophic factor and vascular endothelial growth factor gene expression in damaged brain tissue in an experimental stroke model [9]. The similarity of the pathogenic mechanisms of TBI and cerebral ischaemia indicate that therapeutic strategies that are successful in treating one may also be beneficial in treating the other [10].

Treatment options for TBI are limited due to its complex pathogenesis and the heterogeneity of its presentation, which includes haematomas, contusions, hypoxia, and vascular, axonal, and other types of central nervous system injuries [11, 12]. Among the processes that impact TBI, the generation of reactive oxygen species (ROS) by mitochondria occurs within the first minutes after TBI and thus leads to the disruption of calcium ion (Ca^{2+}) homeostasis, which is the "final common pathway" for toxic cellular degradation [13, 14]. Maintaining regional neuronal Ca^{2+} homeostasis and mitochondrial function is crucial to prevent secondary neuronal injury [15, 16]. Thus, mitochondrial-targeted drugs and drugs acting on specific intracellular Ca^{2+} signalling pathways or subcellular components show promise as therapeutic interventions for TBI [17, 18]. In fact, upregulation of the neuronal calcium channel $\alpha_2\delta$ subunit modulates the activation of mitochondrial Ca^{2+} buffering in pathological conditions [19]. There is also evidence that GABA-B receptor agonists provide neuroprotection against N-methyl-D-aspartate-induced neurotoxicity mediated by the mitochondrial permeability transition pore [20]. Since both isomers of phenibut bind to the $\alpha_2\delta$ subunit of VDCC and only R-phenibut binds to the GABA-B receptor, these both isomers could be used to specify the possible molecular mechanisms of phenibut in different experimental models.

This is the first investigation of the potential therapeutic effects of R-phenibut following TBI in mice. In addition, to evaluate possible molecular mechanisms underlying the actions of R-phenibut against anoxia-reoxygenation-induced mitochondrial damage, the effects on mitochondrial functionality were evaluated in an *in vitro* model of anoxia-reoxygenation and compared for R- and S-phenibut.

2. Materials and Methods

2.1. Animals and Treatment. Forty-eight Swiss-Webster male mice (25-40 g; Laboratory Animal Centre, University of Tartu, Tartu, Estonia) were used in a lateral fluid percussion injury (latFPI) model of TBI [21, 22]. Additionally, 6 Swiss-Webster male mice were used for the preparation of brain homogenate and the isolation of brain mitochondria for *in vitro* assays. Forty-two ICR male mice (Laboratory Animal Breeding Facility, Riga Stradins University, Latvia) were used in a pharmacokinetic study. All animals were housed under standard conditions (21-23°C, 12 h light-dark cycle) with unlimited access to standard food (Lactamin AB, Mjölby, Sweden) and water in an individually ventilated cage housing system (Allentown Inc., Allentown, New Jersey, USA). Each cage contained bedding consisting of Eco-Pure ™ Shavings wood chips (Datesand, Cheshire, UK), nesting material, and wooden blocks from TAPVEI (TAPVEI, Paekna, Estonia). For enrichment, a transparent tinted (red) nontoxic durable polycarbonate safe harbour mouse retreat (AnimaLab, Poznan, Poland) was used. The mice were housed with up to 5 mice per standard cage (38 × 19 × 13 cm). All studies involving animals were reported in accordance with the ARRIVE guidelines [23, 24]. The experimental procedures were performed in accordance with the guidelines reported in the EU Directive 2010/63/EU and in accordance with local laws and policies; all procedures were approved by the Latvian Animal Protection Ethical Committee of Food and Veterinary Service in Riga, Latvia.

The dose of R-phenibut was selected based on the previous studies, where pharmacological efficacy was observed in dose-range between 10 and 50 mg/kg, while R-phenibut at doses higher than 100 mg/kg showed sedative and coordination inhibitory effects [6, 8, 9]. Mice were randomly assigned to four experimental groups: sham-operated mice, saline-treated latFPI mice, and latFPI mice that received R-phenibut (JSC Olainfarm, Olaine, Latvia) at a dose of 10 mg/kg or 50 mg/kg. Six mice were excluded because of a dural breach that occurred during surgery (4 mice from the sham-operated, 1 mouse from the control, and 1 mouse from the R-phenibut 50 mg/kg groups), and four mice died immediately after latFPI and were excluded from the study (3 mice from the control and 1 mouse from the R-phenibut 50 mg/kg groups). The final number of included animals per group was as follows: sham-operated mice ($n = 8$), saline-treated latFPI mice (control group, $n = 8$), and latFPI mice that received R-phenibut at a dose of 10 mg/kg ($n = 12$) or 50 mg/kg ($n = 10$). R-Phenibut and saline were initially administered intraperitoneally (i.p.) 2 h after injury and then once daily for an additional 7 days for a total treatment period of 1 week. During the treatment period, the animals were weighed at 0, 1, 2, 4, and 7 days after latFPI between 9:00 and 10:00 am. To avoid the influence of subjective factors on the rating process, all experimental procedures were performed in a blinded fashion.

2.2. Determination of R-Phenibut in the Plasma and Brain Tissue after p.o. and i.p. Administration. The concentrations of R-phenibut in the brain tissue extracts and plasma were measured by ultraperformance liquid chromatography-tandem mass spectrometry (UPLC/MS/MS). To determine the concentration of R-phenibut in the plasma and brain, mice received an i.p. and p.o. R-phenibut at a dose of 50 mg/kg 15 and 30 min and 1, 2, 4, 6, and 24 h ($n = 3$ in each time point) before the plasma and brain tissue collection. The blood and brain samples were prepared as described previously [25]. The chromatographic separation was performed using an ACQUITY UPLC system (Waters, USA) on an ACQUITY UPLC BEH Shield RP18 (1.7 μm, 2.1 × 50 mm) (Waters) with a gradient elution from 5 to 98% acetonitrile in 0.1% formic acid aqueous solution at a flow rate of 0.15 ml/min. The analyte was ionized by electrospray ionization in positive ion mode on a Quattro Micro triple quadrupole mass spectrometer (Waters). The mass spectrometer was set up as follows: capillary voltage of 3.3 kV; source and desolvation temperatures of 120 and 400°C, respectively. Cone voltage was 20 V, and collision energy was 18 eV. R-Phenibut analysis was performed in the MRM mode. Precursor to production transition was $m/zm/z$ 180.0→116.1. Data acquisition and processing were performed using the MassLynx V4.1 and QuanLynxV4.1 software (Waters).

2.3. Lateral Fluid Percussion Injury-Induced Brain Trauma. To induce TBI, the latFPI model was generated as previously described [21, 22] with slight modifications. Mice were

anaesthetized with 4% isoflurane contained in a mixture of oxygen and nitrous oxide (70 : 30, AGA, Riga, Latvia), and anaesthesia with 2% isoflurane (Chemical Point, Deisenhofen, Germany) was maintained during the surgical procedures using a face mask. The depth of anaesthesia was monitored by a toe pinch using tweezers. Before trauma induction, mice received subcutaneous (s.c.) administration of tramadol (KRKA, Novo Mesto, Slovenia) (10 mg/kg). Eye cream was applied to prevent the eyes from drying out. A midline longitudinal scalp incision was made, and the skull was exposed. A craniectomy that was centred at 2 mm posterior to bregma and 2 mm right of midline was performed using a 3 mm outer-diameter trephine. Any animal noted to have a dural breach was euthanized and excluded from the study. A plastic cap was attached over the craniotomy using dental cement (Fulldent, Switzerland), and a moderate severity (1.5 ± 0.2 atm) brain injury was induced with a commercially available fluid percussion device (AmScien Instruments, Richmond, USA). Immediately after the injury, apnoea was noted, and when spontaneous breathing returned, anaesthesia was resumed. The cement and cap were removed, and the skin was sutured using resorbable sutures (6-0, silk). The animal was placed in a separate cage to allow full recovery from anaesthesia. Sham-injured animals were subjected to an identical procedure as the latFPI animals except for the induction of trauma.

2.4. Neurological Severity Score (NSS). The neurobehavioural status of mice was obtained by the NSS using the method described previously [26]. The animals were trained on the NSS beams and equipment prior to the baseline measurements. The general neurological state of mice was evaluated at baseline (day before latfTBI) and 1, 4, and 7 days postinjury before the next dose of R-phenibut or saline administration. The NSS consisted of 9 individual clinical parameters, including motor function, alertness, and physiological behaviour tasks. The mice were assessed for the following items: presence of paresis; impairment of seeking behaviour; absence of perceptible startle reflex; inability to get down from a rectangle platform (34×27 cm); inability to walk on 3, 2, and 1 cm wide beams; and inability to balance on a vertical beam of 7 mm width and horizontal round stick of 5 mm diameter for 10 sec. If a mouse showed impairment on one of these items, a value of 1 was added to its NSS score. Thus, higher scores on the NSS indicate greater neurological impairment.

2.5. Tissue Preparation for Histological Analysis. The animals used for histological analysis were randomly selected from each group. Seven days after TBI, the mice were anaesthetized using i.p. administration of ketamine (200 mg/kg) and xylazine (15 mg/kg). The depth of anaesthesia was monitored by a toe pinch using tweezers. Animals were transcardially perfused at a rate of 3 ml/minutes with 0.01 M phosphate-buffered saline (PBS, pH = 7.4) for 5 minutes until the blood was completely removed from the tissue. Perfusion was then performed with 4% paraformaldehyde (PFA) fixative solution for 5-7 minutes until stiffening of the mouse body occurred. After perfusion, the brains were carefully dissected and postfixed in 4% PFA overnight at 4°C. The brains were cryoprotected with a 10-20-30% sucrose-PBS gradient for 72 hours. Coronal sections of the brain (20 μm) were made using a Leica CM1850 cryostat (Leica Biosystems, Buffalo Grove, IL, United States) and mounted on Superfrost Plus microscope slides (Thermo Scientific, Waltham, MA, United States).

2.6. Cresyl Violet (Nissl) Staining and Interleukin-1beta (IL-1β) Immunofluorescence Staining. Nissl and IL-1β staining techniques were used to evaluate neuronal cell damage. Nissl-stained dark neurons (N-DNs) indicated the typical morphological change in injured neurons following TBI [27, 28]. The number of N-DNs and cells expressing IL-1β in the cerebral neocortex in the cortical impact area were determined at day 7 after latFPI. For Nissl staining, coronal frozen sections (20 μm) of the mouse brain were used. The sections were incubated in graded ethanol solutions (96% ethanol for 3 minutes and 70% ethanol for 3 minutes). After washing with distilled water for 3 minutes, the sections were stained with 0.01% cresyl violet acetate (ACROS organics) solution for 14 minutes. The sections were then washed with distilled water for 3 minutes and dehydrated in ethanol. The stained sections were coverslipped using DPX mounting medium (Sigma-Aldrich, St. Louis, MO, United States).

For IL-1β staining, the sections were washed once with PBS containing 0.2% Tween 20 for 5 minutes (on a rotary shaker at 250 rpm). The antigen retrieval procedure was performed with 0.05 M Na citrate (pH = 6.0) containing 0.05% Tween 20 for 30 minutes at 85°C. The sections were then washed with PBS (0.2% Tween 20) 3 times for 5 minutes each. Protein blocking was performed using 5% BSA solution, and the sections were incubated for 1 hour at room temperature. The sections were washed with PBS (0.2% Tween 20) 3 times for 5 minutes each. The slices were incubated with primary antibody against anti-IL-1β (1 : 1000; Abcam, Cat# ab9722) for 16 h at +4°C. The antibody was diluted in PBS containing 3% BSA and 0.3% Triton™ X-100. After incubation with the primary antibody, the sections were washed with PBS (0.2% Tween 20) 4 times for 5 minutes each. The sections were subsequently incubated for 1 h at room temperature with goat anti-rabbit IgG H&L (Alexa Fluor® 488, 1 : 200; Abcam, Cat# ab150077) diluted in PBS containing 5% BSA. The sections were washed with PBS (0.2% Tween 20) 4 times for 5 minutes each. The stained sections were mounted using Fluoromount™ aqueous mounting medium (Sigma-Aldrich, St. Louis, MO, United States, Cat# F4680) and finally coverslipped. Images were obtained with a Nikon Eclipse TE300 microscope (Nikon Instruments, Tokyo, Japan).

N-DNs were defined as hyperbasophilic neurons with a shrunken morphology. The number of N-DNs per field of vision was calculated in three randomly selected sections at the epicentre of the injury. The number of N-DNs and cells expressing IL-1β per field of vision were calculated using ImageJ software at 10-fold magnification for N-DNs and at 4-fold magnification for IL-1β. For analysis of expression of IL-1β, eight-bit images were generated from the pictures and were cropped to contain the regions of interest. Images

for IL-1β staining were thresholded to select a specific signal over the background, and the stained area for each region was calculated and used for statistical analysis. Three individual measurements were performed for each sample. The schematic illustration of the brain region was created using BioRender software (https://biorender.com).

2.7. Mitochondrial Respiration and H_2O_2 Production Measurements. To evaluate mitochondrial functionality, mouse brain homogenate or isolated brain mitochondria were prepared. Briefly, brain tissues were homogenized 1 : 20 (w/v) in a medium containing 320 mM sucrose, 10 mM Tris, and 1 mM EDTA (pH 7.4). The homogenate was centrifuged at 1000 g for 10 min, and the supernatant was centrifuged at 6200 g for 10 min. The mitochondrial pellet obtained was washed once and resuspended in the isolation medium. Mitochondrial respiration and H_2O_2 production measurements were performed at 37°C using Oxygraph-2k (O2k; Oroboros Instruments, Austria) with O2k-Fluo-Modules in MiR05Cr (110 mM sucrose, 60 1mM K-lactobionate, 0.5 mM EGTA, 3 mM $MgCl_2$, 20 mM taurine, 10 mM KH_2PO_4, 20 mM HEPES, pH 7.1, 0.1% BSA essentially fatty acid free, and creatine 20 mM). H_2O_2 flux (ROS flux) was measured simultaneously with respirometry in the O2k-fluorometer using the H_2O_2-sensitive probe Ampliflu™ Red (AmR) [29, 30]. 10 μM AmR, 1 U/ml horse radish peroxidase (HRP), and 5 U/ml superoxide dismutase (SOD) were added to the chamber. H_2O_2 detection is based on the conversion of AmR into the fluorescent resorufin. Calibrations were performed with H_2O_2 added at 0.1 μM step. H_2O_2 flux was corrected for background (AmR slope before addition of sample). H_2O_2/O flux ratio (%) was calculated as H_2O_2 flux/(0.5 O_2 flux).

2.8. In Vitro Anoxia-Reoxygenation Model. Mitochondrial functionality after anoxia-reoxygenation was determined in mouse brain tissue homogenate prepared as described previously [31]. To induce anoxia maximal respiration rate, the sample was stimulated by the addition of substrates, pyruvate + malate (5 + 2 mM), succinate (10 mM), and ADP (5 mM), and preparation was left to consume all O_2 in the respiratory chamber (within 10-20 min), thereby entering into an anoxic state [32]. 15 minutes after anoxia, the vehicle or R-phenibut (0.5 μg/ml) was added to the chamber and O_2 was reintroduced to the chamber by opening the chamber to achieve reoxygenation. After 8 minutes of reoxygenation, the chamber was closed and O_2 flux was monitored for additional 2 minutes. At the end of the experiment, antimycin A (2.5 μM) was added to determine residual oxygen consumption (ROX).

2.9. Substrate-Uncoupler-Inhibitor Titration (SUIT) Protocol. To determine the effect of R-phenibut on mitochondrial electron transfer system functionality, mitochondria were isolated from mouse brain as described previously, and mitochondrial respiration and H_2O_2 production measurements were performed in the presence or absence of R-phenibut at 0.5 μg/ml concentration [30]. In addition, effects of S-phenibut (0.5 μg/ml) were tested to determine whether the effects of R-phenibut in mitochondria involve the GABA-B receptor or the $\alpha_2\delta$ subunit of VDCC. Pyruvate and malate (5 mM and 2 mM, respectively) were used to determine N-pathway complex I (CI) linked LEAK (L) respiration. ADP was added at 5 mM concentration to determine oxidative phosphorylation-dependent respiration (OXPHOS state, P). Then, glutamate (10 mM) was added as an additional substrate for N-pathway. Succinate (10 mM, complex II (CII) substrate) was added to reconstitute convergent NS-pathway CI&II-linked respiration. Titrations with the uncoupler CCCP (0.5–1 μM steps) were performed to determine the electron transfer system (ETS) capacity. Rotenone (0.5 μM, inhibitor of complex I) was added to determine the CII-linked OXPHOS capacity. Then, antimycin A (2.5 μM, inhibitor of complex III) was added to evaluate residual (non-mitochondrial) oxygen consumption (ROX). Oxygen fluxes were compared after correction for ROX.

2.10. Ca^{2+}-Induced Mitochondrial Swelling Measurement. Swelling of isolated brain mitochondria was assessed by measuring changes in absorbance at 540 nm as described previously with slight modifications [33–35]. Mitochondria (0.125 mg/ml) were preincubated with R- or S- phenibut at a concentration of 0.5 μg/ml for 15 min in a buffer containing 120 mM KCl, 10 mM Tris, 5 mM KH_2PO_4 pH 7.4, and pyruvate (5 mM), malate (2 mM), and ADP (5 mM) as substrates. R- and S-enantiomers of phenibut were used to determine whether the effects of R-phenibut on Ca^{2+}-induced mitochondrial swelling involve the GABA-B receptor or the $\alpha_2\delta$ subunit of VDCC. Swelling was induced by the addition of 200 μM $CaCl_2$, and changes in absorbance were monitored for 10 min. All experiments were performed at 37°C.

2.11. Statistical Analysis. All results are expressed as the mean ± S.E.M or S.D. (for mitochondrial studies). Health outcomes, animal behaviour, and Ca^{2+}-induced mitochondrial swelling were analysed using two-way repeated-measures analysis of variance (ANOVA). Dunnett's post hoc test was performed when appropriate. The histological data and mitochondrial functionality were evaluated by one-way ANOVA. Whenever the analysis of variance indicated a significant difference, further multiple comparisons were made using Tukey's multiple comparison test as the post hoc test. p values less than 0.05 were considered to be significant. The statistical calculations were performed using the GraphPad Prism software package (GraphPad Software, Inc., La Jolla, California, USA).

The sample size calculations for latFPI-induced brain trauma were based on the effects of R-phenibut in our previous experiments. For example, it was calculated that R-phenibut demonstrates a medium effect in the ET-1-induced middle cerebral artery occlusion model [9] and a large effect in the formalin-induced paw-licking test [6]. Through a power calculation (using G-power software) for a two-way ANOVA test (repeated measures), four-group comparison, four measurements per group (0, 1, 4, and 7 days after TBI) with $\alpha = 0.05$, a power of 80%, and a standardized effect size Cohen's $f = 0.5$, a total sample size of 8 mice per group was deemed sufficient. Since TBI-induced

brain trauma can result in death of some animals, our sample size of $n = 12$ would allow identifying smaller differences, with the same statistical power, for the same significance level.

3. Results

3.1. R-Phenibut Crosses the Blood-Brain Barrier. As shown in Figure 1(a), R-phenibut in plasma could be detected 15 min after a single i.p. and p.o. injection. The maximal concentrations of R-phenibut in the plasma were observed 15 min after the i.p. injection and 30 min after the p.o. administration (Figure 1(a)). The maximal concentration of R-phenibut in the plasma after the i.p. injection was 16.8 μg/ml; at the same time, the maximal concentration of R-phenibut in the plasma after the p.o. injection was 24 μg/ml (see Figure 1(a)). R-Phenibut in the plasma was not detected 24 h after both the i.p. and p.o. injections. R-Phenibut in the brain tissue extracts was detected already 15 min after a single i.p. and p.o. injection (Figure 1(b)). The maximal concentrations of R-phenibut in the brain tissues were 0.64 μg/g and 0.17 μg/g tissue after the i.p. and p.o. injections, respectively (Figure 1(a)). The maximal concentrations of R-phenibut in the brain tissues were observed 15 min after i.p. injection and 60 till 240 min after p.o. administration. 24 h after both the i.p. and p.o. injections, R-phenibut in the brain tissues was 0.02 μg/g and 0.012 μg/g, respectively.

3.2. Health Outcome Monitoring after latFPI. The body weight of the sham group animals was not decreased at 1, 2, 4, and 7 days after TBI. A two-way repeated-measures ANOVA showed a significant interaction between time and treatment ($F_{(12,118)} = 4.6$, $p < 0.0001$) and main effects of time ($F_{(1.4,42.7)} = 25.7$, $p < 0.0001$) and treatment ($F_{(3,34)} = 6.7$, $p = 0.0011$). The control group animals lost significantly more weight after TBI than the sham-operated group animals ($p < 0.05$). Treatment with R-phenibut at both doses had no effect on weight loss compared to weight loss in the control group (Figure 2).

3.3. R-Phenibut Treatment Improved Neurological Status after TBI. TBI induced significant functional deficits in control mice compared with sham-operated mice ($p < 0.0001$). The average NSS in the control group was 6.1 ± 0.4, 5.3 ± 0.3, and 5.0 ± 0.6 on postinjury days 1, 4, and 7, respectively. The average NSS score between baseline value and the first day postcraniotomy in the sham-operated group was significantly higher ($p < 0.01$). There was a significant time × treatment interaction observed between groups (two-way repeated-measures ANOVA: ($F_{(9,102)} = 5.7$, $p < 0.0001$) for time × treatment interaction; ($F_{(3,34)} = 22.2$, $p < 0.0001$) for treatment; ($F_{(2.7,92)} = 161.8$, $p < 0.0001$) for time; Figure 3). R-Phenibut treatment at a dose of 50 mg/kg significantly ameliorated functional deficits by 28%, 25%, and 30% after TBI on postinjury days 1, 4, and 7, respectively ($p < 0.05$; Figure 3).

3.4. R-Phenibut Treatment Reduced Early Neuronal Cell Death and Neuroinflammation in the Brain Cortex after TBI. To assess histopathological changes in the ipsilateral brain site, N-DNs and cells expressing IL-1β (Figure 4) were quantified in the sham-operated, control, and R-phenibut treatment groups 7 days after TBI. N-DNs and IL-1β-expressing cells were found in the ipsilateral hemisphere of control group animals (Figures 4(a) and 4(b)). Histological analysis showed that R-phenibut treatment at a dose of 50 mg/kg significantly reduced the number of N-DNs and cells expressing IL-1β in the neocortex after TBI ($p < 0.05$). Significant differences were found in the N-DNs and IL-1β-positive cell numbers in the ipsilateral cortex around the lesion site between the control group (9.1 ± 6.4/per field of vision for N-DNs and 379 ± 82/per field of vision for IL-1β-expressing cells) and the R-phenibut treatment group at a dose of 50 mg/kg (3.0 ± 1.9/per field of vision for N-DNs and 246 ± 31/per field of vision for IL-1β-expressing cells; $p < 0.05$; Figures 4(d) and 4(e)). There was no statistically significant difference between the control group and the R-phenibut treatment group at the dose of 10 mg/kg. No N-DNs were observed in the sham-operated mice.

3.5. R-Phenibut Protects Brain Mitochondria against Anoxia-Reoxygenation Damage. To determine whether R-phenibut-induced neuroprotection could be a result of the preservation of mitochondrial functionality, ROS production and the mitochondrial respiration rate were assessed after anoxia-reoxygenation *in vitro*. To better mimic the conditions observed *in vivo*, R-phenibut at the concentration of 0.5 μg/ml was added to the chamber immediately before reoxygenation. Anoxia-reoxygenation induced 33% and 59% increases in the H_2O_2 production rate and the H_2O_2/O ratio, respectively (Figure 5). R-Phenibut treatment significantly decreased the anoxia-reoxygenation-induced increase in the H_2O_2 production rate and the H_2O_2/O ratio ($p < 0.05$).

3.6. R-Phenibut Reduces ROS Production and Attenuates Ca^{2+}-Induced Mitochondrial Swelling. To determine whether the protective effect of R-phenibut is related to its direct action on mitochondria, measurements of mitochondrial respiration, ROS production, and Ca^{2+}-induced swelling were performed in isolated mouse brain mitochondria in the presence or absence of the compounds. As seen in Figure 6, R-phenibut and S-phenibut at 0.5 μg/ml did not induce any changes in the mitochondrial respiration rate (Figure 6(a)), while H_2O_2 production and the H_2O_2/O ratio (Figures 6(b) and 6(c)) were significantly decreased by 31-53% in the LEAK and OXPHOS states. These results show that R-phenibut and S-phenibut reduce ROS production without affecting the mitochondrial electron transfer system capacities, indicating the improvement of mitochondrial coupling. In addition, both R- and S-phenibut attenuated calcium-induced brain mitochondrial swelling (two-way repeated-measures ANOVA: main effect of treatment ($F_{(40,360)} = 4.576$, $p < 0.0001$), time ($F_{(2.611,46.99)} = 104.5$, $p < 0.0001$), and interaction between treatment and time ($F_{(40,360)} = 4.576$, $p < 0.0001$); Figure 6(d)).

Thus, the phenibut treatment-induced protection of mitochondria against anoxia-reoxygenation could be due to a reduction in ROS production and the modulation of Ca^{2+} signalling.

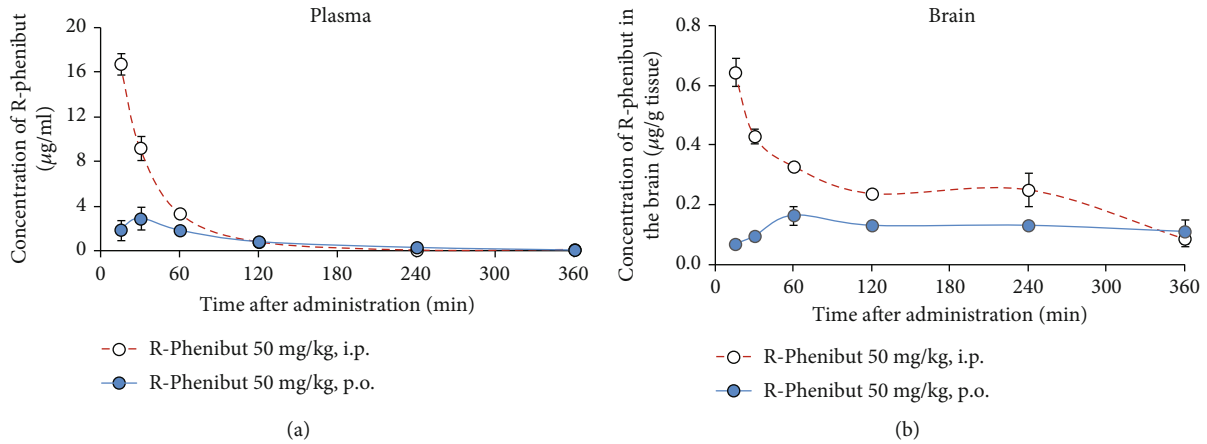

Figure 1: The concentration of R-phenibut in the mouse plasma and brain tissue after a single administration. Mice received an i.p. and p.o. injection of R-phenibut at a dose of 50 mg/kg. The amount of compound in the plasma (a) and brain tissue extracts (b) was measured 15 and 30 min and 1, 2, 4, and 6 h after R-phenibut administration ($n = 3$). Values are represented as the mean ± S.E.M..

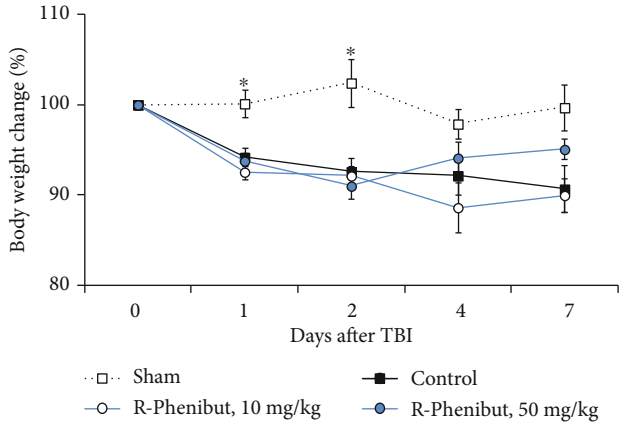

Figure 2: Body weight changes of the sham-operated, control, and R-phenibut treatment groups. Mice were weighed before and 1, 2, 4, and 7 days after latFPI. Data are expressed as the percentage change in body weight relative to the initial body weight of each animal (%). Data are shown as the mean ± S.E.M. ($n = 8 - 12$). *Indicates a significant difference compared to the sham-operated group (two-way repeated-measures ANOVA followed by Dunnett's multiple comparison test; $^{*}P < 0.05$).

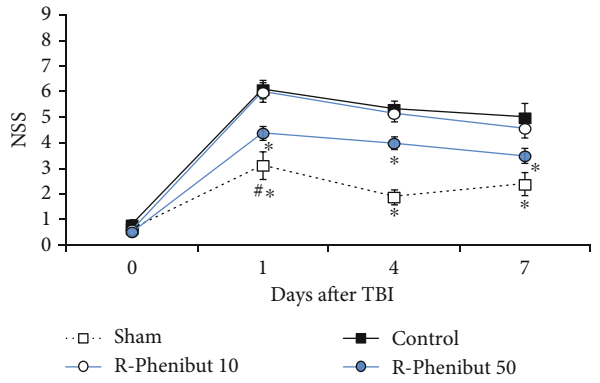

Figure 3: Effects of R-phenibut on the neurological severity score (NSS) after TBI. R-Phenibut and saline were initially administered i.p. 2 h after injury and then once daily for an additional 7 days for a total treatment period of 1 week. Data are shown as the mean ± S.E.M. ($n = 8 - 12$). *Indicates a significant difference compared to the control group; #indicates a significant difference compared to the sham-operated group (two-way repeated-measures ANOVA followed by Dunnett's multiple comparison test; $^{*}P < 0.05$; $^{\#}P < 0.01$).

4. Discussion

In the current study, we examined the effects of R-phenibut treatment on brain trauma induced by latFPI. For the first time, we showed that R-phenibut could be detected in the mouse brain 15 min after a single p.o. or i.p. injection and found in brain extracts even 24 h after the administration. The present study confirms that R-phenibut, which is an antagonist of the $\alpha_2\delta$ subunit of VDCC and an agonist of GABA-B receptors, improves sensorimotor functional outcomes and significantly ameliorates brain damage and neuronal death in the acute phase after TBI via mechanisms related to Ca^{2+} homeostasis and oxidative stress.

The binding characteristics of R-phenibut were previously investigated using radiolabeled gabapentin that was the first ligand shown to bind to the $\alpha_2\delta_1$ and $\alpha_2\delta_2$ subunits with high affinity ($K_d = 59$ and 153 nM, respectively), while at the same time demonstrating no binding activity to the $\alpha_2\delta_3$ and $\alpha_2\delta_4$ subunits [36, 37]. The pathologies associated with gene disruption of $\alpha_2\delta_1$ protein include neuropathic pain and cardiac dysfunction, while in case of $\alpha_2\delta_2$ protein, the pathologies are related to epilepsy and cerebellar ataxia [38]. We showed previously that pharmacological activity of R-phenibut is associated with neuropathic pain rather than epilepsy [6]; thus, we could speculate that the effects of R-phenibut are $\alpha_2\delta_1$ protein binding-related.

The $\alpha_2\delta$ subunits of VDCC are widely expressed by excitatory neurons in the cerebral cortex, hippocampus, and other brain regions [39, 40]. Furthermore, the $\alpha_2\delta$ subunits of VDCC have been shown to be involved in processes that are not directly linked to calcium channel function, such as synaptogenesis [41]. Other studies have reported that the administration of VDCC ligands in rodent models of TBI

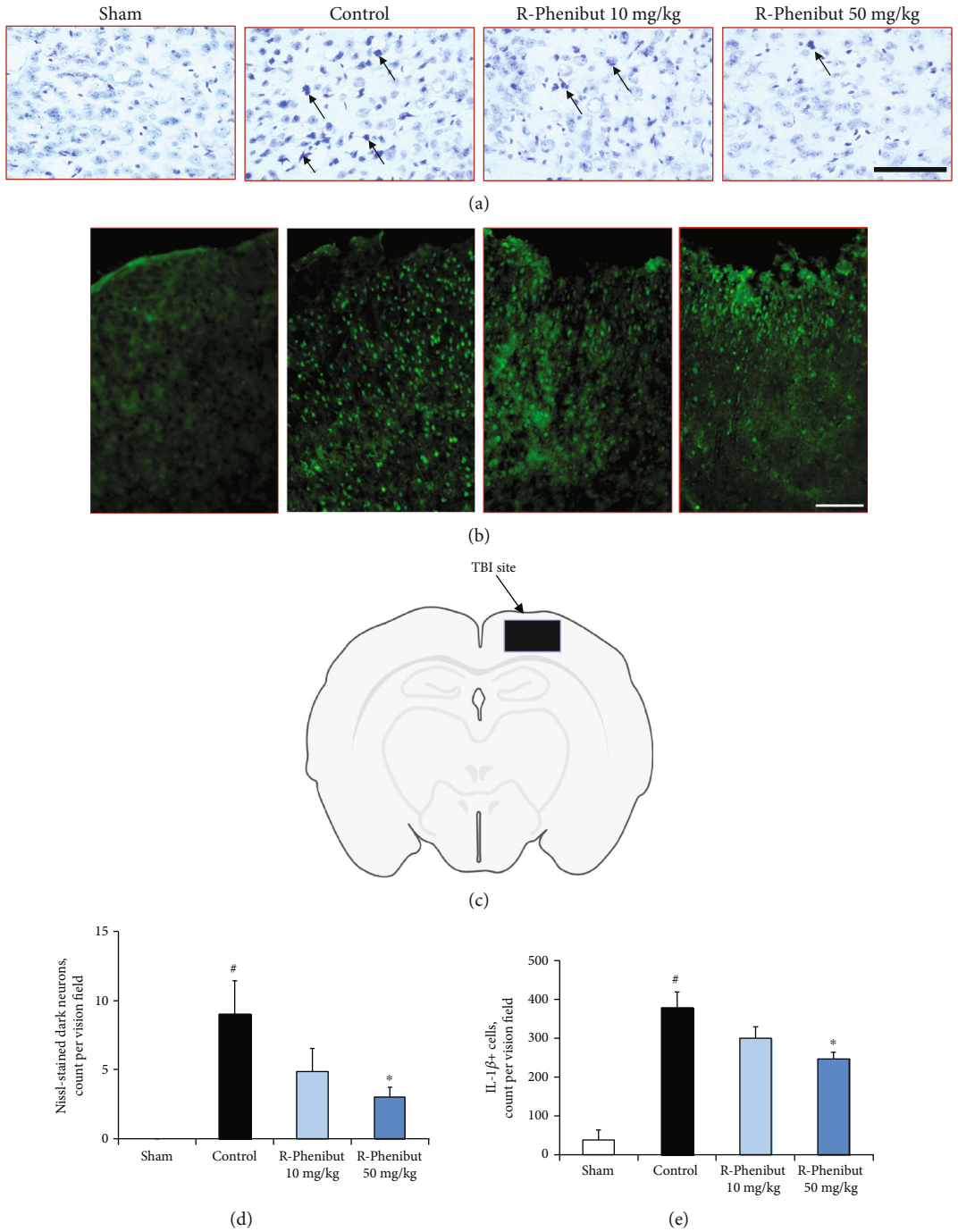

Figure 4: Cresyl violet (Nissl) and IL-1β immunofluorescence staining 7 days post-TBI. (a) Cresyl violet-stained sections of the mouse neocortex ipsilateral to the injury site. R-Phenibut treatment at doses of 10 mg/kg and 50 mg/kg reduced the number of N-DNs. Scale bar = 100 μm. (b) IL-1β expression based on immunofluorescence staining in the mouse neocortex ipsilateral to the injury site. R-Phenibut treatment at doses of 10 mg/kg and 50 mg/kg reduced the number of IL-1β-positive cells. Scale bar = 250 μm. (c) Schematic illustration of the brain region indicated in the filled area, which was selected for the quantitative analysis of cell injury. (d) Quantitative assessment of N-DNs in the ipsilateral cortex at postinjury day 7. Data are expressed as the mean ± S.E.M. ($n = 7$ for the R-phenibut 50 mg/kg group and n = 6 for the sham, control, and R-phenibut 10 mg/kg groups). (e) Quantitative assessment of IL-1β-positive cells in the ipsilateral cortex at postinjury day 7. Data are expressed as the mean ± S.E.M. ($n = 4$ for the control group and $n = 3$ for the sham, R-phenibut 10 mg/kg, and 50 mg/kg groups). $^{\#}$Indicates a significant difference compared to the sham-operated group; *indicates a significant difference compared to the control group (one-way ANOVA followed by Tukey's multiple comparison test; $^{*}P < 0.05$).

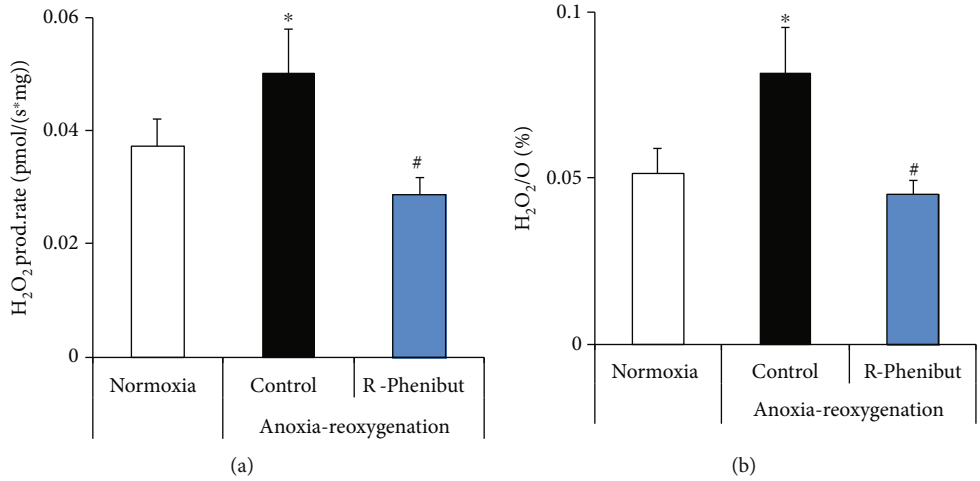

FIGURE 5: The effects of R-phenibut (0.5 μg/ml) on ROS production in an *in vitro* anoxia-reoxygenation model. After anoxia-reoxygenation, the H_2O_2 production rate (a) and H_2O_2/O ratio (b) were significantly decreased in the R-phenibut group. The results are presented as the mean ± S.D. of 6 independent replicates. *Indicates a significant difference compared to normoxia; #indicates a significant difference compared to the anoxia-reoxygenation control group (one-way ANOVA followed by Tukey's multiple comparison test; $^*P < 0.05$).

reduced cell death and improved cognitive function [40]. Similar to phenibut, ligands of the $\alpha_2\delta$ subunit of VDCC, such as pregabalin, at a high dose of 60 mg/kg reduce neuronal loss and improve functional outcomes 24 h after trauma in experimental models of TBI [41, 42]. Moreover, pregabalin at a dose of 30 mg/kg has been shown to improve functional recovery and to demonstrate anti-inflammatory and antiapoptotic effects in a rat model of spinal cord injury [43, 44].

Cytoskeletal protein loss results in altered neuronal morphology after TBI [45, 46]. N-DNs represent a typical pathomorphological change in injured neurons after TBI, showing abnormal basophilia and shrinkage [27, 28]. N-DNs appear in the neocortex immediately after TBI and can be observed even two weeks postinjury [27, 47]. In addition, IL-1 is a major driver of the secondary neuronal injury cascade after TBI [48]. It is involved in the recruitment of other types of immune cells, neuronal apoptosis, and blood-brain barrier disruption after TBI [49–51]. Furthermore, IL-1β antagonism was shown to be neuroprotective in clinical trials and in rodent models of TBI [52–54]. The present study shows that treatment with R-phenibut at a dose of 50 mg/kg significantly reduced the number of N-DNs and significantly reduced IL-1β expression in the neocortex after TBI. The histopathological findings of the current study revealed that R-phenibut could attenuate neuronal damage, inflammation, and degeneration.

For the first time, we showed that R-phenibut limits mitochondrial dysfunction in the brain induced by anoxia-reoxygenation. Compared with other types of cells, neurons are endowed with less robust antioxidant defence systems [55]. As mitochondrial dysfunction has been shown to be involved in TBI, perturbations in energy metabolism are likely to contribute to the pathogenesis of TBI [56, 57]. In TBI, oxidative cell damage is caused by an imbalance between the production and accumulation of ROS, in which mitochondria are the major intracellular source of ROS. Accordingly, there is accumulating evidence that antioxidant agents and membrane lipid peroxidation inhibitors, such as tirilazad, U-78517F and U-83836E, are effective in treating preclinical models of TBI [17]. Mitochondrial-targeted drugs, such as mitoquinone and thymoquinone-containing antioxidants, have been shown to decrease neurological deficits and β-amyloid-induced neurotoxicity after TBI [58, 59]. Meanwhile, the inhibition of ROS production has been shown to inhibit secretion of IL-1β [60].

Notably, the immunosuppressant drug cyclosporine A, which is an IL-1β receptor antagonist, has been shown to decrease pathological changes in the brain after TBI by blocking the mitochondrial permeability transition pore [61]. Our results indicate that R-phenibut treatment improves mitochondrial tolerance and thus protects brain energetics against anoxia-reoxygenation damage by reducing ROS production. R-Phenibut treatment reduces ROS production without affecting the mitochondrial electron transfer system capacities, indicating the improvement of mitochondrial coupling. Another study has demonstrated that phenibut has neuroprotective effects *in vitro* but does not possess antioxidant potential [62]. Perfilova et al. recently showed that phenibut can limit heart and brain mitochondrial damage in rats exposed to stress [63].

To determine the molecular mechanisms underlying the actions of R-phenibut against anoxia-reoxygenation-induced mitochondrial damage, the activity of the R- and S-enantiomers of racemic phenibut was compared. We found that both R-phenibut and S-phenibut reduced mitochondrial ROS production and inhibited Ca^{2+}-induced mitochondrial swelling. This suggests that the protective effects of R-phenibut in mitochondria do not involve the GABA-B receptor (in contrast to R-phenibut, S-phenibut does not bind to the GABA-B receptor) and might be mediated by the $\alpha_2\delta_1$ subunit of VDCC. It was shown previously that increased intracellular Ca^{2+}, as a result of increased activity of $\alpha_2\delta_1$, could be rapidly taken up by mitochondria and subsequently released into the cytoplasm avoiding Ca^{2+} accumulation and maintaining intracellular Ca^{2+} signalling [19]. This could explain why, in the presence of R- and S-phenibut, reduced Ca^{2+}-induced mitochondrial swelling was observed. Both R-phenibut and S-phenibut demonstrate mitochondrial-

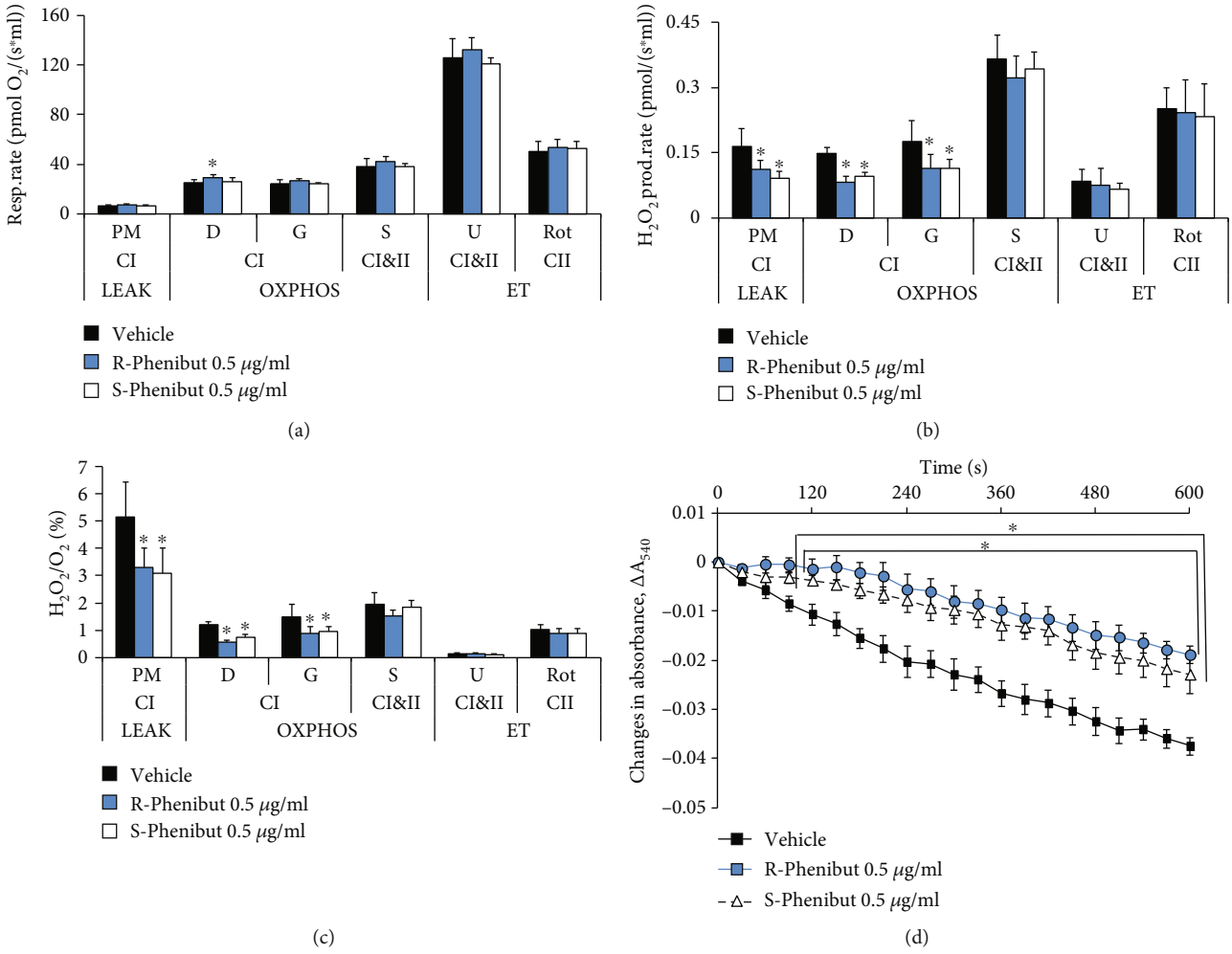

Figure 6: The effects of R-phenibut and S-phenibut (0.5 μg/ml) on mitochondrial functionality and Ca^{2+}-induced swelling in isolated mouse brain mitochondria. R-Phenibut and S-phenibut did not affect the mitochondrial respiration rate (a) but significantly decreased the H_2O_2 production rate (b) and H_2O_2/O ratio (c). The results are presented as the mean ± S.D. of 5 independent measurements. P: pyruvate; M: malate; D: ADP; G: glutamate; S: succinate; U: uncoupler; Rot: rotenone; CI: complex I; CII: complex II; LEAK: substrate metabolism-dependent state; OXPHOS: oxidative phosphorylation-dependent state; ET: electron transfer capacity state. *Indicates a significant difference compared to the control group (one-way ANOVA followed by Tukey's multiple comparison test, $^*P < 0.05$). Both R-phenibut and S-phenibut at a concentration of 0.5 μg/ml significantly attenuated Ca^{2+}-induced swelling (d). The results are presented as the mean ± S.D. of 7 independent replicates. *Indicates a significant difference compared to the control group (two-way repeated-measures ANOVA followed by Dunnett's multiple comparison test; $^*P < 0.05$).

protective properties against anoxia-reoxygenation and Ca^{2+}-induced stress. Since there is no evidence of $\alpha_2\delta$ localization in the mitochondrial membrane, it is possible that compounds could alter Ca^{2+} signalling pathways and protect mitochondria by targeting mitochondrial-specific or mitochondrial-endoplasmatic reticulum-associated Ca^{2+} transporters.

Our study has several limitations. One of the limitations of this study is that the level of ROS in mouse brain after treatment of R-phenibut following TBI was not measured. Another limitation is the increase in the NSS score between the baseline value and the first day postcraniotomy in the sham-operated group. The increase of the NSS score in sham-operated mice was reported previously and can be related to the distinct injury caused by craniotomy procedures [64]. Similar to other studies, the NSS score of injured mice showed maximum deficits on postinjury day 1 and remained elevated at 1, 2, 4, and 7 days after latFPI [64, 65]. A potential limitation of this study is that only male mice were used in experiments.

5. Conclusions

In conclusion, R-phenibut treatment reduces TBI-induced neuronal death and improves functional recovery, suggesting its therapeutic potential. The present study suggests that the neuroprotective properties of phenibut may be mediated by its effects on mitochondrial calcium influx and ROS generation.

Data Availability

The data used to support the findings of this study are available from the corresponding author upon request.

Conflicts of Interest

The authors declare that there is no conflict of interest regarding the publication of this paper.

Acknowledgments

This study was supported by the framework of the EU-ERA-NET NEURON projects TRAINS and CnsAflame.

References

[1] A. M. Rubiano, N. Carney, R. Chesnut, and J. C. Puyana, "Global neurotrauma research challenges and opportunities," *Nature*, vol. 527, no. 7578, pp. S193–S197, 2015.

[2] L. J. Carroll, J. D. Cassidy, C. Cancelliere et al., "Systematic review of the prognosis after mild traumatic brain injury in adults: cognitive, psychiatric, and mortality outcomes: results of the international collaboration on mild traumatic brain injury prognosis," *Archives of Physical Medicine and Rehabilitation*, vol. 95, no. 3, pp. S152–S173, 2014.

[3] M. Majdan, D. Plancikova, A. Brazinova et al., "Epidemiology of traumatic brain injuries in Europe: a cross-sectional analysis," *Lancet Public Health*, vol. 1, no. 2, pp. e76–e83, 2016.

[4] E. Kupats, J. Vrublevska, B. Zvejniece et al., "Safety and tolerability of the anxiolytic and nootropic drug phenibut: a systematic review of clinical trials and case reports," *Pharmacopsychiatry*, vol. 53, no. 5, pp. 201–208, 2020.

[5] I. Lapin, "Phenibut (beta-phenyl-GABA): a tranquilizer and nootropic drug," *CNS Drug Reviews*, vol. 7, no. 4, pp. 471–481, 2001.

[6] L. Zvejniece, E. Vavers, B. Svalbe et al., "R-phenibut binds to the $\alpha 2$–δ subunit of voltage-dependent calcium channels and exerts gabapentin-like anti-nociceptive effects," *Pharmacology, Biochemistry, and Behavior*, vol. 137, pp. 23–29, 2015.

[7] I. Belozertseva, J. Nagel, B. Valastro, L. Franke, and W. Danysz, "Optical isomers of phenibut inhibit [H^3]-gabapentin binding in vitro and show activity in animal models of chronic pain," *Pharmacological Reports*, vol. 68, no. 3, pp. 550–554, 2016.

[8] M. Dambrova, L. Zvejniece, E. Liepinsh et al., "Comparative pharmacological activity of optical isomers of phenibut," *European Journal of Pharmacology*, vol. 583, no. 1, pp. 128–134, 2008.

[9] E. Vavers, L. Zvejniece, B. Svalbe et al., "The neuroprotective effects of R-phenibut after focal cerebral ischemia," *Pharmacological Research*, vol. 113, pp. 796–801, 2016.

[10] H. M. Bramlett and W. D. Dietrich, "Pathophysiology of cerebral ischemia and brain trauma: similarities and differences," *Journal of Cerebral Blood Flow & Metabolism*, vol. 24, no. 2, pp. 133–150, 2004.

[11] Y. Xiong, A. Mahmood, and M. Chopp, "Animal models of traumatic brain injury," *Nature Reviews Neuroscience*, vol. 14, no. 2, pp. 128–142, 2013.

[12] L. Zvejniece, G. Stelfa, E. Vavers et al., "Skull fractures induce neuroinflammation and worsen outcomes after closed head injury in mice," *Journal of Neurotrauma*, vol. 37, no. 2, pp. 295–304, 2020.

[13] A. Görlach, K. Bertram, S. Hudecova, and O. Krizanova, "Calcium and ROS: a mutual interplay," *Redox Biology*, vol. 6, pp. 260–271, 2015.

[14] D. N. Granger and P. R. Kvietys, "Reperfusion injury and reactive oxygen species: the evolution of a concept," *Redox Biology*, vol. 6, pp. 524–551, 2015.

[15] M. Bains and E. D. Hall, "Antioxidant therapies in traumatic brain and spinal cord injury," *Biochimica et Biophysica Acta*, vol. 1822, no. 5, pp. 675–684, 2012.

[16] J. T. Weber, "Altered calcium signaling following traumatic brain injury," *Frontiers in Pharmacology*, vol. 3, p. 60, 2012.

[17] E. D. Hall, R. A. Vaishnav, and A. G. Mustafa, "Antioxidant therapies for traumatic brain injury," *Neurotherapeutics*, vol. 7, no. 1, pp. 51–61, 2010.

[18] G. Cheng, R. Kong, L. Zhang, and J. Zhang, "Mitochondria in traumatic brain injury and mitochondrial-targeted multipotential therapeutic strategies," *British Journal of Pharmacology*, vol. 167, no. 4, pp. 699–719, 2012.

[19] M. D'Arco, W. Margas, J. S. Cassidy, and A. C. Dolphin, "The upregulation of $\alpha 2\delta$-1 subunit modulates activity-dependent Ca2+ signals in sensory neurons," *The Journal of Neuroscience*, vol. 35, no. 15, pp. 5891–5903, 2015.

[20] T. Kinjo, Y. Ashida, H. Higashi et al., "Alleviation by GABAB receptors of neurotoxicity mediated by mitochondrial permeability transition pore in cultured murine cortical neurons exposed to N-methyl-D-aspartate," *Neurochemical Research*, vol. 43, no. 1, pp. 79–88, 2018.

[21] J. Flygt, K. Ruscher, A. Norberg et al., "Neutralization of interleukin-1β following diffuse traumatic brain injury in the mouse attenuates the loss of mature oligodendrocytes," *Journal of Neurotrauma*, vol. 35, no. 23, pp. 2837–2849, 2018.

[22] N. Marklund, "Rodent models of traumatic brain injury: methods and challenges," *Methods in Molecular Biology*, vol. 1462, pp. 29–46, 2016.

[23] C. Kilkenny, W. Browne, I. C. Cuthill, M. Emerson, D. G. Altman, and NC3Rs Reporting Guidelines Working Group, "Animal research: reporting in vivo experiments: the ARRIVE guidelines," *The Journal of Gene Medicine*, vol. 12, no. 7, pp. 561–563, 2010.

[24] J. C. McGrath, G. B. Drummond, E. M. McLachlan, C. Kilkenny, and C. L. Wainwright, "Guidelines for reporting experiments involving animals: the ARRIVE guidelines," *British Journal of Pharmacology*, vol. 160, no. 7, pp. 1573–1576, 2010.

[25] L. Zvejniece, B. Zvejniece, M. Videja et al., "Neuroprotective and anti-inflammatory activity of DAT inhibitor R-phenylpiracetam in experimental models of inflammation in male mice," *Inflammopharmacology*, vol. 28, no. 5, pp. 1283–1292, 2020.

[26] M. A. Flierl, P. F. Stahel, K. M. Beauchamp, S. J. Morgan, W. R. Smith, and E. Shohami, "Mouse closed head injury model induced by a weight-drop device," *Nature Protocols*, vol. 4, no. 9, pp. 1328–1337, 2009.

[27] H. Ooigawa, H. Nawashiro, S. Fukui et al., "The fate of Nissl-stained dark neurons following traumatic brain injury in rats: difference between neocortex and hippocampus regarding survival rate," *Acta Neuropathologica*, vol. 112, no. 4, pp. 471–481, 2006.

[28] R. Hicks, H. Soares, D. Smith, and T. McIntosh, "Temporal and spatial characterization of neuronal injury following lateral fluid-percussion brain injury in the rat," *Acta Neuropathologica*, vol. 91, no. 3, pp. 236–246, 1996.

[29] M. Makrecka-Kuka, G. Krumschnabel, and E. Gnaiger, "High-resolution respirometry for simultaneous measurement of oxygen and hydrogen peroxide fluxes in permeabilized cells,

tissue homogenate and isolated mitochondria," *Biomolecules*, vol. 5, no. 3, pp. 1319–1338, 2015.

[30] G. Krumschnabel, M. Fontana-Ayoub, Z. Sumbalova et al., "Simultaneous high-resolution measurement of mitochondrial respiration and hydrogen peroxide production," *Methods in Molecular Biology*, vol. 1264, pp. 245–261, 2015.

[31] J. Burtscher, L. Zangrandi, C. Schwarzer, and E. Gnaiger, "Differences in mitochondrial function in homogenated samples from healthy and epileptic specific brain tissues revealed by high-resolution respirometry," *Mitochondrion*, vol. 25, pp. 104–112, 2015.

[32] M. Makrecka, B. Svalbe, K. Volska et al., "Mildronate, the inhibitor of L-carnitine transport, induces brain mitochondrial uncoupling and protects against anoxia-reoxygenation," *European Journal of Pharmacology*, vol. 723, pp. 55–61, 2014.

[33] T. Kristián, J. Gertsch, T. E. Bates, and B. K. Siesjö, "Characteristics of the calcium-triggered mitochondrial permeability transition in nonsynaptic brain mitochondria: effect of cyclosporin A and ubiquinone O," *Journal of Neurochemistry*, vol. 74, no. 5, pp. 1999–2009, 2000.

[34] C. P. Baines, R. A. Kaiser, N. H. Purcell et al., "Loss of cyclophilin D reveals a critical role for mitochondrial permeability transition in cell death," *Nature*, vol. 434, no. 7033, pp. 658–662, 2005.

[35] T. Kobayashi, S. Kuroda, M. Tada, K. Houkin, Y. Iwasaki, and H. Abe, "Calcium-induced mitochondrial swelling and cytochrome c release in the brain: its biochemical characteristics and implication in ischemic neuronal injury," *Brain Research*, vol. 960, no. 1-2, pp. 62–70, 2003.

[36] E. Marais, N. Klugbauer, and F. Hofmann, "Calcium channel alpha(2)delta subunits-structure and gabapentin binding," *Molecular Pharmacology*, vol. 59, no. 5, pp. 1243–1248, 2001.

[37] N. Qin, S. Yagel, M.-L. Momplaisir, E. E. Codd, and M. R. D'Andrea, "Molecular cloning and characterization of the human voltage-gated calcium channel $\alpha 2\delta$-4 subunit," *Molecular Pharmacology*, vol. 62, no. 3, pp. 485–496, 2002.

[38] A. C. Dolphin, "The $\alpha 2\delta$ subunits of voltage-gated calcium channels," *Biochimica et Biophysica Acta*, vol. 1828, no. 7, pp. 1541–1549, 2013.

[39] C. P. Taylor and R. Garrido, "Immunostaining of rat brain, spinal cord, sensory neurons and skeletal muscle for calcium channel alpha2-delta ($\alpha 2$-δ) type 1 protein," *Neuroscience*, vol. 155, no. 2, pp. 510–521, 2008.

[40] G. Gurkoff, K. Shahlaie, B. Lyeth, and R. Berman, "Voltage-gated calcium channel antagonists and traumatic brain injury," *Pharmaceuticals (Basel)*, vol. 6, no. 7, pp. 788–812, 2013.

[41] C. Calikoglu, H. Aytekin, O. Akgül et al., "Effect of pregabalin in preventing secondary damage in traumatic brain injury: an experimental study," *Medical Science Monitor*, vol. 21, pp. 813–820, 2015.

[42] M. Shamsi Meymandi, Z. Soltani, G. Sepehri, S. Amiresmaili, F. Farahani, and M. Moeini Aghtaei, "Effects of pregabalin on brain edema, neurologic and histologic outcomes in experimental traumatic brain injury," *Brain Research Bulletin*, vol. 140, pp. 169–175, 2018.

[43] K.-Y. Ha, Y.-H. Kim, K.-W. Rhyu, and S.-E. Kwon, "Pregabalin as a neuroprotector after spinal cord injury in rats," *European Spine Journal*, vol. 17, no. 6, pp. 864–872, 2008.

[44] K.-Y. Ha, E. Carragee, I. Cheng, S.-E. Kwon, and Y.-H. Kim, "Pregabalin as a neuroprotector after spinal cord injury in rats: biochemical analysis and effect on glial cells," *Journal of Korean Medical Science*, vol. 26, no. 3, pp. 404–411, 2011.

[45] J. K. Newcomb, A. Kampfl, R. M. Posmantur et al., "Immunohistochemical study of calpain-mediated breakdown products to alpha-spectrin following controlled cortical impact injury in the rat," *Journal of Neurotrauma*, vol. 14, no. 6, pp. 369–383, 1997.

[46] R. M. Posmantur, J. K. Newcomb, A. Kampfl, and R. L. Hayes, "Light and confocal microscopic studies of evolutionary changes in neurofilament proteins following cortical impact injury in the rat," *Experimental Neurology*, vol. 161, no. 1, pp. 15–26, 2000.

[47] L. Talley Watts, J. A. Long, J. Chemello et al., "Methylene blue is neuroprotective against mild traumatic brain injury," *Journal of Neurotrauma*, vol. 31, no. 11, pp. 1063–1071, 2014.

[48] E. A. Newell, B. P. Todd, J. Mahoney, A. A. Pieper, P. J. Ferguson, and A. G. Bassuk, "Combined blockade of interleukin-1α and -1β signaling protects mice from cognitive dysfunction after traumatic brain injury," *eNeuro*, vol. 5, no. 2, pp. -ENEURO.0385–ENEU17.2018, 2018.

[49] M. Sun, R. D. Brady, D. K. Wright et al., "Treatment with an interleukin-1 receptor antagonist mitigates neuroinflammation and brain damage after polytrauma," *Brain, Behavior, and Immunity*, vol. 66, pp. 359–371, 2017.

[50] N. J. Rothwell and G. N. Luheshi, "Interleukin 1 in the brain: biology, pathology and therapeutic target," *Trends in Neurosciences*, vol. 23, no. 12, pp. 618–625, 2000.

[51] K.-T. Lu, Y.-W. Wang, J.-T. Yang, Y.-L. Yang, and H.-I. Chen, "Effect of interleukin-1 on traumatic brain injury-induced damage to hippocampal neurons," *Journal of Neurotrauma*, vol. 22, no. 8, pp. 885–895, 2005.

[52] F. Clausen, A. Hånell, M. Björk et al., "Neutralization of interleukin-1beta modifies the inflammatory response and improves histological and cognitive outcome following traumatic brain injury in mice," *The European Journal of Neuroscience*, vol. 30, no. 3, pp. 385–396, 2009.

[53] R. Tehranian, S. Andell-Jonsson, S. M. Beni et al., "Improved recovery and delayed cytokine induction after closed head injury in mice with central overexpression of the secreted isoform of the interleukin-1 receptor antagonist," *Journal of Neurotrauma*, vol. 19, no. 8, pp. 939–951, 2002.

[54] J. Lazovic, A. Basu, H.-W. Lin et al., "Neuroinflammation and both cytotoxic and vasogenic edema are reduced in interleukin-1 type 1 receptor-deficient mice conferring neuroprotection," *Stroke*, vol. 36, no. 10, pp. 2226–2231, 2005.

[55] R. A. Floyd and J. M. Carney, "Free radical damage to protein and DNA: mechanisms involved and relevant observations on brain undergoing oxidative stress," *Annals of Neurology*, vol. 32, no. S1, pp. S22–S27, 1992.

[56] C. Werner and K. Engelhard, "Pathophysiology of traumatic brain injury," *British Journal of Anaesthesia*, vol. 99, no. 1, pp. 4–9, 2007.

[57] M. Prins, T. Greco, D. Alexander, and C. C. Giza, "The pathophysiology of traumatic brain injury at a glance," *Disease Models & Mechanisms*, vol. 6, no. 6, pp. 1307–1315, 2013.

[58] E. E. Genrikhs, E. V. Stelmashook, O. V. Popova et al., "Mitochondria-targeted antioxidant SkQT1 decreases trauma-induced neurological deficit in rat and prevents amyloid-β-induced impairment of long-term potentiation in rat

hippocampal slices," *Journal of Drug Targeting*, vol. 23, no. 4, pp. 347–352, 2015.

[59] J. Zhou, H. Wang, R. Shen et al., "Mitochondrial-targeted antioxidant MitoQ provides neuroprotection and reduces neuronal apoptosis in experimental traumatic brain injury possibly via the Nrf2-ARE pathway," *American Journal of Translational Research*, vol. 10, no. 6, pp. 1887–1899, 2018.

[60] R. L. Schmidt and L. L. Lenz, "Distinct licensing of IL-18 and IL-1β secretion in response to NLRP3 inflammasome activation," *PLoS One*, vol. 7, no. 9, article e45186, 2012.

[61] R. L. Veech, C. R. Valeri, and T. B. VanItallie, "The mitochondrial permeability transition pore provides a key to the diagnosis and treatment of traumatic brain injury," *IUBMB Life*, vol. 64, no. 2, pp. 203–207, 2012.

[62] D. Huynh, C. S. Wai, A. Liang, T. J. Maher, and A. Pino-Figueroa, "In vitro neuroprotective activity of phenibut," *The FASEB Journal*, vol. 26, 672.6 pages, 2012.

[63] V. N. Perfilova, T. A. Popova, I. I. Prokofiev, I. S. Mokrousov, O. V. Ostrovskii, and I. N. Tyurenkov, "Effect of phenibut and glufimet, a novel glutamic acid derivative, on respiration of heart and brain mitochondria from animals exposed to stress against the background of inducible NO-synthase blockade," *Bulletin of Experimental Biology and Medicine*, vol. 163, no. 2, pp. 226–229, 2017.

[64] J. T. Cole, A. Yarnell, W. S. Kean et al., "Craniotomy: true sham for traumatic brain injury, or a sham of a sham?," *Journal of Neurotrauma*, vol. 28, no. 3, pp. 359–369, 2011.

[65] L. D. Schurman, T. L. Smith, A. J. Morales et al., "Investigation of left and right lateral fluid percussion injury in C57BL6/J mice: in vivo functional consequences," *Neuroscience Letters*, vol. 653, pp. 31–38, 2017.

International Journal of
Molecular Sciences

MDPI

Article

Reduced GFAP Expression in Bergmann Glial Cells in the Cerebellum of Sigma-1 Receptor Knockout Mice Determines the Neurobehavioral Outcomes after Traumatic Brain Injury

Gundega Stelfa [1,2,*], Edijs Vavers [1], Baiba Svalbe [1], Rinalds Serzants [1,3], Anna Miteniece [1,4], Lasma Lauberte [1], Solveiga Grinberga [5], Baiba Gukalova [5], Maija Dambrova [1,3] and Liga Zvejniece [1]

1 Laboratory of Pharmaceutical Pharmacology, Latvian Institute of Organic Synthesis, Aizkraukles Str. 21, LV-1006 Riga, Latvia; edijs.vavers@farm.osi.lv (E.V.); baibas@farm.osi.lv (B.S.); rinalds.serzants@farm.osi.lv (R.S.); anna.miteniece18@imperial.ac.uk (A.M.); lasma@farm.osi.lv (L.L.); maija.dambrova@farm.osi.lv (M.D.); liga@farm.osi.lv (L.Z.)
2 Faculty of Veterinary Medicine, Latvia University of Life Sciences and Technologies, K Helmana Str. 8, LV-3001 Jelgava, Latvia
3 Department of Pharmaceutical Chemistry, Riga Stradins University, Dzirciema Str. 16, LV-1007 Riga, Latvia
4 Department of Life Sciences, Imperial College London, Exhibition Road, London SW7 2AZ, UK
5 Laboratory of Physical Organic Chemistry, Latvian Institute of Organic Synthesis, Aizkraukles Str. 21, LV-1006 Riga, Latvia; solveiga@osi.lv (S.G.); baiba.gukalova@osi.lv (B.G.)
* Correspondence: gundega@farm.osi.lv; Tel.: +371-66155159

Abstract: Neuroprotective effects of Sigma-1 receptor (S1R) ligands have been observed in multiple animal models of neurodegenerative diseases. Traumatic brain injury (TBI)-related neurodegeneration can induce long-lasting physical, cognitive, and behavioral disabilities. The aim of our study was to evaluate the role of S1R in the development of neurological deficits after TBI. Adult male wild-type CD-1 (WT) and S1R knockout (S1R-/-) mice were subjected to lateral fluid percussion injury, and behavioral and histological outcomes were assessed for up to 12 months postinjury. Neurological deficits and motor coordination impairment were less pronounced in S1R-/- mice with TBI than in WT mice with TBI 24 h after injury. TBI-induced short-term memory impairments were present in WT but not S1R-/- mice 7 months after injury. Compared to WT animals, S1R-/- mice exhibited better motor coordination and less pronounced despair behavior for up to 12 months postinjury. TBI induced astrocyte activation in the cortex of WT but not S1R-/- mice. S1R-/- mice presented a significantly reduced GFAP expression in Bergmann glial cells in the molecular layer of the cerebellum compared to WT mice. Our findings suggest that S1R deficiency reduces TBI-induced motor coordination impairments by reducing GFAP expression in Bergmann glial cells in the cerebellum.

Keywords: sigma-1 receptor; traumatic brain injury; lateral fluid percussion injury; neurobehavior; cerebellum; astrocytes

Citation: Stelfa, G.; Vavers, E.; Svalbe, B.; Serzants, R.; Miteniece, A.; Lauberte, L.; Grinberga, S.; Gukalova, B.; Dambrova, M.; Zvejniece, L. Reduced GFAP Expression in Bergmann Glial Cells in the Cerebellum of Sigma-1 Receptor Knockout Mice Determines the Neurobehavioral Outcomes after Traumatic Brain Injury. *Int. J. Mol. Sci.* **2021**, *22*, 11611. https://doi.org/10.3390/ijms222111611

Academic Editors: Carmen Abate and Tangui Maurice

Received: 30 August 2021
Accepted: 23 October 2021
Published: 27 October 2021

1. Introduction

Traumatic brain injury (TBI) is a complex neurodegenerative condition that is induced by biomechanical forces applied to the brain [1]. TBI is the main injury-related cause of permanent disability, with more than 50 million individuals suffering from TBIs each year [2]. Brain injury is commonly viewed as an acute self-limiting problem; however, the consequences of adult brain injuries can develop over years or even decades after the initial insult [3,4]. TBI is considered a "biphasic injury" that is characterized by direct physical and irreversible primary damage to the brain tissue and delayed secondary injury, which can be prevented and reduced by therapeutic intervention [5]. In addition, the progressive, long-lasting consequences of TBI have received increasing attention in both experimental and clinical studies [6–8].

Among the putative targets of neuroprotective drugs, the Sigma-1 receptor (S1R) has attracted increasing attention as a novel molecular target for treating neurological disorders [9]. S1R is a unique endoplasmic reticulum protein that is widely expressed in multiple organs, including the central nervous system [10]. S1R has been reported to play a role in both neurodegenerative and ischemic diseases, including Alzheimer's disease, Parkinson's disease, amyotrophic lateral sclerosis, stroke, and TBI [9]. Genetic inactivation and pharmacological inhibition of S1R are associated with neurodegenerative phenotypes [9,11,12]. Specific agonists of S1R have previously been shown to provide potent neuroprotection by attenuating neurodegeneration and preventing microglial cell activation in adult animal models of TBI and in neonatal hypoxic/ischemic brain damage [13,14]. However, S1R antagonists also exert neuroprotective effects on experimental models of brain ischemia. For example, mice treated with the antagonist S1RA presented significantly reduced cerebral infarct size and neurological deficits caused by permanent middle cerebral artery occlusion (MCAO) [15]. Additionally, the nonselective S1R antagonist haloperidol induces neuroprotection after brain ischemia [16]. Interestingly, after genetic inactivation and pharmacological blockade of S1R, antinociceptive effects on mice with traumatic spinal cord injury (SCI) were detected [17]. On the other hand, activation of S1R after SCI is presumed to be detrimental for neuron survival and motor function recovery [18]. Thus, different S1R ligands may exert various effects in a variety of neurodegenerative disease models.

The aim of this study was to investigate behavioral and histological outcomes in an S1R knockout (S1R-/-) mouse model of lateral fluid percussion injury over a 12-month period. We also evaluated posttraumatic behavioral and histological outcomes of pharmacological blockade of S1R using the S1R antagonist BD-1063.

2. Results

2.1. S1R-/- Mice Exhibit Improved Acute Sensorimotor Ability and Motor Coordination following TBI

Sensorimotor function was assessed using the neurological severity score (NSS) and rota-rod (RR) test. TBI induced significant neurological impairments in WT TBI mice ($p = 0.006$) but not in S1R-/- TBI mice 24 h after injury compared to the respective sham groups ($p = 0.191$, effect of group ($F_{3,32} = 16.1$; $p < 0.0001$), repeated measures (RM) two-way ANOVA followed by Fisher's least-significant difference (LSD) test, Figure 1A). In addition, S1R-/- TBI mice exhibited a significantly decreased NSS (1.78 ± 0.57) compared to WT TBI mice (4.20 ± 0.79) at 24 h postinjury ($p = 0.024$). Compared to WT sham mice, the NSSs of WT TBI mice indicated sensorimotor deficits for up to 9 months postinjury ($p < 0.05$). From the second week to 9 months postinjury, the NSS was also significantly increased in the S1R-/- TBI group compared with the S1R-/- sham animals. No differences were observed at 12 months postinjury across all experimental groups ($p > 0.05$, Figure 1A).

In the accelerating RR test, WT TBI animals spent less time on the RR 24 h after injury compared to WT sham animals ($p = 0.038$, effect of group ($F_{3,29} = 8$, $p = 0.0006$), and time ($F_{4,87} = 5$, $p = 0.002$), RM two-way ANOVA followed by Fisher's LSD test, Figure 1B). We did not observe any impairment of motor coordination in S1R-/- TBI animals compared to S1R-/- sham animals ($p > 0.05$, Figure 1B). Moreover, motor coordination was not significantly different at any time point after injury compared to baseline values in S1R-/- sham and TBI animals ($p > 0.05$). We observed impaired motor coordination in WT sham animals starting at 6 months postinjury compared to baseline measurements (Figure 1B). WT TBI animals spent less time on the RR starting at 24 h after injury compared to baseline values (Figure 1B).

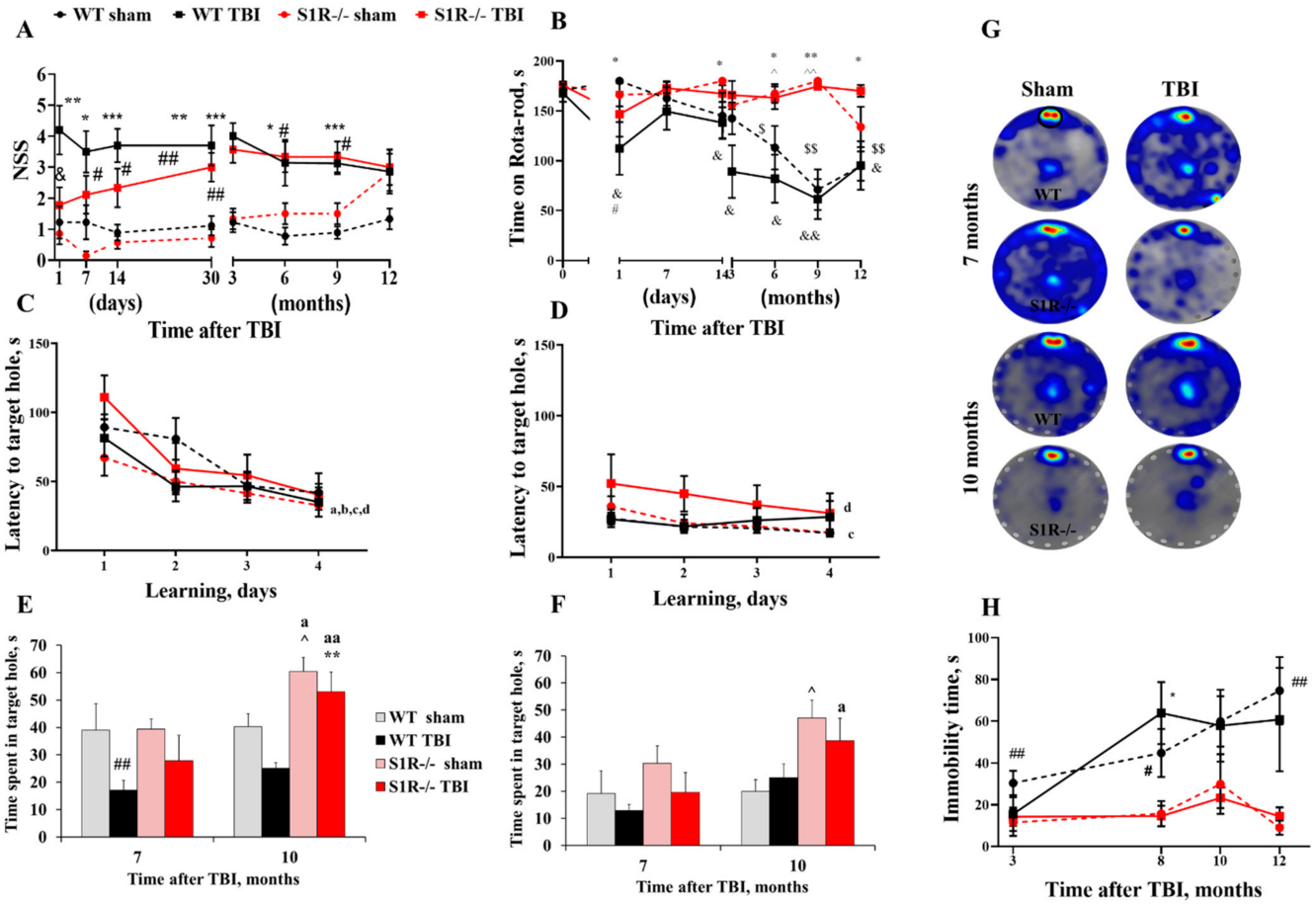

Figure 1. Long-term behavioral changes after traumatic brain injury (TBI). Behavioral testing revealed functional deficits in the (**A**) neurological severity score (NSS), (**B**) rota-rod (RR), (**C**–**G**) Barnes maze (BM), and (**H**) tail suspension tests. (**A**) Wild-type (WT) TBI mice showed neurological deficits compared to WT sham mice 24 h after injury. WT sham $n = 9$, WT TBI $n = 7$–10, Sigma-1 receptor knockout (S1R-/-) sham $n = 6$–8, S1R-/- TBI $n = 6$–9. * $p < 0.05$ WT TBI vs. S1R-/- TBI, # $p < 0.05$, ## $p < 0.01$ sham vs. TBI (the black symbols represent differences between WT groups, and the red symbols represent differences between S1R-/- groups). (**B**) WT TBI mice spent less time on the RR than WT sham mice 24 h after injury. Motor coordination was impaired in the WT TBI group at all time points after injury compared to baseline values. Motor coordination remained unaffected in S1R-/- mice after TBI. WT sham $n = 8$, WT TBI $n = 6$–9, S1R-/- sham $n = 7$, S1R-/- TBI $n = 6$–9. * $p < 0.05$, ** $p < 0.01$, *** $p < 0.001$ WT TBI vs. S1R-/- TBI, ^ $p < 0.05$, ^^ $p < 0.01$ WT sham vs. S1R-/- sham, ## $p < 0.01$ WT sham vs. WT TBI, $ $p < 0.05$, $$ $p < 0.01$ WT sham vs. baseline, & $p < 0.05$, && $p < 0.01$ WT TBI vs. baseline. In terms of BM performance, (**C**) all groups showed a reduced latency to find the target hole, indicating no impairments in the learning task (**C**) 7 and (**D**) 10 months after injury. (**E**) During the short-term memory evaluation, WT TBI animals spent significantly less time in the target hole than WT sham animals at 7 months postinjury. ** $p < 0.01$ WT TBI vs. S1R-/- TBI ##, ^ $p < 0.05$ WT sham vs. S1R-/- sham, ## $p < 0.01$ WT sham vs. WT TBI, a $p < 0.05$, aa $p < 0.01$ 7 vs. 10 months. (**F**) TBI did not induce long-term memory impairments at 7 and 10 months after the injury. WT sham $n = 9$, WT TBI $n = 10$, S1R-/- sham $n = 7$, S1R-/- TBI $n = 9$. ^ $p < 0.05$ WT sham vs. S1R-/- sham, a $p < 0.05$ 7 vs. 10 months. (**G**) Heat maps representing weighted occupancy across probe trials conducted 7 and 10 months after TBI. Warmer colors indicate longer dwelling times. The target hole area is denoted with a black circle. (**H**) WT sham and TBI mice showed a time-dependent increase in immobility time after injury. WT sham $n = 8$–9, WT TBI $n = 6$–9, S1R-/- sham $n = 5$–8, S1R-/- TBI $n = 7$–8. * $p < 0.05$ WT TBI vs. S1R-/- TBI, ^ $p < 0.05$, ^^ $p < 0.01$ WT sham vs. S1R-/- sham. All values are presented as means ± standard errors of the means (SEM). p values for differences between groups were calculated using repeated measures two-way analysis of variance (RM two-way ANOVA) followed by Fisher's least-significant difference (LSD) test.

2.2. S1R-/- Mice Have Preserved Cognitive Ability after TBI

Spatial learning and memory function were evaluated using the Barnes maze (BM) to test whether any long-term effects on cognitive function were present in WT and S1R-/- mice after TBI. Learning ability was evaluated as the latency to reach the target hole over 4 learning days. Learning was unaffected in all experimental groups at 7 months (RM two-way ANOVA, effect of time $F_{3,87} = 37.75$, $p < 0.0001$, effect of group $F_{3,29} = 0.884$, $p = 0.460$, Figure 1C) and 10 months after injury (effect of time $F_{3,81} = 3$, $p = 0.020$, effect of group $F_{3,27} = 2$, $p = 0.202$, Figure 1D). Time spent in the target hole area, which previously contained an escape hole, was measured 24 h (short-term memory) and 7 days (long-term memory) after the last learning day to assess spatial memory processes. TBI induced short-term memory impairments in WT mice (effect of group $F_{3,24} = 7.958$, $p < 0.001$, Figure 1E). WT TBI animals spent significantly less time in the target hole than WT sham animals at 7 months postinjury ($p < 0.01$, Figure 1E). At 10 months postinjury, WT TBI animals appeared to perform worse than WT sham animals; however, the difference failed to reach significance ($p = 0.070$, Figure 1E). Short-term memory was not impaired in S1R-/- TBI mice compared to S1R-/- sham mice after injury ($p > 0.05$, Figure 1E). Long-term memory was not affected in any experimental groups after injury ($p > 0.05$, Figure 1F). We also observed that S1R-/- sham and TBI mice displayed improvements in short-term memory function at 10 months compared to 7 months (effect of time $F_{1,8} = 12.3$, $p < 0.01$, S1R-/- sham $p = 0.011$, TBI $p < 0.01$, Figure 1E), while WT sham and TBI mice performed similarly over time ($p > 0.05$, Figure 1E).

Next, we used the y-maze test to evaluate spatial working memory. We did not observe any differences in spontaneous alternations between the experimental groups ($p > 0.05$, Table S1), indicating that spatial working memory was not affected after TBI.

2.3. S1R-/- Mice Show Reduced Despair-like Behavior and Increased Anxiety, Regardless of Injury Status

Depressive-like behavior was assessed using the tail suspension test (TST). A significant effect of time on immobility in the TST was observed (RM two-way ANOVA, $F_{3,66} = 5.21$, $p = 0.004$, Figure 1H). Over the course of the experiment, immobility time was unchanged in S1R-/- sham and TBI mice ($p > 0.05$, Figure 1H). WT sham and TBI mice showed a time-dependent increase in immobility time after injury. WT sham mice spent more time in an immobile state at 10 and 12 months postinjury ($p = 0.032$ and $p = 0.018$, respectively) than at 3 months. WT TBI mice showed a significant increase in immobility at 8 months ($p = 0.032$) postinjury compared to 3 months; however, at later time points, the difference failed to reach significance. In addition, the immobility time was significantly decreased in S1R-/- sham mice compared to WT sham mice at 3 ($p = 0.047$), 8 ($p = 0.045$) and 12 months postinjury ($p < 0.01$, Figure 1H). S1R-/- TBI mice spent less time in an immobile state than WT TBI mice at 8 months postinjury ($p = 0.010$, Figure 1H).

The evaluation of anxiety-like behavior by quantification of the cumulative time spent in the closed and open quadrants showed a significant group effect (RM two-way ANOVA, $F_{3,34} = 4.98$, $p = 0.005$, Table S2). Post hoc tests revealed that the WT sham and TBI groups spent equivalent amounts of time in the open quadrants of the maze, indicating no change in anxiety as a consequence of TBI ($p > 0.05$, Table S2). We observed differences between WT and S1R-/- mice, regardless of their injury status. S1R-/- sham mice spent less time in open quadrants than WT sham mice 1 month after the injury ($p = 0.025$, Table S2). By 8 months, S1R-/- sham mice tended to spend less time in open quadrants than WT sham mice ($p = 0.058$). Similarly, S1R-/- TBI mice spent less time in open quadrants than WT TBI mice at 1 ($p = 0.081$) and 8 months ($p = 0.014$) postinjury.

No significant differences were observed between experimental groups in the distance traveled, suggesting that all groups retained similar motor activity and a similar ability to explore the open field arena within a 12-month period after injury ($p > 0.05$, Table S3). In addition, total activity did not differ between experimental groups in metabolic cages with

running wheels ($p > 0.05$, Table S3). No significant changes were observed in drinking and feeding behaviors at 1, 3, and 6 months after TBI ($p > 0.05$, Table S4).

2.4. S1R-/- Mice Exhibit Decreased Glial Fibrillary Acidic Protein (GFAP) Staining in the Molecular Layer of the Cerebellum

We compared the Iba1 and GFAP staining intensity between the experimental groups of WT and S1R-/- mice to evaluate microglial (Iba1) and astrocyte (GFAP) activation 12 months after TBI (Figure 2B). We examined the cortex, hippocampus (hippocampal cornu ammonis 3 (CA3) region), and thalamus (lateral nucleus of thalamus) as respective impact site regions. We also evaluated the astrocyte (GFAP, Glt-1) staining intensity and number of Purkinje cells (Calbindin D28K) in the grey matter of the cerebellum, which is associated with motor-related and cognitive functions that were prominently affected after TBI. TBI induced a significant increase in GFAP staining in the ipsilateral and contralateral cortex of WT mice compared to sham mice (Mann–Whitney U-test, $p = 0.015$ and $p = 0.015$, respectively, Figure 2D). S1R-/- TBI mice showed significantly decreased GFAP staining in the contralateral cortex compared with WT TBI mice (Mann–Whitney U-test, $p = 0.007$, Figure 2D). TBI induced a significant decrease in GFAP staining in the molecular layer of the cerebellum in WT mice compared to sham mice (Mann–Whitney U-test, $p = 0.037$, Figure 3B). Surprisingly, S1R-/- animals displayed almost no GFAP staining in the molecular layer of the cerebellum after injury (Figure 3B). GFAP staining in the cerebellum of S1R-/- mice was significantly different from that in WT animals ($p < 0.00$ S1R-/- sham vs. WT sham, $p = 0.019$ S1R-/- TBI vs. WT TBI, Figure 3B). The intensity of GFAP staining was also significantly decreased at baseline (before TBI) in S1R-/- mice compared to WT mice (Mann–Whitney U-test, $p < 0.001$, Figure S1). There were no significant differences in Glt-1 staining intensity and number of Purkinje cells in the grey matter of the cerebellum between experimental groups (Mann–Whitney U-test, $p > 0.05$, Figure 3C,D). No differences in the Iba1 staining intensity in the cortex, hippocampus, or thalamus were observed between WT and S1R-/- mice from either the sham or TBI groups (Figure 2C).

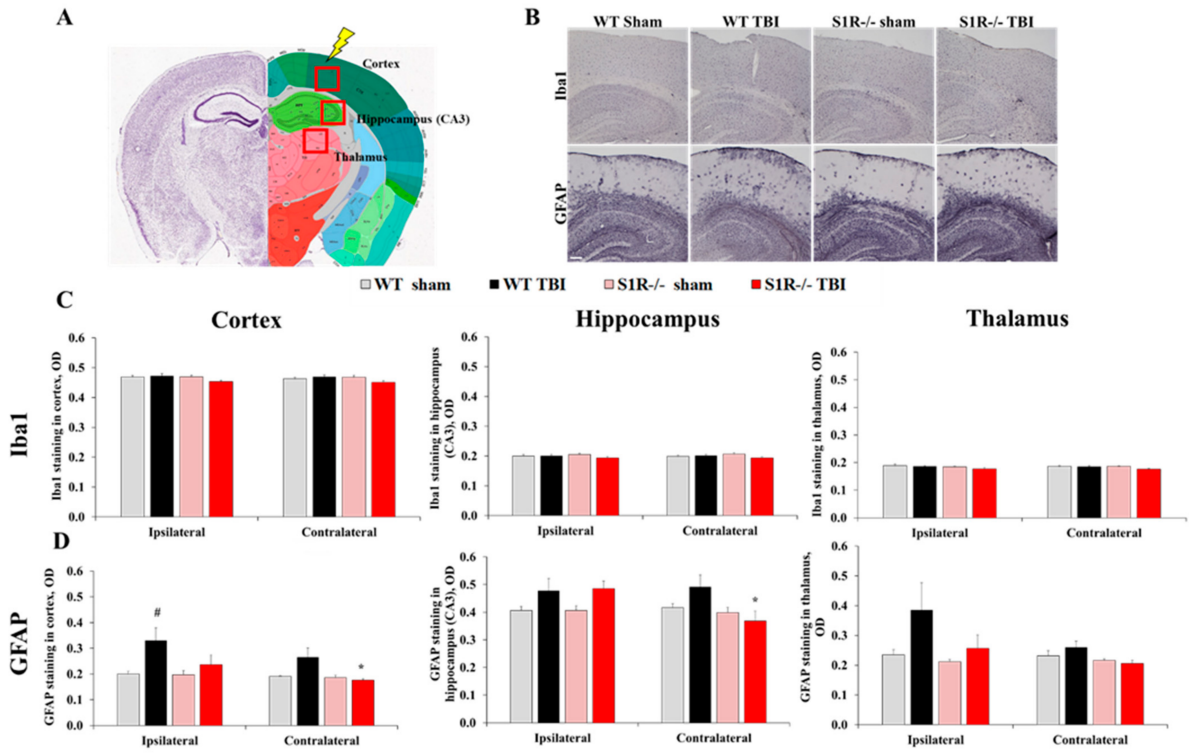

Figure 2. Staining of microglia (Iba1) and astrocytes (GFAP) in WT and S1R-/- mouse brain slices at 12 months postinjury. (**A**) The anatomical positions of the analyzed brain regions were validated using the Allen Mouse Brain Atlas (http://mouse.brain-map.org/static/atlas, accessed on 15 October 2021). (**B**) Representative images of Iba1 and GFAP staining in the cortex and hippocampus (total magnification = 40×, scale bar = 100 µm). Measured optical densities (OD) of the staining

intensity of (**C**) Iba1 and (**D**) GFAP in the cortex, hippocampus, and thalamus between the WT and S1R-/- animal groups. All values are presented as the means ± SEM. *p* values for differences between groups were calculated using the Mann–Whitney U-test, (*n* = 5): * $p < 0.05$ WT vs. S1R-/-, # $p < 0.05$ WT sham vs. WT TBI.

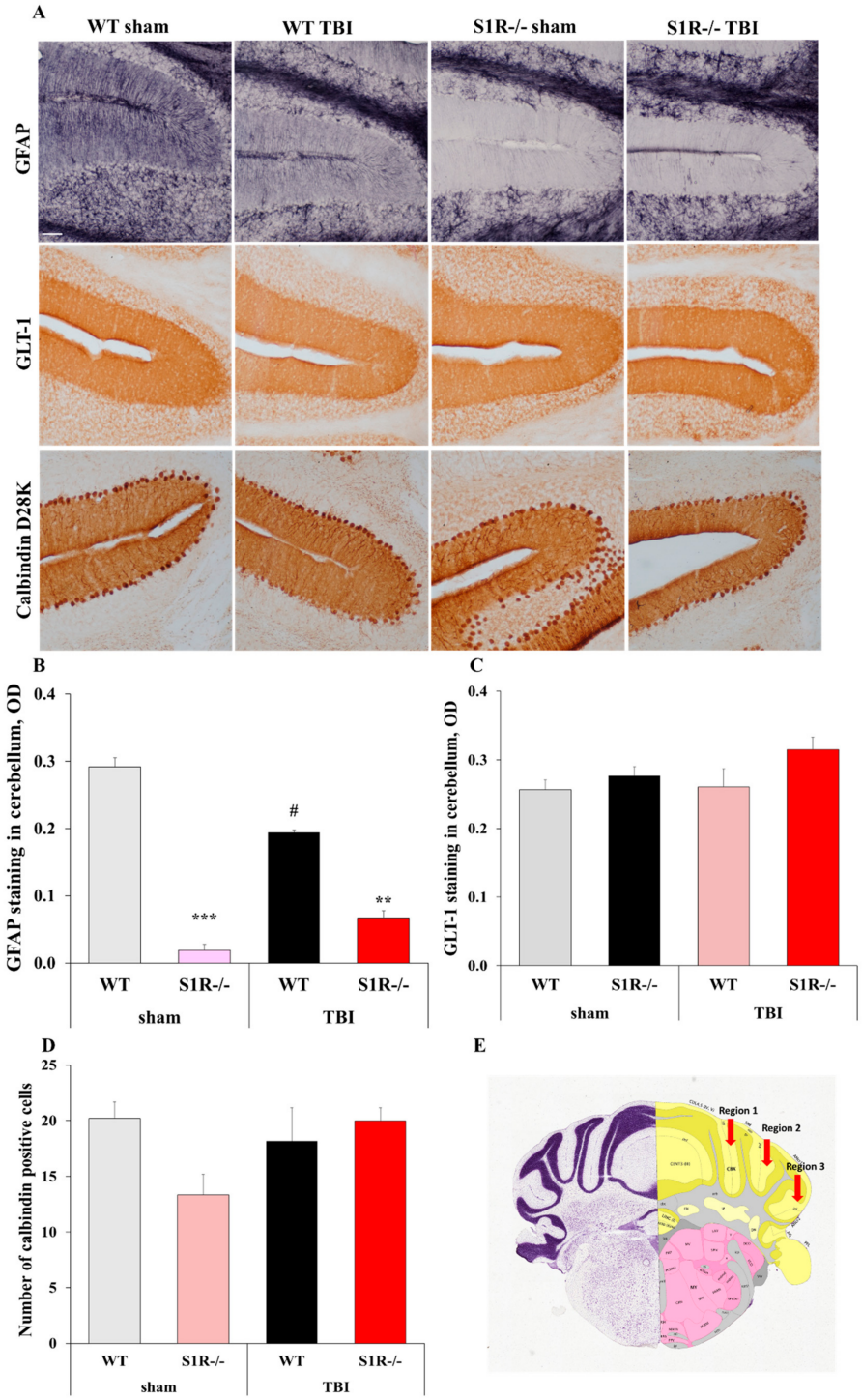

Figure 3. Staining of astrocytes (GFAP, Glt-1) and Purkinje cells (Calbindin D28K) in WT and S1R-/- mouse cerebellum slices at 12 months postinjury. (**A**) Representative images of GFAP, Glt-1, and Calbindin D28K staining in the grey matter of the cerebellum (total magnification = 100×, scale bar = 50 µm). OD of the GFAP (**B**), Glt-1 (**C**) staining intensity in the molecular layer of the cerebellum between the WT and S1R-/- experimental groups. (**D**) Total cell counts of Purkinje cells in the molecular layer of the cerebellum between WT and S1R-/- experimental groups. (**E**) Anatomical positions of the analyzed regions in the cerebellum (red arrows). All values are presented as the means ±SEM. *p* values for differences between groups were calculated using the Mann–Whitney U-test, (*n* = 5): ** $p < 0.01$, *** $p < 0.001$ WT vs. S1R-/-, # $p < 0.05$ WT sham vs. WT TBI.

2.5. Health Outcome Measures after TBI

S1R deficiency did not affect the general health condition of mice after TBI. Postinjury apnea was not significantly different between the WT TBI (46.7 ± 13.3) and S1R-/- TBI groups (28.3 ± 6.2) (p = 0.228, Figure S2). Overall mortality was not significantly affected by the injury (chi-square test, p = 0.175, Figure S2). After injury, the body weight was not significantly different between experimental groups, indicating that mice maintained good general health throughout the study (Figure S2). Posttraumatic seizure episodes were observed in both WT (5/12) and S1R-/- (1/12) animals. The first episode of seizures in each group was observed at 8 days postinjury. None of the sham animals displayed seizures after the injury.

2.6. BD-1063 Does Not Influence Acute Injury Measures or Behavioral and Histological Outcomes Following TBI

An assessment of NSS from baseline to 7 days after TBI revealed significant time ($F_{2,48}$ = 5, p = 0.017) and group ($F_{3,33}$ = 8, p = 0.0003) effects (RM two-way ANOVA, followed by Fisher's LSD test, Figure 4A). The NSS was significantly higher in TBI animals than in sham animals at 1, 3, and 7 days postinjury. In the RR test, the TBI and TBI + BD1063 10 and 30 mg/kg groups spent similar amounts of time on the RR as the sham animals (effect of time $F_{2,49}$ = 0.2, p = 0.78 and group $F_{3,33}$ = 1, p = 0.35, RM two-way ANOVA, Fisher's LSD test, Figure 4B). BD-1063 treatment did not affect sensorimotor ability and motor coordination. After the subcutaneous BD-1063 injection at a dose of 30 mg/kg for 7 days, the detected concentration of the test compound in the brain was 6.3 ± 0.03 µg/g. However, in the brain tissue, no significant differences were observed in S1R gene expression between the BD-1063 30 mg/kg treatment (1.1-fold) and saline (1.0-fold) groups.

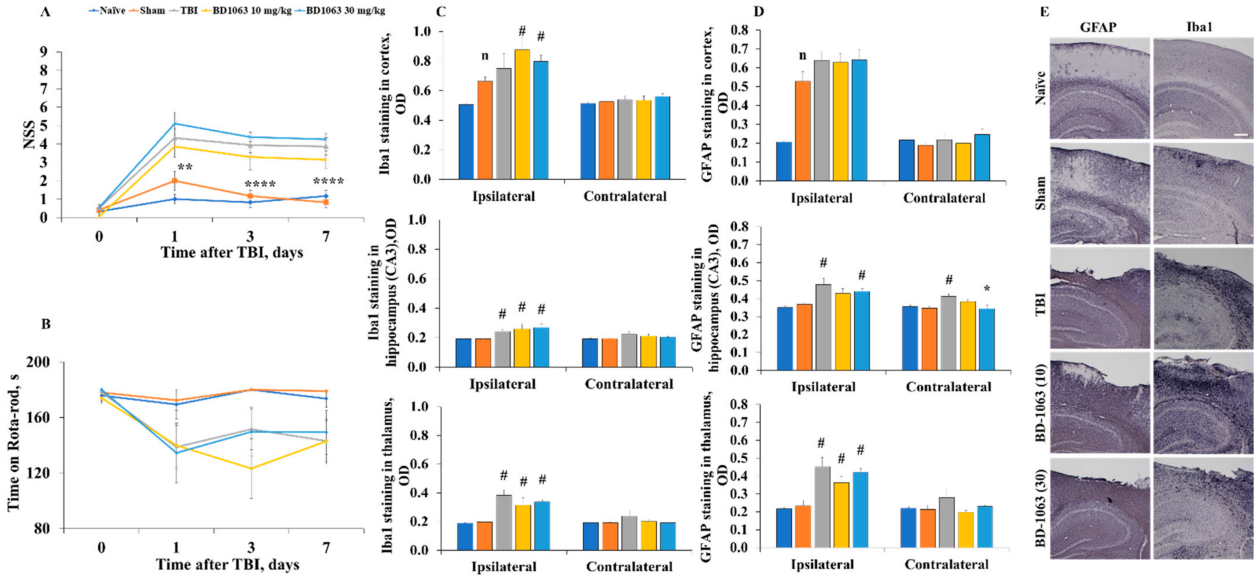

Figure 4. Posttraumatic behavioral and histological outcomes after pretreatment with the S1R antagonist BD-1063. (**A**) TBI mice had a significantly higher NSS up to 7 days postinjury. (**B**) All experimental groups spent similar time on the RR. BD-1063 treatment did not influence behavioral outcomes after TBI. Data are presented as the means ± SEM (naïve n = 6, sham n = 9, TBI n = 15, BD-1063 10 mg/kg n = 7, BD-1063 30 mg/kg n = 8). p values for differences between groups were calculated using RM two-way ANOVA followed by Fisher's LSD test: * $p < 0.05$, ** $p < 0.01$, **** $p < 0.0001$ sham vs. TB. OD of the intensity of (**C**) Iba1 and (**D**) GFAP staining in the cortex, hippocampus, and thalamus. TBI induced significantly increased staining for Iba1 in the ipsilateral thalamus and for GFAP in the ipsilateral hippocampus and thalamus. (**E**) Representative images of Iba1 and GFAP staining at 7 days postinjury (total magnification = 40×, scale bar = 100 µm). Data are presented as the means ± SEM (n = 5). p values for differences between groups were calculated using the Kruskal–Wallis test followed by Dunn's test: # $p < 0.05$ compared with the sham group, * $p < 0.05$ compared with the TBI group. Differences between naïve and sham groups were calculated using the Mann–Whitney U-test: ^{n} $p < 0.05$ compared with the naïve animals.

We performed immunohistochemical staining to assess TBI-induced activation of microglia (Iba1) and astrocytes (GFAP) in the experimental groups (Figure 4C). The TBI group displayed significant increases in the intensity of Iba1 staining in the ipsilateral thalamus (lateral nucleus of the thalamus, $p = 0.023$, Kruskal–Wallis test followed by Dunn's test; Figure 4C) and GFAP staining in the ipsilateral hippocampus (hippocampal cornu ammonis 3 (CA3) region, $p = 0.018$, Kruskal–Wallis test followed by Dunn's test; Figure 4D) and thalamus ($p = 0.007$, Kruskal–Wallis test followed by Dunn's test; Figure 4D). Increased GFAP staining was also observed in the contralateral hippocampus of the TBI group ($p = 0.0043$, Kruskal–Wallis test followed by Dunn's test; Figure 4C). Due to the surgical procedure, sham animals presented significantly increased Iba1 (Figure 4C) and GFAP (Figure 4D) staining in the ipsilateral cortex 7 days after TBI ($p = 0.015$ compared with naïve animals, Mann–Whitney U-test), while no increase in staining was observed in the hippocampus and thalamus ($p > 0.05$, Figure 4C,D). Treatment with BD-1063 did not result in any significant differences in Iba1 and GFAP staining in the cortex, hippocampus, or thalamus compared with the TBI group (Figure 4C,D).

The duration of apnea and time to regain the righting reflex were equal for the TBI and BD-1063 treatment groups (ordinary one-way ANOVA, $p > 0.05$). No differences in body weight were observed between experimental groups after injury (RM two-way ANOVA, $p > 0.05$).

3. Discussion

In the present study, we used a lateral fluid percussion injury model of TBI to evaluate the role of S1R in the development of neurological deficits for up to 12 months after TBI. This model resulted in neurological and motor dysfunction in WT mice that was less pronounced in S1R-/- mice at 24 h after injury. TBI induced long-term cognitive impairments in WT mice but not in S1R-/- mice. WT TBI animals displayed significantly higher astroglia-related GFAP protein expression levels in the cortex, while GFAP protein expression levels in both S1R-/- sham and S1R-/- TBI animals were similar to those in the WT sham group at 12 months postinjury. S1R-/- animals exhibited substantially reduced GFAP expression in Bergmann glial cells in the molecular layer of the cerebellum compared to WT mice before and 12 months after TBI. In addition, we observed age-related behavioral changes in WT mice but not in S1R-/- mice. S1R-/- mice displayed preserved motor coordination and reduced despair-like behavior compared to WT mice over a 12-month period.

TBI is a chronic health condition with serious long-term consequences such as motor dysfunction, depression, cognitive deficits, and emotional changes [4,8,19]. Currently, no effective treatment is available for TBI-induced deficits other than supportive therapy [20]. Therefore, research on treatments that prevent the progression of brain damage after TBI is necessary. Drugs interacting with S1R have potential as treatments for neurological diseases, including TBI [13,14,21]. Here, S1R deficiency was associated with improved motor function and diminished neurological deficits in the acute phase after TBI. Previous studies have also shown that S1R deficiency attenuates neurodegenerative processes. For example, in the MPTP-induced Parkinsonism model, motor deficits and dopaminergic neuron death were less pronounced in S1R-/- mice than in WT mice [22]. Another study indicated that S1R-/- mice present reduced mechanical allodynia, macrophage/monocyte infiltration, and levels of the chemokine CCL2 in dorsal root ganglia after spinal nerve injury [23]. S1R deficiency alters cognitive function, especially in older mice [24], and is associated with more pronounced learning deficits and toxicity in APPSwe AD mice [25]. In contrast, we showed no changes in the spatial learning and memory abilities of S1R-/- mice for up to 10 months after TBI. In addition, we observed that both sham and TBI S1R-/- mice displayed less despair behavior than WT mice over a 12-month period. Our findings indicate an important role for S1R in the development of TBI-induced neurobehavioral deficits in the acute and chronic phases after TBI.

In recent years, accumulating evidence has shown that S1R is implicated in the modulation of neuronal physiology and synaptic plasticity [26]. Various anti-inflammatory

mechanisms have been postulated for S1R ligands that might account for their potential neuroprotective effects [27]. Astrocytes and microglia are considered key players in the initiation of an inflammatory response after injury [28]. Astrocytosis occurs in concert with neuronal degeneration [29,30] and has been noted in rodents, primarily in the cortex, within the first 24 h [31] and up to 12 months after TBI [32]. In the present study, TBI-induced astrocyte activation in the brain tissue was reduced in S1R-/- mice, suggesting that S1R deficiency prevents development of neurodegenerative processes in brain tissue 12 months postinjury. A recent study found that S1R deficiency reduced MPTP-induced astrocyte activation in the substantia nigra [22]. Another study documented increased GFAP expression in mixed astrocyte–neuronal cultures derived from S1R-/- mice, which seemed to counterbalance the cellular response to stressful conditions. [33] Similar to astrocytosis, in the context of many neurological disorders, chronic microglial activation is responsible for neurodegeneration [28]. Recent studies have shown that S1R agonists acutely decrease microglial activation following brain injury in vivo [13–15,21]. Although microglia remain highly activated in different brain regions up to 1 year after controlled cortical impact injury (CCI) [34], we did not observe any differences between the sham and TBI groups in terms of microglial activation at 12 months postinjury. The discrepancy in microglial activation might be due to the use of different types of TBI animal models. The CCI model produces more extensive damage to brain tissue [34] than the latFPI model used in the present study.

Impairments in motor function and coordination are common consequences of TBI and are usually associated with injury to the sensorimotor cortex [35]. However, the cerebellum also plays an important role in the control and coordination of movement that may be specifically related to motor dysfunction after TBI [36]. Here, we showed that both sham and TBI WT mice developed impairments in motor coordination with age, while S1R-/- mice exhibited preserved motor function. One of the possible explanations for motor dysfunction in WT mice is increased astrocyte activation in the cerebellum. Cerebellar astrocytosis reduces the survival of Purkinje cells, which are associated with movement and coordination, and leads to cerebellar dysfunction and motor impairments after TBI [37–39]. Here, S1R-/- mice displayed preserved motor coordination and almost no GFAP expression in the molecular layer of the cerebellum after TBI. Similarly, GFAP expression was substantially decreased in S1R-/- sham mice compared to WT mice. Based on localization, GFAP-positive astrocytes are Bergmann glia [40]. Bergmann glia directly regulate Purkinje cells and influence motor behavior [41,42]. We found no significant difference in total number of PCs in S1R-/- mice. This is in line with previous findings in which PC degeneration and motor dysfunction was associated with both increased GFAP expression and ablation of Bergmann glia [43–45]. Our data show that the improved motor coordination exhibited by S1R-/- mice could be due to decreased GFAP expression in Bergmann glial cells in the molecular layer of cerebellum. These results suggest important involvement of S1R in the regulation of information processing in the cerebellum and control mechanisms of motor behavior. Therefore, decreasing GFAP expression in Bergmann glia may represent a novel therapeutic strategy for motor dysfunction during ageing.

Since S1R-/- mice showed acute improvements in neurological function after TBI, we examined whether pharmacological treatment with an S1R antagonist influenced behavioral and histological outcomes after injury. Treatment with BD-1063 did not affect TBI-induced neurological deficits. Although we measured a sufficient concentration of BD-1063 in the brain tissue (6.3 $\pm$ 0.03 μg/g), no significant difference in S1R gene expression was observed between saline- and BD-1063-treated animals. S1R agonists are able to attenuate neurological deficits and lessen TBI-induced neurodegeneration by reducing microglial activation following brain injury in vivo [13,14,21]. In previous studies, BD-1063 was used to block the effect of S1R agonists [46,47]. Recently, oral treatment with BD-1063 induced neuroprotection in an SCI model by increasing the number of surviving motor neurons and decreasing microglial activation in the ventral horns of L4-L5 spinal

segments [48]. Thus, different S1R ligands may act differently and even adversely in neuroprotection.

In conclusion, S1R deficiency led to improved neurological and motor coordination, reduced despair-like behavior, preserved long-term cognitive function, and prevented TBI-induced neuroinflammation 12 months postinjury. S1R deficiency was associated with reduced GFAP expression in Bergmann glial cells in the cerebellum. These findings suggest a role for S1R in the pathogenesis of TBI and cerebellum-mediated motor behavior.

4. Materials and Methods

4.1. Animals and Experimental Design

Twenty-one S1R knockout (S1R-/-) male mice aged 10 weeks (Laboratorios Dr. Esteve S.A., Barcelona, Spain) were used to explore the effects of genetic deletion of S1R on traumatic brain injury. S1R-/- mice on a CD-1 genetic background were generated as described previously [49]. Twenty-two wild-type male mice (WT) aged 10 weeks (HSD:ICR(CD-1®), ENVIGO, Venray, Netherlands) of the same genetic background as the S1R-/- mice were used. Sixty-nine 12- to 14-week-old WT male mice were used to evaluate the effects of the S1R antagonist BD-1063 on injury. Ten 36-week-old male Swiss-Webster mice (Laboratory Animal Centre, University of Tartu, Tartu, Estonia) were used to investigate BD-1063 concentrations and S1R expression in brain tissue. Three S1R-/- mice (Laboratorios Dr. Esteve S.A., Barcelona, Spain) and three WT males aged 10 weeks were used to evaluate astrocyte activation in the cerebellum of intact animals. All animals were housed under standard conditions (21–23 °C, 12 h dark–light cycle, with lights off at 8 a.m. and on at 8 p.m.) with unlimited access to standard food (Lactamin AB, Mjölby, Sweden) and water in an individually ventilated cage housing system (Allentown Inc., Allentown, NJ, USA). Each cage contained EcoPure™ wood chip shavings (Datesand, Cheshire, UK), nesting material, and wood blocks from TAPVEI (TAPVEI, Paekna, Estonia). For enrichment, a transparent tinted (red) nontoxic durable polycarbonate safe harbor mouse retreat (Animalab, Poznan, Poland) was used. The mice were housed in groups of up to five mice per standard cage (38 × 19 × 13 cm). All studies involving animals were reported in accordance with the ARRIVE guidelines [50,51]. The experimental procedures were performed in accordance with the guidelines reported in EU Directive 2010/63/EU and with local laws and policies; all of the procedures were approved by the Latvian Animal Protection Ethical Committee of Food and Veterinary Service in Riga, Latvia.

A subset of animals subjected to experimental lateral fluid percussion injury was randomly separated into four experimental groups: WT sham (n = 10), S1R-/- sham (n = 10), WT TBI (n = 12), and S1R-/- TBI (n = 12). Mice were weighed before injury (baseline measurement), on the first day after the injury, and then weekly throughout the study as a measure of general health. Body weight was reported as a percent change relative to baseline. Behavioral tests were performed at baseline and 1, 7, and 14 days and 1, 3, 6, 9, and 12 months after injury. Mice were euthanized at 12 months postinjury, and brain tissue was collected for histological analysis. The study design is presented in Figure 5A.

One WT mouse and two S1R-/- animals were excluded due to dural breach during the surgical procedure. No animal subjected to sham injury was excluded. Over the 12 months of this study, 10 mice died prematurely (WT TBI n = 3, S1R-/- TBI n = 4, S1R-/- sham n = 3, Figure S2). For behavioral tests, all data points (including those generated by mice that eventually died prematurely) were included. For the histological analysis, only mice that survived up to the 12-month time point were included, and all available brain tissues were analyzed.

Treatment with the S1R antagonist BD-1063 was performed to evaluate the effect of pharmacological blockade of S1R. Mice were randomly divided into five groups: naïve (n = 6), sham (n = 12), TBI (n = 18), TBI + BD-1063 10 mg/kg (n = 16), and TBI + BD-1063 30 mg/kg (n = 16). The dose of BD-1063 was chosen based on previous in vivo studies [47]. Naïve and sham groups received the corresponding vehicle with the same volume and treatment regimen. BD-1063 (TOCRIS, Bristol, UK) at doses of 10 or 30 mg/kg or vehicle

(0.9% NaCl solution) was injected subcutaneously (sc) for 6 consecutive days prior to TBI. The last injection (total of 7 injections) was administered 1 h before TBI. Mice were weighed before (baseline measurement) and 1, 2, 3, and 7 days after injury as a measure of general health. Body weight was reported as a percent change relative to baseline. Behavioral tests were performed at baseline and 1, 3, and 7 days after injury. The study design is presented in Figure 5B.

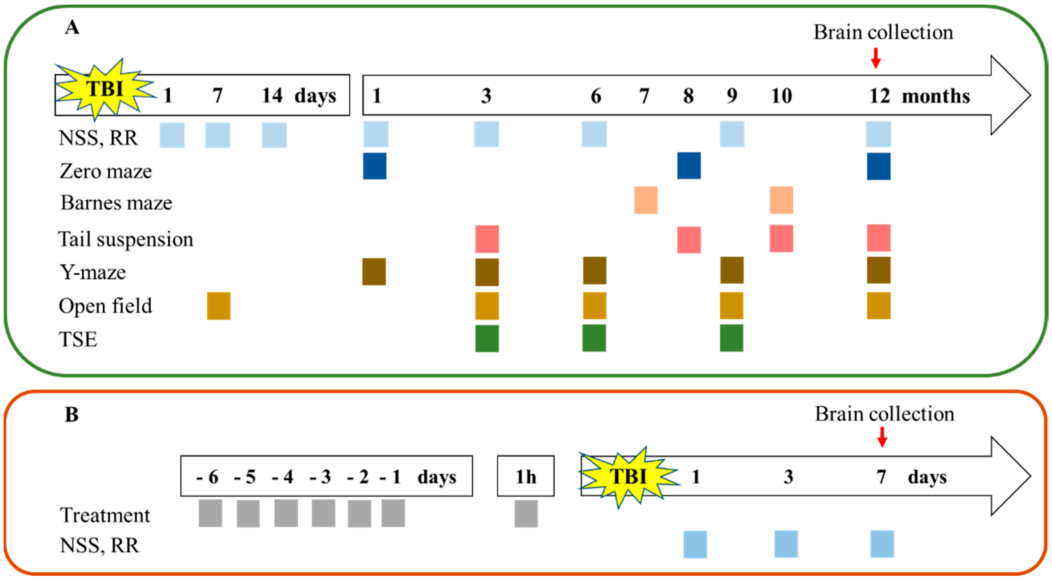

Figure 5. Schematic depicting the experimental design. (**A**) S1R-/- and WT mice were subjected to latFPI, and behavioral outcomes were assessed for up to 12 months postinjury. (**B**) BD-1063 was administered to evaluate the effects of pharmacological blockade of S1R. Behavioral outcomes were evaluated for up to 7 days postinjury. Brain tissues were collected from animals in both experiments for histological analysis at the end point. TBI—traumatic brain injury, NSS—neurological severity score, RR—rota-rod, TSE—PhenoMaster behavioral phenotyping.

Two mice (sham $n = 1$, TBI $n = 1$) died spontaneously during the pretreatment period. Two mice died during surgery (TBI $n = 1$, TBI + BD-1063 30 mg/kg $n = 1$). Fifteen animals were excluded due to dural breach during the surgical procedure (sham $n = 2$, TBI $n = 1$, TBI + BD-1063 10 mg/kg $n = 7$, TBI + BD-1063 30 mg/kg $n = 5$). Four mice died after TBI (TBI + BD-1063 10 mg/kg $n = 2$, TBI + BD-1063 30 mg/kg $n = 2$). For behavioral analyses, all data points (including those generated by mice that died after TBI) were included. Mice were euthanized at 7 days postinjury, and brain tissue was collected for histological analysis. Solutions for BD-1063 injections were prepared immediately before use in sterile saline from stock solutions with a concentration of 10 mg/mL that were previously prepared and stored at −20 °C. All analyses were conducted by investigators blinded to the group allocation. Behavioral tests were performed during the dark phase (from 9 a.m. to 4 p.m.).

4.2. Lateral Fluid Percussion Injury

The lateral fluid percussion injury (latFPI) model was established as previously described [52]. Briefly, anesthesia was induced with 4% isoflurane (Chemical Point, Deisenhofen, Germany) contained in a mixture of oxygen and nitrous oxide (70:30, AGA, Riga, Latvia) and maintained with 2% isoflurane using a face mask. Before trauma induction, the mice received a sc injection of tramadol (KRKA, Novo Mesto, Slovenia) (10 mg/kg). A craniectomy was performed using a 3 mm (outside diameter) circular trephine over the parietal region, 2 mm posterior to bregma and 2 mm right of midline. Injury was induced using a fluid percussion device connected to a pressure measurement instrument (Model FP 302, AmScience Instruments, Richmond, VA, USA). The duration of apnea was monitored immediately after the injury. Sham animals underwent the same procedures as

the animals in the latFPI group except for the induction of trauma. Mice with weight loss >20%, dural breech, or mortality within 24 h postinjury were excluded from the study.

4.3. Neurological Severity Score

The neurobehavioral status of the mice was assessed using the NSS as previously described [53]. The NSS consisted of nine individual clinical parameters, including tasks on motor function, alertness, and physiological behavior. The mice were assessed for the following items: presence of paresis; impairment of seeking behavior; absence of perceptible startle reflex; inability to get down a rectangle platform (34 × 27 cm); inability to walk on 3-, 2-, and 1-cm wide beams; and inability to balance on a vertical beam of 7 mm width and horizontal round stick of 5 mm diameter for at least 15 s. If a mouse showed impairment on one of these items, a value of 1 was added to its NSS score. Higher scores on the NSS thus indicate greater neurological impairment.

4.4. Rota-Rod Test

A rota-rod (Model 47600; Ugo Basile) test with slight modification was used to measure motor coordination [54]. Briefly, mice were pretrained on the rota-rod apparatus (5 rpm) with 2 sessions per animal, each lasting for 240 s. On the experimental day, mice were placed on the rod with an accelerating rotating speed from 5 to 25 rpm over a period of 240 s with a 30 min rest between trials. Time spent walking on the accelerating rota-rod before falling off was measured. The mean of two trials was calculated for each mouse.

4.5. Y-Maze Test

Working memory performance was assessed by recording spontaneous alternation behavior in a Y-maze, as previously described [55]. The mice were individually placed at the end of one arm in a symmetrical Y-shaped runway (arm length 35 cm, width 5 cm, height 21 cm) and allowed to explore the maze for 5 min. A spontaneous alternation behavior was defined as the entry into all three arms on consecutive choices in overlapping triplet sets (i.e., ABC, BCA, CBA). The percent spontaneous alternation behavior was calculated as the ratio of actual to possible alternations (defined as the total number of arm entries − 2) × 100.

4.6. Tail Suspension Test

Despair-like behavior was assessed by tail suspension test, as previously described [56]. Briefly, each animal was suspended with tape (17 cm) from a horizontal rod elevated 30 cm above a clean cage for 6 min. To prevent mice from climbing their tails, a clear hollow cylinder (Ø = 4.5 cm, h = 5.5 cm) was placed around the tail before suspension. Mice were recorded for 6 min using the digital HD video camera recorder (Handycam HDR-CX11E, Sony Corporation, Tokyo, Japan) and immobilization was analyzed during the last 4 min. Immobility included motionless time as well as passive swinging caused by momentum from movement.

4.7. Open Field Test

Locomotor and anxiety-like behavior was assessed using the open-field test. The open field was a square arena (44 × 44 cm) shielded by 30 cm high opaque walls. Square area (20 × 20 cm) was defined as the center. The mouse was gently placed in the center of the field and allowed to explore for 12 min. The distance traveled, velocity, and time spent in the center were recorded and analyzed for 4 min periods using an EthoVision video tracking system (version XT 11.5, Noldus Information Technology, Wageningen, The Netherlands).

4.8. Elevated Zero Maze Test

Anxiety was assessed using the elevated zero maze test. The apparatus consisted of a black circular platform (width: 4.5 cm, diameter 50 cm), placed 44 cm from the ground and

divided into four equal quadrants. Two opposite quadrants had 15 cm high dark, opaque walls (closed quadrants), while the other two had no walls (open quadrants). Mice were placed in the center of open quadrant, and allowed to explore for 5 min. Time spent in each quadrant was registered using an EthoVision video tracking system (version XT 11.5; Noldus, Wageningen, The Netherlands).

4.9. Barnes Maze Test

Spatial learning and memory were assessed using the Barnes maze test as previously described with slight modifications [57]. The test was performed on a brightly lit grey circular platform (diameter 92 cm) with 20 equally spaced holes (diameter 5 cm) located around the perimeter, an escape box fitted under in one of the holes, and visual cues in the periphery. On the first day, the animal was placed at the center of the platform using a glass beaker and allowed to acclimate for 2 min; the mouse was then guided to the target hole and allowed to stay there for 1 min. Mice then underwent four days of learning consisting of three consecutive trials separated by brief returns to their home cages. If the mouse did not enter the escape box (defined as all four paws leaving the surface of the platform) within the 180 s trial, the experimenter guided the mouse to the escape hole as before and allowed it to rest for 1 min before returning the animal to its home cage. During the 90 s probe trials (24 h and 7 days after the last learning), the escape box was removed, and the time spent in the area of the target hole was recorded using the EthoVision (version XT 11.5; Noldus, Wageningen, The Netherlands).

4.10. TSE PhenoMaster System (Indirect Calorimetry)

The feeding and drinking behavior and locomotor activity were tested using an eight-cage calorimetry system (PhenoMaster, TSE Systems, Bad Homburg, Germany), which allowed continuous and undisturbed recording. Mouse behaviors were continuously recorded for 72 h with the following measurements recorded every 15 min: water intake (mg/kg body weight), food intake (g/kg body weight), and locomotor activity (voluntary running wheel).

4.11. Determination of BD-1063 in the Brain Tissue Using UPLC/MS

The concentration of BD-1063 in brain tissue was measured using ultra-performance liquid chromatography–tandem mass spectrometry (UPLC/MS). BD-1063 was administered in mice for 7 consecutive days prior to tissue collection. Animals were euthanized 1 h after the last sc administration of BD-1063 at a dose of 30 mg/kg. Brain tissues were collected immediately after the decapitation of animals. The brains were divided into two hemispheres and one of the hemispheres was used for BD-1063 measurements, while the second half was used for quantitative PCR analysis for S1R. The brain hemisphere was homogenized in ice-cold Milli-Q water at a w/v ratio of 1:5 using bead-beating technology (Omni Bead ruptor 24; Omni International, Kennesaw, GA, USA) in 2 mL tubes [58]. The obtained homogenate was centrifuged at 16,500 rpm for 10 min at 4 °C. The supernatant was then decanted, and the pellet was homogenized in the same volume of Milli-Q water as previously used. The obtained homogenate was centrifuged at 16,500 rpm for 10 min at 4 °C. The supernatants were combined and stored at −80 °C until use.

Brain tissue extract (100 µL) was mixed with 400 µL of IS (Verapamil) solution in acetonitrile to precipitate proteins. The tubes were vortexed to mix and centrifuged at 10,000 rpm for 10 min. A volume of 400 µL of supernatant was transferred to chromatographic vial, diluted with 400 µL of 0.1% formic acid, and subjected to UPLC/MS analysis. The calibration curve was constructed by plotting ratios of peak areas (analyte/IS) versus BD-1063 concentration over the range of 4 to 1000 ng/mL.

UPLC was carried out using the Waters Acquity UPLC system equipped with the Acquity BEH C18 column (2.1 × 50mm, 1.7 µm). The mobile phase consisted of A (aqueous 0.1% formic acid) and B (acetonitrile) at a flow rate of 0.4 mL/min, using a gradient

elution: initial—5% B, 2.5 min—50% B, 3.5 min—98% B, 4.5min—98% B, 4.7 min—5% B, 6 min—5% B. The injection volume was 10 µL. The column temperature was 30 °C.

MS analysis was performed on a triple quadrupole mass spectrometer Quattro micro-Waters in ESI positive mode using multiple reaction monitoring of two transitions for BD-1063 from m/z 273.1 to m/z 137.1 and from m/z 273.1 to m/z 173.1 and the transition for verapamil from m/z 455.3 to m/z 165.2 (cone voltage, 30 V; collision energy, 25 eV). The MS conditions were as follows: desolvation gas (N2) flow, 800 L/h; desolvation temperature, 400 °C; ESI source temperature, 120 °C; and capillary voltage, 3.0 kV. Quantitative analysis was achieved using QuanLynx4.1 software (Waters).

4.12. Quantitative PCR

Brain hemispheres were stored at −80 °C until isolation of RNA. Total RNA was isolated, first-strand cDNA was synthesized, and quantitative PCR analysis for Sig1R was performed as described previously [59]. The primer sequences used in this study were as follows: Sigmar1 (NM_011014.3), 5′-CAT TCG GGA CGA TAC TGG-3′ (forward) and 5′-CCT GGG TAG AAG ACC TCA CTT TT-3′ (reverse) and Actb (NM_007393.5), 5′-CCT CTA TGC CAA CAC AGT GC-3′ (forward) and 5′-CAT CGT ACT CCT GCT TGC TG-3′ (reverse). The primers were obtained from Metabion, Germany. The relative expression levels for each gene were calculated using the ΔΔCt method, normalized to the expression of β-actin, and compared to the expression levels of control group animals.

4.13. Immunohistochemistry

Mice were anesthetized using intraperitoneal administration of ketamine (200 mg/kg) and xylazine (15 mg/kg). The depth of anesthesia was monitored by toe pinch. Animals were transcardially perfused at a speed of 3 mL/min with 0.01 M phosphate-buffered saline (PBS, pH = 7.4) for 5 min until the blood was completely removed from the tissue. After perfusion, brains were carefully dissected and fixed in 4% PFA overnight at 4 °C. Brains were cryoprotected with a 10–20–30% sucrose gradient over 72 h. Coronal sections (35 µm) were cut using a Leica CM1850 cryostat (Leica Biosystems, Buffalo Grove, IL, USA).

Samples were embedded in an optimal cutting temperature compound (Tissue-Tek® O.C.T.™ Compound, Sakura Finetek Europe B.V., Alphen aan den Rijn, The Netherlands) and placed in a dry ice/isopropanol slurry. Frozen samples were stored at −80 °C. Coronal sections (35 µm thick) of brain were cut using a cryostat Leica CM1850 (Leica Biosystems, Buffalo Grove, IL, USA) and stored in antifreeze buffer at −20 °C until staining was performed. The immunohistochemistry of free-floating sections was determined based on a method described previously [59]. The following primary antibodies were used in this study: rabbit anti-Iba1 antibody (1:2000; Abcam, Cat# ab153696, Cambridge, UK), rabbit anti-GFAP antibody (1:2000, Abcam, Cat# ab7260, Cambridge, UK), mouse anti-Calbindin D28K antibody (1:500, Santa Cruz Biotechnology, Cat# sc365360, Dallas, TX, USA), rabbit anti-EAAT2 antibody (1:5000, Abcam, Cat# ab205248, Cambridge, UK). The goat anti-rabbit IgG (H + L) (1:1000, Invitrogen, Cat# 65-6140, Carlsbad, CA, USA) and goat anti-mouse IgG (H + L) (1:1000, Invitrogen, Cat# 31800, Carlsbad, CA, USA) biotinylated antibodies were used as secondary antibodies. Samples stained with biotinylated antibody and incubated with streptavidin (HRP) (1:1000, Abcam, Cat# ab7403, Cambridge, UK) were processed with freshly prepared DAB reagent.

Images were taken with a Nikon Eclipse TE300 microscope (Nikon Instruments, Tokyo, Japan). Identical brain sections corresponding to identical anatomical structures were used for the analysis. The structures were validated using Allen Mouse Brain atlas (http://mouse.brain-map.org/static/atlas, accessed on 15 October 2021). For each antibody staining experiment, sections from all animals were processed in the same staining tray. Staining was quantified using ImageJ software (ImageJ v1.52a). Negative controls replacing the primary antibody with a buffer solution (TBS-T) only were performed. Eight-bit images were generated from the pictures and were cropped to contain the regions of interest. Means of optical density (OD) were used to quantify the

staining intensity of Iba1 and GFAP in specific brain structures. For OD analysis, calibration was performed in accordance with the instructions on the ImageJ software website (https://imagej.nih.gov/ij/docs/examples/calibration/, accessed on 15 October 2021). The number of Purkinje cells (PC) in the cerebellum was assessed in 10× magnification pictures. For each animal, six pictures of different areas of the cerebellum were taken, all including the PC layer. The number of PCs in each picture was counted and corrected for the length of the PC layer, which was measured by drawing a line through the PC layer using ImageJ and measuring the length of the line. Two criteria were used for cell counts: the cell body (1) was well defined (i.e., not blurred), and (2) had the general characteristic morphology of a PC (i.e., round cell body approximately 25–30 µm diameter located between the granule cell and molecular layers).

4.14. Statistical Analysis

The statistical analysis and visualization were performed using GraphPad Prism software (GraphPad Prism Software, Inc., La Jolla, CA, USA). The data were found to be normally distributed using the Shapiro–Wilk test. For behavioral tests, two-way mixed design repeated measures analysis of variance was used to calculate group differences at each time point. In all comparisons, Fisher's least-significant difference post hoc analysis was used when appropriate (one or both main factors were statistically significant). For histological evaluations, the Mann–Whitney U-test or Kruskal–Wallis test with Dunn's post hoc test was used. For overall mortality, the chi-square test was used for comparisons between groups. All data are presented as the means ± standard errors of the means. p values less than 0.05 were considered significant.

Supplementary Materials: The following are available online at https://www.mdpi.com/article/10.3390/ijms222111611/s1.

Author Contributions: Conceptualization, G.S., L.Z. and M.D.; methodology, validation and formal analysis, G.S., B.S., E.V. and L.Z.; behavioral analysis, L.L., E.V. and G.S.; histological analysis, G.S., E.V., A.M. and R.S.; BD-1063 concentration measurements, S.G. and B.G.; data analysis and interpretation, G.S., E.V. and L.Z.; writing—original draft preparation, G.S. and L.Z.; writing—review and editing, G.S., E.V., B.S., L.Z. and M.D. All authors have read and agreed to the published version of the manuscript.

Funding: This study was supported by EU-ERA-NET NEURON project TRAINS No. 9642151 and the European Union's Horizon 2020 research and innovation program under grant agreement No. 857394.

Institutional Review Board Statement: The study was conducted in accordance with the guidelines of the European Union Council (Directive 2010/63/EU). The experimental procedures were approved by the Latvian Animal Protection Ethical Committee of Food and Veterinary Service.

Informed Consent Statement: Not applicable.

Data Availability Statement: Data are available from the authors under reasonable request.

Acknowledgments: The authors thank Laboratorios Esteve, S.A. (Barcelona, Spain) for providing CD-1 background S1R-/- mice.

Conflicts of Interest: The authors declare no conflict of interest.

References

1. Berkner, J.; Mannix, R.; Qiu, J. Clinical traumatic brain injury in the preclinical setting. *Methods Mol. Biol.* **2016**, *1462*, 11–28. [CrossRef] [PubMed]
2. Maas, A.I.R.; Menon, D.K.; Adelson, P.D.; Andelic, N.; Bell, M.J.; Belli, A.; Bragge, P.; Brazinova, A.; Büki, A.; Chesnut, R.M.; et al. Traumatic brain injury: Integrated approaches to improve prevention, clinical care, and research. *Lancet Neurol.* **2017**, *16*, 987–1048. [CrossRef]
3. Blennow, K.; Brody, D.L.; Kochanek, P.M.; Levin, H.; McKee, A.; Ribbers, G.M.; Yaffe, K.; Zetterberg, H. Traumatic brain injuries. *Nat. Rev. Dis. Prim.* **2016**, *2*, 16084. [CrossRef] [PubMed]
4. Wilson, L.; Stewart, W.; Dams-O'Connor, K.; Diaz-Arrastia, R.; Horton, L.; Menon, D.K.; Polinder, S. The chronic and evolving neurological consequences of traumatic brain injury. *Lancet Neurol.* **2017**, *16*, 813–825. [CrossRef]

5. Ng, S.Y.; Lee, A.Y.W. Traumatic brain injuries: Pathophysiology and potential therapeutic targets. *Front. Cell. Neurosci.* **2019**, *13*, 528. [CrossRef] [PubMed]
6. Cheng, W.H.; Martens, K.M.; Bashir, A.; Cheung, H.; Stukas, S.; Gibbs, E.; Namjoshi, D.R.; Button, E.B.; Wilkinson, A.; Barron, C.J.; et al. CHIMERA repetitive mild traumatic brain injury induces chronic behavioural and neuropathological phenotypes in wild-type and APP/PS1 mice. *Alzheimer Res. Ther.* **2019**, *11*, 6. [CrossRef] [PubMed]
7. Tucker, L.B.; Velosky, A.G.; Fu, A.H.; McCabe, J.T. Chronic neurobehavioral sex differences in a murine model of repetitive concussive brain injury. *Front. Neurol.* **2019**, *10*, 509. [CrossRef]
8. Riggio, S. Traumatic brain injury and its neurobehavioral sequelae. *Neurol. Clin.* **2011**, *29*, 35–47. [CrossRef]
9. Nguyen, L.; Lucke-Wold, B.P.; Mookerjee, S.A.; Cavendish, J.Z.; Robson, M.J.; Scandinaro, A.L.; Matsumoto, R.R. Role of sigma-1 receptors in neurodegenerative diseases. *J. Pharmacol. Sci.* **2015**, *127*, 17–29. [CrossRef] [PubMed]
10. Su, T.P.; Junien, J.L. *Sigma Receptors in the Central Nervous System and the Periphery*; Itzhak, Y., Ed.; London Academic Press: Cambridge, MA, USA, 1994; pp. 21–44.
11. Vavers, E.; Svalbe, B.; Lauberte, L.; Stonans, I.; Misane, I.; Dambrova, M.; Zvejniece, L. The activity of selective sigma-1 receptor ligands in seizure models in vivo. *Behav. Brain Res.* **2017**, *328*, 13–18. [CrossRef]
12. Nguyen, L.; Lucke-Wold, B.P.; Mookerjee, S.; Kaushal, N.; Matsumoto, R.R. Sigma-1 receptors and neurodegenerative diseases: Towards a hypothesis of Sigma-1 receptors as amplifiers of neurodegeneration and neuroprotection. *Adv. Exp. Med. Biol.* **2017**, *964*, 133–152. [CrossRef]
13. Dong, H.; Ma, Y.; Ren, Z.; Xu, B.; Zhang, Y.; Chen, J.; Yang, B. Sigma-1 receptor modulates neuroinflammation after traumatic brain injury. *Cell. Mol. Neurobiol.* **2016**, *36*, 639–645. [CrossRef] [PubMed]
14. Wegleiter, K.; Hermann, M.; Posod, A.; Wechselberger, K.; Stanika, R.I.; Obermair, G.J.; Kiechl-Kohlendorfer, U.; Urbanek, M.; Griesmaier, E. The sigma-1 receptor agonist 4-phenyl-1-(4-phenylbutyl) piperidine (PPBP) protects against newborn excitotoxic brain injury by stabilizing the mitochondrial membrane potential in vitro and inhibiting microglial activation in vivo. *Exp. Neurol.* **2014**, *261*, 501–509. [CrossRef]
15. Sánchez-Blázquez, P.; Pozo-Rodrigálvarez, A.; Merlos, M.; Garzón, J. The sigma-1 receptor antagonist, S1RA, reduces stroke damage, ameliorates post-stroke neurological deficits and suppresses the overexpression of MMP-9. *Mol. Neurobiol.* **2018**, *55*, 4940–4951. [CrossRef] [PubMed]
16. Schetz, J.A.; Perez, E.; Liu, R.; Chen, S.; Lee, I.; Simpkins, J.W. A prototypical Sigma-1 receptor antagonist protects against brain ischemia. *Brain Res.* **2007**, *1181*, 1–9. [CrossRef] [PubMed]
17. Castany, S.; Gris, G.; Vela, J.M.; Verdú, E.; Boadas-Vaello, P. Critical role of sigma-1 receptors in central neuropathic pain-related behaviours after mild spinal cord injury in mice. *Sci. Rep.* **2018**, *8*, 3873. [CrossRef]
18. Lattard, A.; Poulen, G.; Bartolami, S.; Gerber, Y.N.; Perrin, F.E. Negative impact of Sigma-1 receptor agonist treatment on tissue integrity and motor function following spinal cord injury. *Front. Pharmacol.* **2021**, *12*, 614949. [CrossRef]
19. Semple, B.D.; Zamani, A.; Rayner, G.; Shultz, S.R.; Jones, N.C. Affective, neurocognitive and psychosocial disorders associated with traumatic brain injury and post-traumatic epilepsy. *Neurobiol. Dis.* **2019**, *123*, 27–41. [CrossRef] [PubMed]
20. Roozenbeek, B.; Lingsma, H.F.; Maas, A.I. New considerations in the design of clinical trials for traumatic brain injury. *Clin. Investig.* **2012**, *2*, 153–162. [CrossRef] [PubMed]
21. Moritz, C.; Berardi, F.; Abate, C.; Peri, F. Live imaging reveals a new role for the sigma-1 (σ1) receptor in allowing microglia to leave brain injuries. *Neurosci. Lett.* **2015**, *591*, 13–18. [CrossRef] [PubMed]
22. Hong, J.; Sha, S.; Zhou, L.; Wang, C.; Yin, J.; Chen, L. Sigma-1 receptor deficiency reduces MPTP-induced parkinsonism and death of dopaminergic neurons. *Cell Death Dis.* **2015**, *6*, e1832. [CrossRef]
23. Bravo-Caparrós, I.; Ruiz-Cantero, M.C.; Perazzoli, G.; Cronin, S.J.F.; Vela, J.M.; Hamed, M.F.; Penninger, J.M.; Baeyens, J.M.; Cobos, E.J.; Nieto, F.R. Sigma-1 receptors control neuropathic pain and macrophage infiltration into the dorsal root ganglion after peripheral nerve injury. *FASEB J.* **2020**, *34*, 5951–5966. [CrossRef]
24. Chevallier, N.; Keller, E.; Maurice, T. Behavioural phenotyping of knockout mice for the sigma-1 (σ_1) chaperone protein revealed gender-related anxiety, depressive-like and memory alterations. *J. Psychopharmacol.* **2011**, *25*, 960–975. [CrossRef] [PubMed]
25. Maurice, T.; Strehaiano, M.; Duhr, F.; Chevallier, N. Amyloid toxicity is enhanced after pharmacological or genetic invalidation of the σ(1) receptor. *Behav. Brain Res.* **2018**, *339*, 1–10. [CrossRef]
26. Ryskamp, D.A.; Korban, S.; Zhemkov, V.; Kraskovskaya, N.; Bezprozvanny, I. Neuronal Sigma-1 receptors: Signaling functions and protective roles in neurodegenerative diseases. *Front. Neurosci.* **2019**, *13*, 862. [CrossRef]
27. Jia, J.; Cheng, J.; Wang, C.; Zhen, X. Sigma-1 receptor-modulated neuroinflammation in neurological diseases. *Front. Cell. Neurosci.* **2018**, *12*, 314. [CrossRef]
28. Kumar, A.; Loane, D.J. Neuroinflammation after traumatic brain injury: Opportunities for therapeutic intervention. *Brain. Behav. Immun.* **2012**, *26*, 1191–1201. [CrossRef]
29. Maragakis, N.J.; Rothstein, J.D. Mechanisms of disease: Astrocytes in neurodegenerative disease. *Nat. Clin. Pract. Neurol.* **2006**, *2*, 679–689. [CrossRef]
30. Pekny, M.; Wilhelmsson, U.; Pekna, M. The dual role of astrocyte activation and reactive gliosis. *Neurosci. Lett.* **2014**, *565*, 30–38. [CrossRef]

31. Rosa, J.M.; Farre-Alins, V.; Navarrete, M.; Palomino-Antolin, A.; Fernandez-Lopez, E.; Narros-Fernandez, P.; Egea, J. TLR4-pathway impairs synaptic number and cerebrovascular functions through astrocyte activation following traumatic brain injury. *Br. J. Pharmacol.* **2021**, *178*, 3395–3413. [CrossRef]
32. Pischiutta, F.; Micotti, E.; Hay, J.R.; Marongiu, I.; Sammali, E.; Tolomeo, D.; Vegliante, G.; Stocchetti, N.; Forloni, G.; De Simoni, M.-G.; et al. Single severe traumatic brain injury produces progressive pathology with ongoing contralateral white matter damage one year after injury. *Exp. Neurol.* **2018**, *300*, 167–178. [CrossRef] [PubMed]
33. Weng, T.-Y.; Hung, D.T.; Su, T.-P.; Tsai, S.-Y.A. Loss of Sigma-1 receptor chaperone promotes astrocytosis and enhances the Nrf2 antioxidant defense. *Oxid. Med. Cell. Longev.* **2017**, *2017*, 4582135. [CrossRef] [PubMed]
34. Loane, D.J.; Kumar, A.; Stoica, B.A.; Cabatbat, R.; Faden, A.I. Progressive neurodegeneration after experimental brain trauma: Association with chronic microglial activation. *J. Neuropathol. Exp. Neurol.* **2014**, *73*, 14–29. [CrossRef]
35. Carron, S.F.; Alwis, D.S.; Rajan, R. Traumatic brain injury and neuronal functionality changes in sensory cortex. *Front. Syst. Neurosci.* **2016**, *10*, 47. [CrossRef] [PubMed]
36. Rapoport, M.; van Reekum, R.; Mayberg, H. The role of the cerebellum in cognition and behavior. *J. Neuropsychiatry Clin. Neurosci.* **2000**, *12*, 193–198. [CrossRef]
37. Mautes, A.E.; Fukuda, K.; Noble, L.J. Cellular response in the cerebellum after midline traumatic brain injury in the rat. *Neurosci. Lett.* **1996**, *214*, 95–98. [CrossRef]
38. Park, E.; McKnight, S.; Ai, J.; Baker, A.J. Purkinje cell vulnerability to mild and severe forebrain head trauma. *J. Neuropathol. Exp. Neurol.* **2006**, *65*, 226–234. [CrossRef]
39. Cerrato, V. Cerebellar astrocytes: Much more than passive bystanders in ataxia pathophysiology. *J. Clin. Med.* **2020**, *9*, 757. [CrossRef]
40. Nolte, C.; Matyash, M.; Pivneva, T.; Schipke, C.G.; Ohlemeyer, C.; Hanisch, U.K.; Kirchhoff, F.; Kettenmann, H. GFAP promoter-controlled EGFP-expressing transgenic mice: A tool to visualize astrocytes and astrogliosis in living brain tissue. *Glia* **2001**, *33*, 72–86. [CrossRef]
41. Wang, F.; Xu, Q.; Wang, W.; Takano, T.; Nedergaard, M. Bergmann glia modulate cerebellar Purkinje cell bistability via Ca^{2+}-dependent K^+ uptake. *Proc. Natl. Acad. Sci. USA* **2012**, *109*, 7911–7916. [CrossRef] [PubMed]
42. Sasaki, T.; Beppu, K.; Tanaka, K.F.; Fukazawa, Y.; Shigemoto, R.; Matsui, K. Application of an optogenetic byway for perturbing neuronal activity via glial photostimulation. *Proc. Natl. Acad. Sci. USA* **2012**, *109*, 20720. [CrossRef] [PubMed]
43. Cui, W.; Allen, N.D.; Skynner, M.; Gusterson, B.; Clark, A.J. Inducible ablation of astrocytes shows that these cells are required for neuronal survival in the adult brain. *Glia* **2001**, *34*, 272–282. [CrossRef]
44. Tyszkiewicz, C.; Pardo, I.D.; Ritenour, H.N.; Liu, C.N.; Somps, C. Increases in GFAP immunoreactive astrocytes in the cerebellar molecular layer of young adult CBA/J mice. *Lab. Anim. Res.* **2021**, *37*, 24. [CrossRef] [PubMed]
45. Wang, X.; Imura, T.; Sofroniew, M.V.; Fushiki, S. Loss of adenomatous polyposis coli in Bergmann glia disrupts their unique architecture and leads to cell nonautonomous neurodegeneration of cerebellar Purkinje neurons. *Glia* **2011**, *59*, 857–868. [CrossRef] [PubMed]
46. Nardai, S.; László, M.; Szabó, A.; Alpár, A.; Hanics, J.; Zahola, P.; Merkely, B.; Frecska, E.; Nagy, Z. N,N-dimethyltryptamine reduces infarct size and improves functional recovery following transient focal brain ischemia in rats. *Exp. Neurol.* **2020**, *327*, 113245. [CrossRef]
47. Katnik, C.; Garcia, A.; Behensky, A.A.; Yasny, I.E.; Shuster, A.M.; Seredenin, S.B.; Petrov, A.V.; Seifu, S.; McAleer, J.; Willing, A.; et al. Treatment with afobazole at delayed time points following ischemic stroke improves long-term functional and histological outcomes. *Neurobiol. Dis.* **2014**, *62*, 354–364. [CrossRef] [PubMed]
48. Gaja-Capdevila, N.; Hernández, N.; Zamanillo, D.; Vela, J.M.; Merlos, M.; Navarro, X.; Herrando-Grabulosa, M. Neuroprotective effects of Sigma 1 receptor ligands on motoneuron death after spinal root injury in mice. *Int. J. Mol. Sci.* **2021**, *22*, 6956. [CrossRef] [PubMed]
49. Langa, F.; Codony, X.; Tovar, V.; Lavado, A.; Giménez, E.; Cozar, P.; Cantero, M.; Dordal, A.; Hernández, E.; Pérez, R.; et al. Generation and phenotypic analysis of sigma receptor type I (sigma 1) knockout mice. *Eur. J. Neurosci.* **2003**, *18*, 2188–2196. [CrossRef] [PubMed]
50. Kilkenny, C.; Browne, W.; Cuthill, I.C.; Emerson, M.; Altman, D.G. Animal research: Reporting in vivo experiments: The ARRIVE guidelines. *Br. J. Pharmacol.* **2010**, *160*, 1577–1579. [CrossRef]
51. McGrath, J.C.; Drummond, G.B.; McLachlan, E.M.; Kilkenny, C.; Wainwright, C.L. Guidelines for reporting experiments involving animals: The ARRIVE guidelines. *Br. J. Pharmacol.* **2010**, *160*, 1573–1576. [CrossRef]
52. Kupats, E.; Stelfa, G.; Zvejniece, B.; Grinberga, S.; Vavers, E.; Makrecka-Kuka, M.; Svalbe, B.; Zvejniece, L.; Dambrova, M. Mitochondrial-protective effects of R-Phenibut after experimental traumatic brain injury. *Oxid. Med. Cell. Longev.* **2020**, *2020*, 9364598. [CrossRef]
53. Zvejniece, L.; Stelfa, G.; Vavers, E.; Kupats, E.; Kuka, J.; Svalbe, B.; Zvejniece, B.; Albert-Weissenberger, C.; Sirén, A.-L.; Plesnila, N.; et al. Skull fractures induce neuroinflammation and worsen outcomes after closed head injury in mice. *J. Neurotrauma* **2019**, *37*, 295–304. [CrossRef]
54. Zvejniece, L.; Svalbe, B.; Veinberg, G.; Grinberga, S.; Vorona, M.; Kalvinsh, I.; Dambrova, M. Investigation into stereoselective pharmacological activity of phenotropil. *Basic Clin. Pharmacol. Toxicol.* **2011**, *109*, 407–412. [CrossRef] [PubMed]

55. Zvejniece, L.; Vavers, E.; Svalbe, B.; Vilskersts, R.; Domracheva, I.; Vorona, M.; Veinberg, G.; Misane, I.; Stonans, I.; Kalvinsh, I.; et al. The cognition-enhancing activity of E1R, a novel positive allosteric modulator of sigma-1 receptors. *Br. J. Pharmacol.* **2014**, *171*, 761–771. [CrossRef]
56. Can, A.; Dao, D.T.; Terrillion, C.E.; Piantadosi, S.C.; Bhat, S.; Gould, T.D. The tail suspension test. *J. Vis. Exp.* **2012**, *59*, e3769. [CrossRef] [PubMed]
57. Gawel, K.; Gibula, E.; Marszalek-Grabska, M.; Filarowska, J.; Kotlinska, J.H. Assessment of spatial learning and memory in the Barnes maze task in rodents-methodological consideration. *Naunyn Schmiedebergs Arch. Pharmacol.* **2019**, *392*, 1–18. [CrossRef]
58. Verollet, R. A major step towards efficient sample preparation with bead-beating. *Biotechniques* **2008**, *44*, 832–833. [CrossRef] [PubMed]
59. Vavers, E.; Zvejniece, B.; Stelfa, G.; Svalbe, B.; Vilks, K.; Kupats, E.; Mezapuke, R.; Lauberte, L.; Dambrova, M.; Zvejniece, L. Genetic inactivation of the sigma-1 chaperone protein results in decreased expression of the R2 subunit of the GABA-B receptor and increased susceptibility to seizures. *Neurobiol. Dis.* **2021**, *150*, 105244. [CrossRef] [PubMed]

frontiers | Frontiers in Neurology

TYPE Original Research
PUBLISHED 20 September 2022
DOI 10.3389/fneur.2022.985895

OPEN ACCESS

EDITED BY
Hengli Tian,
Shanghai Jiao Tong University School of Medicine, China

REVIEWED BY
Alina Arulsamy,
Monash University, Malaysia
Bridgette D. Semple,
Monash University, Australia

*CORRESPONDENCE
Gundega Stelfa
gundega@farm.osi.lv

SPECIALTY SECTION
This article was submitted to Neurotrauma, a section of the journal Frontiers in Neurology

RECEIVED 04 July 2022
ACCEPTED 22 August 2022
PUBLISHED 20 September 2022

CITATION
Stelfa G, Svalbe B, Vavers E, Duritis I, Dambrova M and Zvejniece L (2022) Moderate traumatic brain injury triggers long-term risks for the development of peripheral pain sensitivity and depressive-like behavior in mice. *Front. Neurol.* 13:985895. doi: 10.3389/fneur.2022.985895

Moderate traumatic brain injury triggers long-term risks for the development of peripheral pain sensitivity and depressive-like behavior in mice

Gundega Stelfa[1,2]*, Baiba Svalbe[1], Edijs Vavers[1], Ilmars Duritis[2], Maija Dambrova[1,3] and Liga Zvejniece[1]

[1]Laboratory of Pharmaceutical Pharmacology, Latvian Institute of Organic Synthesis, Riga, Latvia, [2]Faculty of Veterinary Medicine, Latvia University of Life Sciences and Technologies, Jelgava, Latvia, [3]Department of Pharmaceutical Chemistry, Faculty of Pharmacy, Rīga Stradiņš University, Riga, Latvia

As traumatic brain injury (TBI) is one of the major causes of permanent disability, there is increasing interest in the long-term outcome of TBI. While motor deficits, cognitive impairment and longer-term risks of neurodegenerative disease are well-established consequences in animal models of TBI, pain is discussed less often despite its high prevalence. The current study addresses the need to characterize the extent of chronic pain and long-term behavioral impairments induced by moderate lateral fluid percussion injury (latFPI) in mice up to 12 months post-TBI and evaluates the validity of the model. Adult male BALB/c mice were subjected to latFPI, and the results were compared with outcomes in sham-operated mice. Mouse behavior was assessed at 1 and 7 days and 1, 3, 6, 9, and 12 months post-injury using sensory-motor (neurological severity score, NSS), cold (acetone) and mechanical sensitivity (von Frey), depressive-like behavior (tail suspension), locomotor (open field), motor coordination (rotarod) and cognitive (Morris water maze, y-maze, passive avoidance) tests. Animals with TBI demonstrated significantly higher NSS than the sham-operated group for up to 9 months after the injury. Cold sensitization was significantly increased in the contralateral hind paw in the TBI group compared to that of the sham group at 3, 6, and 9 months after TBI. In the von Frey test, the withdrawal threshold of the contralateral and ipsilateral hind paws was reduced at 6 months after TBI and lasted for up to 12 months post-injury. latFPI induced progressive depressive-like behavior starting at 6 months post-injury. No significant deficits were observed in memory, motor coordination or locomotion over the 12-month assessment period. The present study demonstrates that moderate TBI in mice elicits long-lasting impairment of sensory-motor function, results in progressive depression and potentiates peripheral pain. Hence, the latFPI model provides a relevant preclinical setting for the study of the link between brain injury and chronic sequelae such as depression and peripheral pain.

KEYWORDS

long-term behavioral outcome, lateral fluid percussion injury, pain, depression, traumatic brain injury

Introduction

Traumatic brain injury (TBI) is one of the leading causes of trauma-related permanent disability worldwide, especially in people under the age of 45 (1–3). Worldwide estimates suggest that more than 50 million new TBIs occur each year, with approximately 70–90% of patients having mild to moderate TBI (4). While many symptoms of mild to moderate TBI dissipate rapidly after injury, these patients frequently experience unusually high rates of chronic pain (5). It is widely recognized that the experience of pain is a frequent occurrence in TBI patients (6). In most of these instances, chronic pain is located in the head and is associated with brain tissue damage (7). Pain in TBI patients has also been reported in seemingly intact body regions, such as the upper and lower limbs (7, 8). However, chronic post-TBI pain in non-head body regions could also be associated with local injury (e.g., fractures, wounds), peripheral neuropathy or a related spinal injury (7). Therefore, the anatomical source of pain in TBI patients is often not identifiable when pain is chronic (9). To date, the mechanisms for chronic pain in TBI patients are largely unknown (7). Psychological disorders, including depression, following TBI are commonly reported comorbidities of posttraumatic pain (5). Depression and pain following TBI are believed to exacerbate each other, and both are rooted in common biological mechanisms, such us shared neurotransmitter pathways in periaqueductal gray, which is a key anatomic structure in the pain modulation system (10, 11). In animal models of TBI, the response to the peripheral pain reflex, such as mechanical and thermal sensitivity, has been studied up to 2 months after controlled cortical injury (CCI) and fluid percussion injury (FPI) (12). Only a small subset of experimental TBI models evaluated long-term consequences after injury (>6 months after TBI, see Supplementary Table S1). It has been demonstrated that mice subjected to cortical impact injury (CCI), which is often characterized by extensive brain tissue loss, demonstrate persisting behavioral deficits, such as depressive-like behavior, cognitive decline and motor dysfunction, up to 12 months after injury (13–16) (see Supplementary Table S1). However, more moderate CCI produces less extensive morphological damage (tissue loss at the cortical region) and less prominent behavioral deficits (17) (see Supplementary Table S1). Only a few studies have evaluated long-term behavioral changes in rats following FPI, mostly limited to single time points or memory evaluation (18–20).

We recently reported that CD-1 background mice develop neurological and cognitive impairments over a 12-month assessment period after lateral FPI (latFPI) (21). It should be noted that behavioral outcomes after TBI could depend on the background strains of mice (22). Most long-term follow-up TBI studies have been performed on C57Bl/6 background mice. It is known that different mouse strains vary in their inherent behavioral characteristics (23). For example, C57BL/6 and BALB/c mice exhibit differences in anxiety-like and depressive-like behavior, pain sensitivity, motor performance, learning and memory (24–27). The aim of the present study was to characterize the development of pain sensitivity and depressive-like behavior up to 1 year after the latFPI model in BALB/c background male mice. In addition, cognitive function, general activity and sensorimotor and coordination abilities were evaluated to provide a complete and relevant description of the long-term behavioral changes induced by TBI in mice. We found increased pain sensitivity with ongoing depressive-like behavior up to 1 year after latFPI in mice. The assessment and interplay between both conditions post-TBI should be more detailly investigated in the future preclinical and clinical studies, that may lead to the rational design of therapies that both reduce and improve functional outcomes after TBI.

Materials and methods

Animals

Twenty male Balb/c mice (Envigo, Venray, Netherlands) 10-week-old, weighing 20–26 g, were used in this study. All animals were housed under standard conditions (21–23°C, 12 h light-dark cycle) with unlimited access to standard food (Lactamin AB, Mjölby, Sweden) and water in an individually ventilated cage housing system (Allentown Inc., Allentown, New Jersey, USA). Each cage contained bedding of EcoPure^{TM} Shavings wood chips (Datesand, Cheshire, UK), nesting material and a wooden block from TAPVEI (TAPVEI, Paekna, Estonia). For the enrichment, transparent tinted (red) non-toxic durable polycarbonate safe harbor mouse retreat (Animalab, Poznan, Poland) was used. The mice were housed with up to 5 mice per standard cage (38 × 19 × 13 cm). All studies involving animals were reported in accordance with the ARRIVE guidelines (28). The experimental procedures were performed in accordance with the guidelines reported in the EU Directive 2010/63/EU and in accordance with local laws and policies; all procedures were approved by the Latvian Animal Protection Ethical Committee of Food and Veterinary Service in Riga, Latvia.

The lateral fluid percussion injury model

The lateral fluid percussion injury model was performed as previously described (29). Briefly, mice were anesthetized using 5% isoflurane dissolved in 100% oxygen. After the onset of anesthesia, the concentration of isoflurane was decreased to 2.5%. Before trauma induction, the mice received a subcutaneous administration of tramadol at a dose of 10 mg/kg (KRKA, Novo Mesto, Slovenia). A craniectomy was performed using a 3 mm (outside diameter) circular trephine over the parietal region, 2 mm posterior to bregma and 2 mm right of

midline. The bone flap was gently pulled from the underlying dura, leaving it intact. An injury hub (Leur-Loc syringe hub cut from a 23-gauge needle) was affixed to the skull using dental cement and then filled with sterile saline. An injury of 0.83 ± 0.09 ATM was induced using a fluid percussion device connected to a pressure measurement instrument (Model FP 302, AmScience Instruments, Richmond, VA, USA). Duration of apnea was monitored immediately after the injury. After the injury, the bone flap was put back, the wound was closed, and the mouse was placed in an awakening cage. Sham-injured animals underwent the same procedures as the animals in the latFPI group, except for trauma induction.

Behavioral tests

Animals were randomly separated into two experimental groups, sham-operated (n = 10) and latFPI (n = 10). The body weight of the mice was measured before injury (baseline measurement), on the first 3 days after the injury and then weekly throughout the study as a measure of general health. Behavioral tests were performed at baseline, 1 and 7 days, and 1, 3, 6, 9, and 12 months after the injury. Behavioral testing was conducted by an experimenter blinded to the study group. Tests were performed from the least aversive to the most aversive (neurological severity score < rotarod < open-field < Y-maze < acetone < von Frey < passive avoidance < tail suspension < Morris water maze test) with at least 2-day intervals among them to relieve animal's stress. The timeline of experimental procedures and the number of animals at each behavioral testing time point are given in Figure 1.

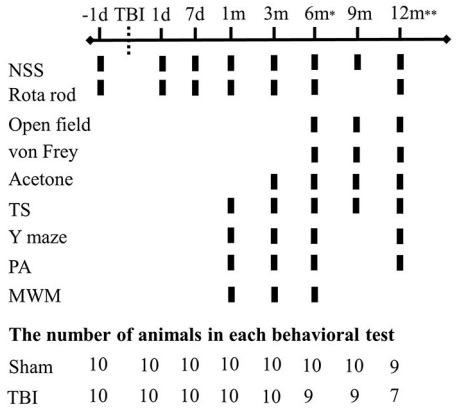

FIGURE 1
Experimental schedule for behavioral evaluation. Functional deficits were assessed at multiple intervals up to 12 months post-injury (n = 10/group). (d-days, m-months, NSS-neurological severity score, TS-tail suspension, PA-passive avoidance, MWM-Morris water maze). *One animal died in the TBI group. **Two animals died in the TBI group and one animal died in the sham group.

Neurological severity score (NSS)

The neurobehavioral status of mice was assessed using the NSS as previously described (29). The NSS consisted of nine individual clinical parameters, including tasks on motor function, alertness and physiological behavior. The mice were assessed for the following items: the presence of paresis; impairment of seeking behavior; absence of perceptible startle reflex; inability to get down a rectangle platform (34 × 27 cm); inability to walk on 3-, 2-, and 1-cm wide beams; and inability to balance on a vertical beam of 7 mm width and a horizontal round stick of 5 mm diameter for at least 15 s. If a mouse showed impairment on one of these items, a value of 1 was added to its NSS score. Higher scores on the NSS thus indicate more significant neurological impairment.

Electronic von frey test

Mechanically evoked pain-like behavior (mechanical sensitivity) was measured using an electronic von Frey plantar aesthesiometer (Dynamic Plantar Aesthesiometer, Model 37400-002, Ugo Basile, Gemonio VA, Italy) as previously described (30). During the test, the mice were placed on a metallic grid floor in an individual plastic observation chamber (10 cm W x 10 cm L x 14 cm H) and allowed to habituate to the environment for 30 min. The von Frey filament was applied to the midplantar surface of the hind paw. The withdrawal threshold was defined as the average latency time (s) required for causing withdrawal of the stimulated paw over three trials.

Acetone evaporation test

Cold-evoked pain-like behavior (cold sensitivity) was measured by applying a drop of acetone to the plantar surface of the hind paw (31). 1 day before the experiment and on the experimental day, mice were placed in individual plastic cages (10 cm W × 10 cm L × 14 cm H) on an elevated wire mesh metal floor and habituated for at least 30 min. On the experimental day, acetone was loaded into a 1-ml syringe without a needle. Air bubbles were cleared from the syringe before acetone application. One drop of acetone (approximately 40 μl) was applied to the paw from the bottom of the elevated cage through the wire mesh metal floor and onto the plantar surface of the hind paw. For 45 s, the mouse was scored on lifting, biting, and licking the paw. Each hind paw was measured twice with an interstimulation interval of approximately 15 min. The reaction duration was measured and analyzed as a cumulative reaction time.

Rotarod test

A rotarod test with slight modification was used to measure motor coordination (32). Briefly, mice were pre-trained (5 rpm) on the rotarod apparatus (Model 47650, Ugo Basile, Gemonio VA, Italy) with two sessions per animal, each lasting 240 s. On an experimental day, mice were placed on the rod with an accelerating rotating speed from 5 to 25 rpm for 240 s with a 30 min rest between trials. Time spent walking on the accelerating rotarod before falling off was measured. The mean of two trials was calculated for each mouse.

Passive avoidance test

The passive avoidance test was performed as previously described (32). Briefly, on the training day, each mouse was individually placed in the light compartment of an apparatus with no access to the dark compartment and allowed to explore for 60 s (Ugo Basile, Comerio, Italy). After this time, the sliding door (4 × 4 cm) was automatically opened, and the mouse was allowed to cross over into the dark compartment. Upon entering the dark compartment, the door was closed, and the mouse received a shock of 0.3 mA for 3 s. After 20 s, the mouse was returned to its home cage. A retention test was performed on the next day (24 h later) without any shock. The time to enter the dark compartment was recorded as the retention latency. The maximum retention latency was set at 540 s.

Y-maze test

Working memory performance was assessed by recording spontaneous alternation behavior in a Y-maze, as previously described (33). The experiment was conducted in a dimly red-lit room. The mice were individually placed at the end of one arm in a symmetrical Y-shaped runway (arm's length 35, width 5, height 21 cm) and allowed to explore the maze for 5 min. The total number and sequence of arm entries were manually recorded, and the percentage of alternation behavior was calculated.

Morris water maze test

The Morris water maze (MWM) was used to assess spatial cognition as previously described (34). The MWM apparatus was a blue-painted circular fiberglass pool (height: 60 cm, diameter: 150 cm) located in a test room surrounded by several cues. The experiment was conducted in a dimly red-lit room. The pool was virtually divided into four equal imaginary quadrants identified as a target, opposite, left and right. During the training trials, the animals were trained to find the hidden platform in the pool for four consecutive days, four trials per day. The mice were gently placed into the water facing the pool wall at one of four imaginary starting positions (target, opposite, left and right) around the perimeter of the pool. The trials were performed for up to a maximum of 90 s. If the mouse reached the platform within 90 s, it was allowed to remain there for 15 s; if not—mouse was guided to the platform and then allowed to rest on the platform for 15 s. The inter-trial interval was at least 20 min. After every trial, mice were placed in a drying cage and allowed to dry before they were returned to their home cages. The results were expressed as latency in finding the hidden platform. Probe trials were performed 24 h and 6 days after the last training trial with removal of the platform from the pool. All mice began swimming from a position opposite the target quadrant and were allowed to spend 90 s in the pool. In the probe trial, time in the target quadrant and swimming distance were analyzed using EthoVision video tracking system (version XT 11.5, Noldus Information Technology, Wageningen, Netherlands).

Tail suspension test

Depression-like behavior was assessed by tail suspension test, as previously described (21). Briefly, each animal was suspended with tape (17 cm) from a horizontal rod elevated 30 cm above a clean cage for 6 min. To prevent mice from climbing their tails, a clear hollow cylinder (Ø = 4.5 cm, H = 5.5 cm) was placed around the tail before the suspension. Mice were recorded for 6 min using the digital HD video camera recorder (Handycam HDR-CX11E, Sony Corporation, Tokyo, Japan), and immobilization was analyzed during the last 4 min.

Open-field test

Locomotor activity was assessed by an open-field test. The open-field was a square arena (44 × 44 cm) shielded by 30 cm high opaque walls. The Square area (20 × 20 cm) was defined as the center. The mouse was gently placed in the center of the field and allowed to explore for 12 min. The distance traveled, velocity and time spent in the center were recorded and analyzed for 4 min sessions using the EthoVision video tracking system (version XT 11.5, Noldus Information Technology, Wageningen, Netherlands).

Statistical analysis

The statistical calculations were performed using the GraphPad Prism 8.1 software (Graph Pad Prism software, Inc., La Jolla, CA, USA). The Shapiro-Wilk test was used to test the distribution of the data. A two-way mixed-design analysis of variance with repeated measures (two-way RM ANOVA) was used to calculate group differences at each time-point, which included one between-subjects variable (latFPI vs. sham) and one within-subjects variable (time). In all comparisons, Fisher Least Significant Difference (LSD) *post-hoc* analysis was used when appropriate (one

or both main factors were statistically significant). Area under curve (AUC) values were compared with an ordinary one-way ANOVA. Statistical outliers were identified using Grubbs' test ($\alpha = 0.05$). Two statistical outliers were removed from the sham group at 3 month-time point in acetone and MWM tests. All data are presented as mean ± standard error means (SEM). *P*-values <0.05 were considered significant.

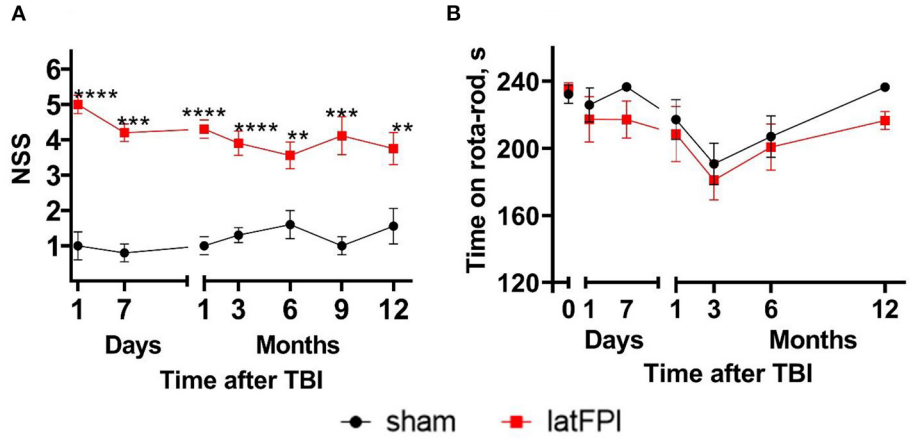

FIGURE 2
Neurological status of mice following latFPI. Brain-injured animals showed significant neurological impairments up to 12 months post-injury compared to sham-operated animals **(A)**. Motor coordination was not affected by latFPI during the 12-month assessment period **(B)**. Data are expressed as mean ± SEM. $^{**}p < 0.01$; $^{***}p < 0.001$; $^{****}p < 0.0001$ vs. sham group (two-way RM ANOVA followed by Fisher's LSD test).

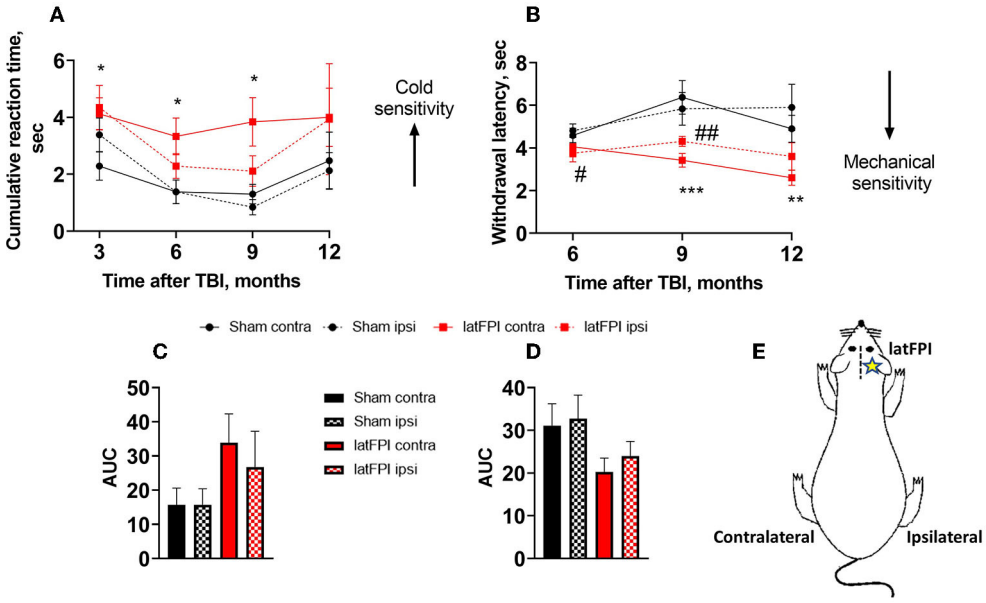

FIGURE 3
Cold and mechanical sensitivity following latFPI in mice. The cumulative reaction time of contralateral and ipsilateral hind paw licking or shaking in the acetone test **(A)** and latency of contralateral and ipsilateral hind paw withdrawal in the electronic von Frey test **(B)** were recorded 3, 6, 9, and 12 months post-injury. Data are expressed as mean ± SEM. $^{*}p < 0.05$; $^{**}p < 0.001$ contralateral latFPI vs. contralateral sham hind paw. $\#p < 0.05$; $\#\#p < 0.001$ ipsilateral latFPI vs. ipsilateral sham hind paw (two-way RM ANOVA followed by Fisher's LSD test). The area under the curve (AUC) in the acetone **(C)** and von Frey tests **(D)**. The AUC was calculated over the whole post-injury period. Schematic drawing of contralateral and ipsilateral sides. The contralateral hind paw corresponds to the opposite side of the lesion, and the ipsilateral hind paw corresponds to the lesion side **(E)**. Data are expressed as mean ± SEM. $^{*}p < 0.05$; $^{**}p < 0.01$; $^{***}p < 0.01$ vs. sham group (one-way ANOVA followed by Dunnett's test).

Results

latFPI impairs sensorimotor ability up to 12 months post-injury

Sensorimotor function was assessed using the NSS. The NSS was significantly higher for the latFPI group than for the sham-operated mice up to 12 months post-injury ($p < 0.0001$, Figure 2A). Brain-injured animals mostly failed in grip strength and balance tasks. The accelerating rotarod test was used to monitor motor coordination throughout the study. Time on rotarod was not significantly different between latFPI and sham animals at any time point post-injury (Figure 2B).

latFPI induces chronic cold and mechanical sensitivity

Peripheral cold sensitivity was evaluated by acetone test. The cumulative reaction time of the contralateral hind paw (opposite side to the lesion) was increased in the latFPI group compared to the sham group at 3 months (4.1 ± 0.6 s vs. 2.3 ± 0.5 s, $p = 0.026$), 6 months (3.3 ± 0.7 s vs. 1.0 ± 0.2 s, $p = 0.007$) and 9 months post-injury (3.8 ± 0.9 s vs. 1.2 ± 0.2 s, $p = 0.014$, Figure 3A). The AUC was not significantly different between latFPI (34 ± 9 for contralateral, 27 ± 10 for ipsilateral hind paw) and sham mice (16 ± 5 for contralateral, 16 ± 5 for ipsilateral hind paw, $p = 0.234$, Figure 3C).

Peripheral mechanical sensitivity was evaluated by the von Frey test. A significant decrease in the mechanical withdrawal latency of the contralateral hind paw was observed in the latFPI group compared to the sham group at 9 months (3.4 ± 0.3 s vs. 5.9 ± 0.7 s, $p = 0.001$) and 12 months post-injury (2.6 ± 0.4 s vs. 4.9 ± 0.4 s, $p = 0.0113$, Figure 3B). The withdrawal latency was also significantly decreased in the ipsilateral hind paw in latFPI mice compared to sham mice 12 months post-injury (3.6 ± 0.6 s vs. 5.9 ± 0.7 s, $p = 0.0157$, Figure 3B). The AUC was not significantly different between latFPI (20 ± 3 for contralateral, 24 ± 4 for ipsilateral hind paw) and sham animals (31 ± 5 for contralateral, 33 ± 5 for ipsilateral hind paw, $p = 0.1627$, Figure 3D).

latFPI results in progressive depression-like behavior

Depressive-like behavior was assessed by the tail suspension test. Immobility time was significantly increased in the latFPI group 6 months (94.7 ± 7.9 vs. 66.4 ± 10.0, $p = 0.040$) and 12 months (136.8 ± 10.5 vs. 70.2 ± 13.3, $p = 0.001$, $p = 0.001$) post-injury compared to the sham group (Figure 4). Throughout the experiment, brain-injured animals displayed significantly longer immobility times starting at 6 months compared to 1 month post-injury ($p = 0.009$, Figure 4). Immobility time remained unchanged over time in sham animals (Figure 4).

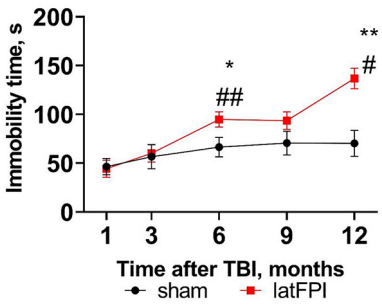

FIGURE 4
Depressive-like behavior was determined by the time spent immobile in the tail suspension test 1, 3, 6, 9, and 12 months after latFPI. Data are expressed as mean ± SEM. *$p < 0.05$, **$p < 0.01$ vs. sham, #$p < 0.05$, ##$p < 0.001$ compared to 1 month (two-way RM ANOVA followed by Fisher's LSD test).

latFPI produces no spatial learning and memory impairments

MWM was performed to evaluate spatial learning and memory. During the learning trials, no differences in latency to reach the platform were seen between groups, indicating comparable learning of the task (data not shown). During the probe trial, which was carried out 24 h following the last day of learning, both groups spent a similar amount of time in the target quadrant (Figure 5A). In addition, both groups showed a preference for the target quadrant compared to other quadrants of the pool (Supplementary Figure S1A), indicating that latFPI exposure did not impair hippocampal-dependent memory of a previously learned platform location at any time point. At 7 days following the last day of learning, brain-injured mice did not show a preference for any of the quadrants 3 months after injury ($p > 0.05$ for target vs. other quadrants, Figure 5B). There was a trend toward decreased time spent in the target quadrant in latFPI animals ($p = 0.0565$); however, the difference failed to reach significance between groups (mean % 54 ± 6 for sham vs. 30 ± 8 for latFPI, Figure 5B). No differences in any evaluated parameters were seen at 1- and 6-months post-injury. There were no differences between groups in swimming distance, suggesting no effect on enhanced or impaired physical function that could account for group differences (Supplementary Table S2).

Y-maze testing revealed no significant changes in spontaneous alterations or total arm entries, indicating no impairments in working memory (Figures 6A,B). Likewise, there was no significant effect of injury on contextual memory

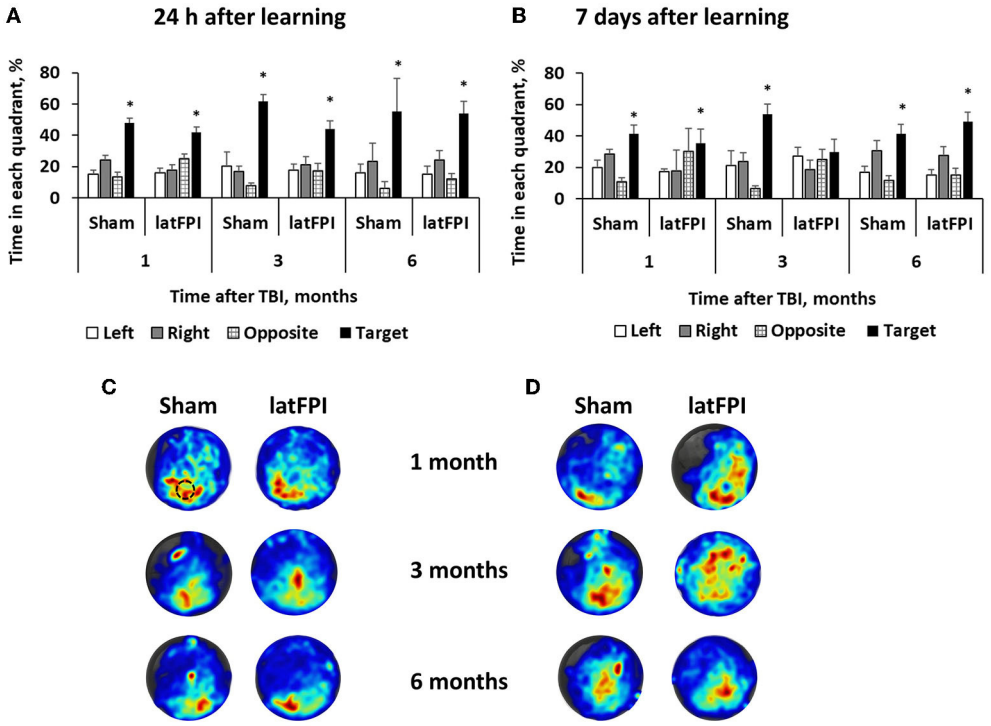

FIGURE 5
Assessment of spatial memory by the Morris water maze 1, 3 and 6 months after latFPI. Percentage of time spent in each quadrant 24 h **(A)** and 7 days **(B)** after the last training day. Heatmaps representing weighted occupancy across the entire 90 s probe trial 24 h **(C)** and 7 days **(D)** after the last training day 1, 3, and 6 months post-injury. Hot colors indicate longer dwell times. The platform area is denoted with a black circle. Data are expressed as mean ± SEM for the entire 90 sec, $*p < 0.05$ target quadrant vs. at least 2 other quadrants (one-way ANOVA followed by Dunnett's multiple comparison test).

assessed by the passive avoidance test. Sham and TBI mice exhibited a similar time to enter the dark compartment 24 h after learning up to 12 months post-injury (Figure 6D). We observed increased step-through latency on the learning day over time, suggesting potential habituation due to repeated measures in the same environment (Figure 6C).

latFPI has no impact on general health and activity

No animal subjected to sham injury was excluded. The length of the apnea for the animals subjected to latFPI was 47.2 ± 6.7 s. The body weight was slightly decreased up to 3 days post-injury for latFPI mice compared to sham mice, but there were no differences between groups during the whole period (Supplementary Figure S1A). Some mice were lost throughout the year of the study, but the deaths were spontaneous (one from the sham group and three from the TBI group) (Supplementary Figure S1B). latFPI mice showed no locomotion deficits within 12 months post-injury. In the open field test, brain-injured mice were more active at 6 months post-injury than sham mice ($p = 0.004$), although this effect had dissipated at 9 and 12 months post-injury (Supplementary Table S3). In the Y-maze test, the number of arm entries in the latFPI group was similar to that in the sham group (Supplementary Table S2, Figure 6B).

Discussion

In the present study, we demonstrated that brain injury to mice results in long-lasting and continually evolving alterations in behavior (Figure 7). Over time, a single latFPI induced persistent cold and mechanical peripheral pain up to 12 months after injury. Our experimental data also revealed that TBI increased immobility time in the tail suspension test, suggesting the development of depression-like behavior. This is the first study to examine the prevalence of persistent peripheral pain over long-term follow-up in mice after experimental TBI, suggesting that latFPI in mice provides a suitable platform to investigate the biological mechanisms of peripheral pain and depression following TBI.

Among the long-term consequences of TBI, one of the most recently debated yet severely understudied is pain (7). Pain is an acute response to brain injury and typically lasts several weeks in patients (8). However, in a small group of

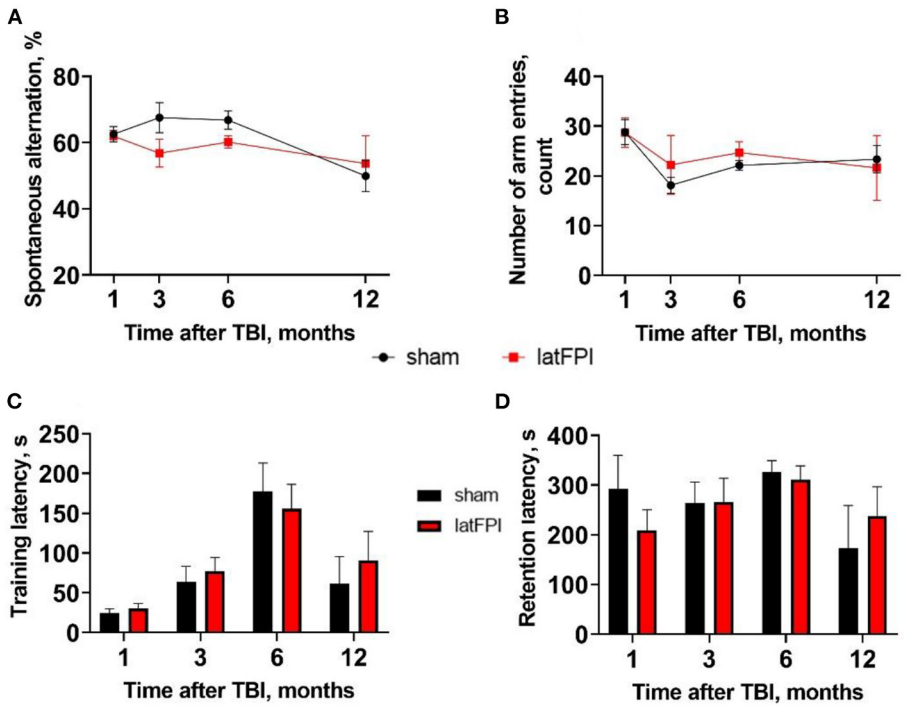

FIGURE 6
Assessment of working and contextual memory after latFPI. Spontaneous alternation behavior **(A)** and the number of arm entries **(B)** in the Y-maze test 1, 3, 6, and 12 months after latFPI. Latency time to enter dark compartment on the training **(C)** and retention day **(D)** in the passive-avoidance test 1, 3, 6, 12 months after latFPI in mice. Data are expressed as mean ± SEM (two-way RM ANOVA followed by Fisher's LSD test).

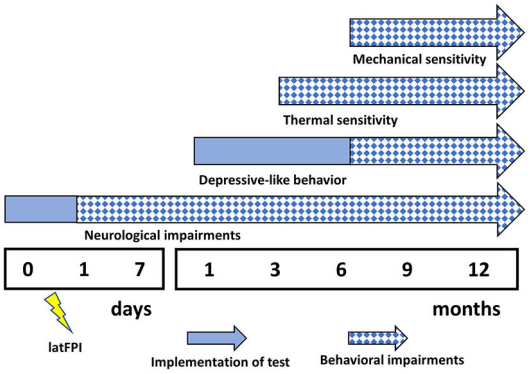

FIGURE 7
Summary of behavioral impairments following latFPI. Neurological impairments were evaluated by neurological severity score, depressive-like behavior by tail suspension test, thermal and mechanical pain sensitivity by acetone and von Frey test, respectively.

patients, pain persists beyond the healing of damaged tissue and becomes chronic (7). The most common long-term pain condition reported in TBI patients is a posttraumatic headache, and in most cases, it is associated with a direct brain tissue injury (5, 7). However, headache is not the only type of pain present after TBI. Clinical studies indicate that chronic pain is located in body regions that have not been injured during trauma, such as the back and lower extremities (8, 35, 36). The mechanisms that drive the development of chronic pain are not well-understood, whether the pain is due to neuropathy, central pain, or secondary to direct tissue injury. Despite emerging evidence that non-head pain is common after TBI, only recently have animal studies begun to explore the mechanisms supporting the development of pain after TBI. Moreover, these studies were limited by short-term follow-up assessment points and pain evaluation in periorbital regions (12, 37–41). A few studies have examined pain-like behavior in peripheral regions, such as hind paws (39, 42, 43). Increased mechanical sensitivity has been observed within 3 weeks after TBI, suggesting that these animals experience acute pain associated with disrupted communication between the brain and spinal cord (43). Here, we showed that latFPI causes cold and mechanical sensitization in body regions distant from the central nervous system. Namely, mechanical sensitivity was observed in contralateral and ipsilateral hind paws starting at 6 months after TBI. Interestingly, cold sensitivity was observed only in the contralateral hind paw, and significant differences were observed starting 3 months after injury. Clinical research

shows that sensation to thermal and tactile stimulation tends to be unilateral, mainly located on the side of the body that was contralateral to the TBI side (8). There is evidence that the surgical procedure per se may lead to increased pain sensitivity in the periorbital and plantar regions in rats (12) and mice (38). However, these findings have been observed at early time points post-TBI and could be explained by direct tissue damage and the inflammatory response to injury.

It is noteworthy that both pain and depression are often cooccurring after TBI, and a significant predictor of persistent pain in patients is an early presence of depressive symptoms after TBI (44). Depressive-like symptoms following TBI have commonly been reported as comorbidities of posttraumatic pain (5, 45). In our study, moderate latFPI induced progressive depressive-like behavior starting at 6 months post-injury. Since the latFPI and sham groups did not differ in locomotor activity in the open field, Y-maze or MWM, the increased immobility time in the tail suspension test reflected the increase in depressive-like behavior. These data are consistent with recently published results in mice suffering from progressive and severe depression-like behavior 6 months after CCI (16). Our previous findings revealed that moderate latFPI also induces depressive-like behavior in male CD-1 mice (21). However, there are also reports where depression-like behavior is not observed within 12 months after closed head injury (46). Our results suggest that moderate latFPI induces progressive depression-like behavior, and this model is suitable for studying common clinical symptoms of depression that are diagnosed following TBI.

Assessment of learning and memory is widely used in preclinical research to determine the duration and severity of cognitive impairments following TBI. Cognitive deficits in experimental TBI models have been observed up to 1 year or longer after the initial injury (Supplementary Table S1). In these long-term studies, cognitive impairments have been observed after severe TBI accompanied by extensive brain tissue loss (13, 15, 16, 47, 48). In cases where brain tissue damage is not extensive (e.g., tissue loss in the ipsilateral cortex), cognitive impairments are less prominent or not observed (17, 21). In the present study, we did not observe cognitive impairments in any of the evaluated memory tests. Hippocampal-dependent cognitive tasks, such as spatial learning and memory, were not affected up to 6 months post-injury. Only one study showed that hippocampal-dependent learning tasks were affected from 2 to 12 months after latFPI in rats; however, the injury was accompanied by progressive tissue loss resembling severe brain injury (18). While some speculate that water maze performance and sensitivity depend on the difficulty of the protocol (49), we believe that the moderate latFPI model is not suitable to study memory deficits after TBI in mice. Furthermore, we were unable to find any differences between the performance of injured and sham mice on the Y-maze and passive avoidance tests, suggesting that moderate latFPI in the present study did not produce cognitive impairments. It is important to note that localization of craniotomy is crucial while performing latFPI. Even though the surgery is performed similarly between animals, medial and rostral shifts can worsen or lessen injury-dependent hippocampal damage (50).

Of note, using only male mice in our study may be considered as a limitation. The incidence of TBI is higher in male than females, however, the consequences of those injuries may be different for the sexes in both preclinical and clinical studies (51). In particular, it has been reported that women have higher risk for persistent pain and depression after TBI (44, 52, 53). There are concerns that estrous cycle changes may introduce variability in the development of neurological impairments, although this has been debated. Previous preclinical study has failed to identify sex-linked differences in nociceptive sensitization and depressive-like behavior after closed head injury (46, 54). However, this should not be taken as underestimating the importance of sex differences in preclinical TBI research and further studies are needed.

The chronic peripheral pain and depression observed in the present study underlie the clinical importance of severe and long-lasting consequences after TBI. Nevertheless, pain in body regions other than the head is often not assessed systematically in clinical and preclinical TBI research. It is essential that this factor is taken into consideration in evaluating posttraumatic pain. Patients with TBI may benefit from timely assessment and intervention to minimize the development and impact of pain. Acute and continued pain management may be paramount for addressing depression or other neurological impairments in TBI patients.

Data availability statement

The raw data supporting the conclusions of this article will be made available by the authors, without undue reservation.

Ethics statement

The animal study was reviewed and approved by Latvian Animal Protection Ethical Committee of Food and Veterinary Service in Riga, Latvia.

Author contributions

Conceptualization: LZ and MD. Methodology, validation, formal analysis, and data analysis and interpretation: GS, BS, EV, and LZ. Behavioral analysis: GS and BS. Writing—original draft preparation: GS and LZ. Writing—review and editing: GS, BS, EV, ID, LZ, and MD. All

authors have read and agreed to the published version of the manuscript.

Funding

This study was supported by the framework of EU-ERA-NET NEURON CnsAflame and TRAINS.

Conflict of interest

The authors declare that the research was conducted in the absence of any commercial or financial relationships that could be construed as a potential conflict of interest.

Publisher's note

Supplementary material

The Supplementary Material for this article can be found online at: https://www.frontiersin.org/articles/10.3389/fneur.2022.985895/full#supplementary-material

References

1. Riggio S. Traumatic brain injury and its neurobehavioral sequelae. *Neurol Clin.* (2011) 29:35–47. doi: 10.1016/j.ncl.10008

2. Wilson L, Stewart W, Dams-O'Connor K, Diaz-Arrastia R, Horton L, Menon DK, et al. The chronic and evolving neurological consequences of traumatic brain injury. *Lancet Neurol.* (2017) 16:813–25. doi: 10.1016/S1474-4422(17)30279-X

3. Semple BD, Zamani A, Rayner G, Shultz SR, Jones NC. Affective, neurocognitive and psychosocial disorders associated with traumatic brain injury and post-traumatic epilepsy. *Neurobiol Dis.* (2018) 123:27–41. doi: 10.1016/j.nbd.07018

4. Maas AIR, Menon DK, Adelson PD, Andelic N, Bell MJ, Belli A, et al. Traumatic brain injury: integrated approaches to improve prevention, clinical care, and research. *Lancet Neurol.* (2017) 16:987–1048. doi: 10.1016/S1474-4422(17)30371-X

5. Khoury S, Benavides R. Pain with traumatic brain injury and psychological disorders Prog Neuro-Psychopharmacology. *Biol Psychiatry.* (2017) 87:224–33. doi: 10.1016/J.PNPBP.06007

6. Gironda RJ, Clark ME, Ruff RL, Chait S, Craine M, Walker R, et al. Traumatic brain injury, polytrauma, and pain: challenges and treatment strategies for the polytrauma rehabilitation. *Rehabil Psychol.* (2009) 54:247–58. doi: 10.1037/A0016906

7. Irvine KA, David Clark J. Chronic Pain After Traumatic Brain Injury: Pathophysiology and Pain Mechanisms. *Pain Med.* (2018) 19:1315–33. doi: 10.1093/PM/PNX153

8. Ofek H, Defrin R. The characteristics of chronic central pain after traumatic brain injury. *Pain.* (2007) 131:330–40. doi: 10.1016/J.PAIN.06015

9. Walker WC. Pain pathoetiology after TBI: neural and nonneural mechanisms. *J Head Trauma Rehabil.* (2004) 19:72–81. doi: 10.1097/00001199-200401000-00007

10. Bair MJ, Robinson RL, Katon W, Kroenke K. Depression and pain comorbidity: a literature review. *Arch Intern Med.* (2003) 163:2433–45. doi: 10.1001/ARCHINTE.163.20.2433

11. Sullivan-Singh SJ, Sawyer K, Ehde DM, Bell KR, Temkin N, Dikmen S, et al. Comorbidity of pain and depression among persons with traumatic brain injury. *Arch Phys Med Rehabil.* (2014) 95:1100–5. doi: 10.1016/J.APMR.02001

12. Silva Fiorin da F, do Espírito Santo CC, Santos ARS, Fighera MR, Royes LFF. Implication of surgical procedure in the induction of headache and generalized painful sensation in a fluid percussion injury model in rats. *J Neurosci Methods.* (2018) 307:23–30. doi: 10.1016/J.JNEUMETH.06004

13. Shear DA, Tate MC, Archer DR, Hoffman SW, Hulce VD, Laplaca MC, et al. Neural progenitor cell transplants promote long-term functional recovery after traumatic brain injury. *Brain Res.* (2004) 1026:11–22. doi: 10.1016/J.BRAINRES.07087

14. Pöttker B, Stöber F, Hummel R, Angenstein F, Radyushkin K, Goldschmidt J, et al. Traumatic brain injury causes long-term behavioral changes related to region-specific increases of cerebral blood flow. *Brain Struct Funct.* (2017) 222:4005–21. doi: 10.1007/S00429-017-1452-9

15. Pischiutta F, Micotti E, Hay JR, Marongiu I, Sammali E, Tolomeo D, et al. Single severe traumatic brain injury produces progressive pathology with ongoing contralateral white matter damage one year after injury. *Exp Neurol.* (2017) 300:167–78. doi: 10.1016/j.expneurol.11003

16. Mao X, Terpolilli NA, Wehn A, Cheng S, Hellal F, Liu B, et al. Progressive Histopathological damage occurring up to one year after experimental traumatic brain injury is associated with cognitive decline and depression-like behavior. *J Neurotrauma.* (2020) 37:1331–41. doi: 10.1089/NEU.2019.6510

17. Leconte C, Benedetto C, Lentini F, Simon K, Ouaazizi C, Taib T, et al. Histological and Behavioral Evaluation after Traumatic Brain Injury in Mice: A Ten Months Follow-Up Study. *J Neurotrauma.* (2020) 37:1342–57. doi: 10.1089/NEU.2019.6679

18. Pierce JES, Smith DH, Trojanowski JQ, McIntosh TK. Enduring cognitive, neurobehavioral and histopathological changes persist for up to one year following severe experimental brain injury in rats. *Neuroscience.* (1998) 87:359–69. doi: 10.1016/S0306-4522(98)00142-0

19. Immonen RJ, Kharatishvili I, Gröhn H, Pitkänen A, Gröhn OHJ. (2009). Quantitative MRI predicts long-term structural and functional outcome after experimental traumatic brain injury. *Neuroimage.* (2008) 45:1–9. doi: 10.1016/J.NEUROIMAGE.11022

20. Johnstone VPA, Wright DK, Wong K, O'Brien TJ, Rajan R, Shultz SR, et al. Experimental traumatic brain injury results in long-term recovery of functional responsiveness in sensory cortex but persisting structural changes and sensorimotor, cognitive, and emotional deficits. *J Neurotrauma.* (2015) 32:1333–46. doi: 10.1089/NEU.2014.3785

21. Stelfa G, Vavers E, Svalbe B, Serzants R, Miteniece A, Lauberte L, et al. Reduced GFAP expression in bergmann glial cells in the cerebellum of sigma-1 receptor knockout mice determines the neurobehavioral outcomes after traumatic brain injury. *Int J Mol Sci.* (2021) 22. doi: 10.3390./IJMS222111611/S1

22. Fox GB, Levasseur RA, Faden AI. Behavioral Responses of C57BL/6, FVB/N, and 129/SvEMS mouse strains to traumatic brain injury: implications for gene targeting approaches to neurotrauma. *J Neurotrauma.* (2009) 16:377–89. doi: 10.1089/NEU.16377

23. Bothe GWM, Bolivar VJ, Vedder MJ, Geistfeld JG. Behavioral differences among fourteen inbred mouse strains commonly used as disease models. *Comp Med.* (2005) 55:326–34.

24. Mogil JS, Wilson SG, Bon K, Lee SE, Chung K, Raber P, et al. Heritability of nociception I: responses of 11 inbred mouse strains on 12 measures of nociception. *Pain.* (1999) 80:67–82. doi: 10.1016/S0304-3959(98)00197-3

25. Lucki I, Dalvi A, Mayorga AJ. Sensitivity to the effects of pharmacologically selective antidepressants in different strains of mice. *Psychopharmacology.* (2001) 155:315–22. doi: 10.1007/S002130100694

26. An XL, Zou JX, Wu RY, Ying Y, Tai FD, Zeng SY, et al. Strain and sex differences in anxiety-like and social behaviors in C57BL/6J and BALB/cJ mice. *Exp Anim.* (2011) 60:111–23. doi: 10.1538/EXPANIM.60.111

27. Garcia Y, Esquivel N. Comparison of the Response of Male BALB/c and C57BL/6 Mice in behavioral tasks to evaluate cognitive function. *Behav Sci.* (2018) 8. doi: 10.3390./BS8010014

28. Percie du Sert N, Hurst V, Ahluwalia A, Alam S, Avey MT, Baker M, et al. The ARRIVE guidelines 2.0: Updated guidelines for reporting animal research. *Exp Physiol.* (2020) 105:1459–66. doi: 10.1113/EP088870

29. Kupats E, Stelfa G, Zvejniece B, Grinberga S, Vavers E, Makrecka-Kuka M, et al. Mitochondrial-protective effects of r-phenibut after experimental traumatic brain injury. *Oxid Med Cell Longev.* (2020). doi: 10.1155/2020/9364598

30. Zvejniece L, Vavers E, Svalbe B, Veinberg G, Rizhanova K, Liepins V, et al. R-phenibut binds to the α2–δ subunit of voltage-dependent calcium channels and exerts gabapentin-like anti-nociceptive effects. *Pharmacol Biochem Behav.* (2015) 137:23–9. doi: 10.1016/J.PBB.07014

31. Bergeson SE, Blanton H, Martinez JM, Curtis DC, Sherfey C, Seegmiller B, et al. Binge ethanol consumption increases inflammatory pain responses and mechanical and cold sensitivity: tigecycline treatment efficacy shows sex differences. *Alcohol Clin Exp Res.* (2016) 40:2506. doi: 10.1111/ACER.13252

32. Zvejniece L, Svalbe B, Veinberg G, Grinberga S, Vorona M, Kalvinsh I, et al. Investigation into stereoselective pharmacological activity of phenotropil. *Basic Clin Pharmacol Toxicol.* (2011) 109:407–12. doi: 10.1111/J.1742-7843.2011.00742.X

33. Zvejniece L, Vavers E, Svalbe B, Vilskersts R, Domracheva I, Vorona M, et al. The cognition-enhancing activity of E1R, a novel positive allosteric modulator of sigma-1 receptors. *Br J Pharmacol.* (2014) 171:761. doi: 10.1111/BPH.12506

34. Svalbe B, Stelfa G, Vavers E, Zvejniece B, Grinberga S, Sevostjanovs E, et al. Effects of the N-methyl-d-aspartate receptor antagonist, MK-801, on spatial memory and influence of the route of administration. *Behav Brain Res.* (2019) 372:112067. doi: 10.1016/J.BBR.2019.112067

35. Nampiaparampil DE. Prevalence of chronic pain after traumatic brain injury: a systematic review. *JAMA.* (2008) 300:711–9. doi: 10.1001/JAMA.300.6.711

36. Kwan V, Vo M, Noel M, Yeates K. A scoping review of pain in children after traumatic brain injury: is there more than headache? *J. Neurotrauma.* (2018) 35:877. doi: 10.1089/NEU.2017.5281

37. Feliciano DP, Sahbaie P, Shi X, Klukinov M, Clark JD, Yeomans DC, et al. Nociceptive sensitization and BDNF up-regulation in a rat model of traumatic brain injury. *Neurosci Lett.* (2014) 583:55–9. doi: 10.1016/J.NEULET.09030

38. Macolino CM, Daiutolo BV, Albertson BK, Elliott MB. Mechanical allodynia induced by traumatic brain injury is independent of restraint stress. *J Neurosci Methods.* (2014) 226:139–46. doi: 10.1016/J.JNEUMETH.01008

39. Meidahl AC, Klukinov M, Tzabazis AZ, Sorensen JC, Yeomans DC. Nasal application of HSV encoding human preproenkephalin blocks craniofacial pain in a rat model of traumatic brain. *Injury.* (2017) 3:55. doi: 10.1038./gt.2017.55

40. Meidahl AC, Eisenried A, Klukinov M, Cao L, Tzabazis AZ, Yeomans DC, et al. Intranasal oxytocin attenuates reactive and ongoing, chronic pain in a model of mild traumatic brain injury. *Headache.* (2018) 58:545–58. doi: 10.1111/HEAD.13248

41. Wang Z, Wang Q, Wang C, Xu X, Yu H. Tetramethylpyrazine attenuates periorbital allodynia and neuroinflammation in a model of traumatic brain injury. *J Inflamm.* (2017) 14. doi: 10.1186./S12950-017-0161-8

42. Liang DY, Shi X, Liu P, Sun Y, Sahbaie P, Li WW, et al. The Chemokine Receptor CXCR2 Supports Nociceptive Sensitization after Traumatic Brain Injury. *Mol Pain.* (2017) 13. doi: 10.1177./1744806917730212

43. Irvine KA, Sahbaie P, Ferguson AR, Clark JD. Enhanced descending pain facilitation in acute traumatic brain injury. *Exp Neurol.* (2019) 320:112976. doi: 10.1016/J.EXPNEUROL.2019.112976

44. Tham SW, Palermo TM, Wang J, Jaffe KM, Temkin N, Durbin D, et al. Persistent pain in adolescents following traumatic brain injury. *J Pain.* (2013) 14:1242. doi: 10.1016/J.JPAIN.05007

45. Bodnar CN, Morganti JM, Bachstetter AD. Depression following a traumatic brain injury: uncovering cytokine dysregulation as a pathogenic mechanism. *Neural Regen Res.* (2018) 13:1693. doi: 10.4103/1673-5374.238604

46. Tucker LB, Velosky AG, Fu AH, McCabe JT. Chronic neurobehavioral sex differences in a murine model of repetitive concussive brain injury. *Front Neurol.* (2019) 10:509. doi: 10.3389/fneur.2019.00509

47. Dixon CE, Kochanek PM, Yan HQ, Schiding JK, Griffith RG, Baum E, et al. 1-year study of spatial memory performance, brain morphology, and cholinergic markers after moderate controlled cortical impact in rats. *J Neurotrauma.* (1999) 16:109–22. doi: 10.1089/NEU.16109

48. Campos-Pires R, Hirnet T, Valeo F, Ong BE, Radyushkin K, Aldhoun J, et al. (2019). Xenon improves long-term cognitive function, reduces neuronal loss and chronic neuroinflammation, and improves survival after traumatic brain injury in mice. *BJA Br J Anaesth.* (2019) 123:60. doi: 10.1016/J.BJA.02032

49. Kamper JE, Pop V, Fukuda AM, Ajao DO, Hartman RE, Badaut J, et al. Juvenile traumatic brain injury evolves into a chronic brain disorder: Behavioral and histological changes over 6 months. *Exp Neurol.* (2013) 250:8–19. doi: 10.1016/J.EXPNEUROL.09016

50. Thompson HJ, Lifshitz J, Marklund N, Grady MS, Graham DI, Hovda DA, et al. Lateral Fluid Percussion Brain Injury: A 15-Year Review and Evaluation. *J Neurotrauma.* (2005) 22:42–75. doi: 10.1089/NEU.2242

51. Gupte R, Brooks W, Vukas R, Pierce J, Harris J. Sex Differences in traumatic brain injury: what we know and what we should know. *J Neurotrauma.* (2019) 36:3063–91. doi: 10.1089/NEU.2018.6171

52. Iverson KM, Pogoda TK, Gradus JL, Street AE. Deployment-related traumatic brain injury among operation enduring freedom/operation Iraqi freedom veterans: associations with mental and physical health by gender. *J Womens Health).* (2013) 22:267–75. doi: 10.1089/JWH.2012.3755

53. Sung CW, Lee HC, Chiang YH, Chiu WT, Chu SF, Ou JC, et al. Early dysautonomia detected by heart rate variability predicts late depression in female patients following mild traumatic brain injury. *Psychophysiology.* (2016) 53:455–64. doi: 10.1111/PSYP.12575

54. Sahbaie P, Tajerian M, Yang P, Irvine KA, Huang TT, Luo J, et al. Nociceptive and cognitive changes in a murine model of polytrauma. *J pain.* (2018) 19:1392–405. doi: 10.1016/J.JPAIN.06004